International Scientific-Technical and Production Journal

The Paton WELDING JOURNAL

July
2008
7

English translation of the monthly «Avtomaticheskaya Svarka» (Automatic Welding) journal published in Russian since 1948

Founders: *E.O. Paton Electric Welding Institute of the NAS of Ukraine*
International Association «Welding»

Publisher: *International Association «Welding»*

Address:
E.O. Paton Electric Welding Institute,
International Association «Welding»,
11, Bozhenko str., 03680, Kyiv, Ukraine
Tel.: (38044) 287 67 57
Fax: (38044) 528 04 86
E-mail: journal@paton.kiev.ua
http://www.nas.gov.ua/pwj

State Registration Certificate
KV 4790 of 09.01.2001

Subscriptions:
$324, 12 issues per year,
postage and packaging included.
Back issues available.

CONTENTS

CHARACTERISTICS OF FRACTURE RESISTANCE OF PIPELINE MATERIAL WITHIN THE ZONE OF DEFECTS, RISK OF FAILURE

V.I. MAKHNENKO, E.A. VELIKOIVANENKO and **O.I. OLEJNIK**
E.O. Paton Electric Welding Institute, NASU, Kiev, Ukraine

Considered are characteristics of pipeline steels and their welded joints, determining fracture resistance in the zone of detected defects. Attention is focused on corrosion thinning defects, as well as development of corrosion cracks. Proceeding from analysis of the publications and authors' investigations, recommendations are given on quantitative values of the above characteristics under static loading on main pipeline.

Keywords: soil corrosion rate, «uniform» surface corrosion, pitting, groove-like defects, corrosion cracks, probability descriptions, risk of failure

The approach to estimation of the risk of failure allowing for defects detected in a linear part of main pipelines under static loading, which is described in [1, 2], requires the on-line knowledge of corresponding characteristics of a material, which determine its resistance, such as development of corrosion processes causing growth of various thinning defects, growth of stress corrosion cracks, and spontaneous propagation of crack-like defects.

The above mechanisms are most typical for the failure to occur in a linear part of modern main pipelines both at the presence of defects and in estimation of appropriate repair structures related to removal of defects [3].

As known from practice, the corrosion effect, despite serious measures taken to ensure corrosion protection of modern main pipelines [4], is one of the most common mechanisms of formation of defects and respective failures. The rate of surface corrosion (g / (dm^2·year), or mm / year) is an indicator of corrosion losses of metal from the surface of pipes in the case of damage of corrosion protection. Study [5] gives experimental results on soil corrosion of pipeline steel under natural conditions, which were obtained by field stations located in different regions of the former Soviet Union (Table 1) and supplemented by laboratory investigations. The latter show that in the processes of soil corrosion of pipeline steel the strong effect on the rate of corrosion both in uniform and non-uniform fracture (leading to formation of corrosion cavities, i.e. pitting) is exerted by temperature conditions. The laboratory investigations described in study [5] show (Figure 1, Table 2) that within a temperature range of $20 < T \leq 60$ °C the rate of uniform corrosion grows in proportion to the temperature, reaching 25–50 g / (dm^2·year) (0.32–0.65 mm / year through thickness of the pipe wall) at $T \approx 40$ °C for steel 17G1S. However, the rate of corrosion dramatically decreases at a temperature above 80 °C, this being attributable to drying up of the soil environment.

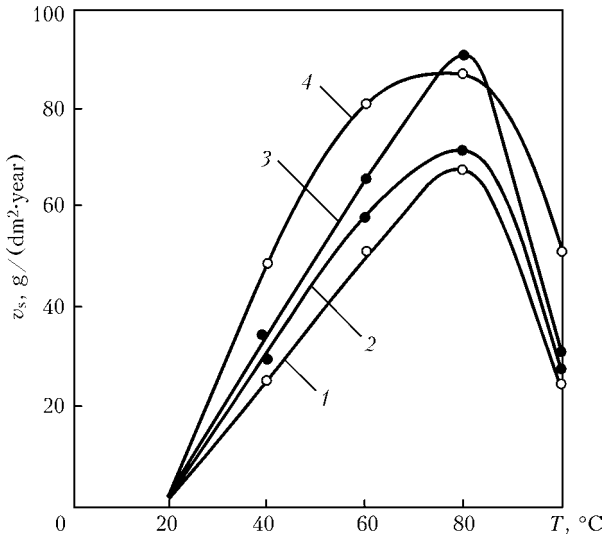

Figure 1. Rate of corrosion of steel 17G1S versus temperature and concentration of sodium chloride in soft water (*1*), in 1 % (*2*), 3 % (*3*) and 6 % (*4*) sodium chloride solution

At non-uniform corrosion leading to formation of macro corrosion pairs, the rate of corrosion may markedly grow to form cavities of 2.5 mm / year deep. Therefore, in 5–6 years a pipeline may corrode to a depth of 10–12 mm through thickness of the pipe wall [5], i.e. the rate of corrosion may amount to about 2 mm / year. The certain effect on the rate of corrosion is exerted by the composition of soil (Table 1, Figure 1). However, this effect is relatively low, allowing for the temperature factor and character of corrosion fracture (uniform, non-uniform).

Similar remark may apply also to the effect of the composition of pipe steel (Table 2).

In this connection, at the absence of direct observations of the rate of corrosion thinning of the pipe wall within the zone of defects under consideration, to estimate the failure risk it is possible to recommend, with a certain degree of conservatism, the following dependence for the mean rate of soil corrosion in the case of the uniform fracture mechanism:

Table 1. Data on soil corrosion of pipeline steel under natural conditions in different regions [5]

Region of location of field station	General characteristic of soil in region of field station	Temperature, °C, at depth, m		Corrosion of steel, g / (dm^2·year), at depth, m		Character of corrosion fracture	Depth of corrosion cavities, mm	Specific electrical resistance of soil in region of field station, Ohm·m
		0.6	1.2	0.6	1.2			
Extreme North								
Salekhard	Loamy soil (frost)	–1.5	–3.0	0	0	Uniform	–	230
Tarka-Sale	Loamy sand	+1.2	–0.9	0.8	0			130
Igrim	Peat soil	+1.3	+0.8	1.6	0.6			100
Surgut	Loamy sand	+2.2	+1.3	1.2	1.3			150
Nadym	Peat soil	+2.3	–1.2	1.4	0			90
Ukhta	Loamy soil	+3.2	–1.1	1.9	0			120
Western and Eastern Siberia								
Tyumen	Loamy soil	+4.6	+2.3	2.2	1.1	Uniform	–	190
Sverdlovsk		+9.2	+4.6	1.7	0.9			110
Chelyabinsk	Loamy sand	+7.2	+3.6	1.6	0.9			130
Novosibirsk		+8.2	+4.1	1.9	0.7			160
Irkutsk	Black earth	+9.0	+5.0	2.1	0.9			100
Chita	Loamy soil	+6.2	+4.2	1.3	1.1			145
Khabarovsk	Black earth	+9.3	+6.5	1.8	1.3			160
Omsk	Loamy sand	+7.2	+4.3	2.0	1.4			180
Krasnoyarsk	Loamy soil	+5.8	+6.4	1.2	0.43			120
Central and Southern regions								
Moscow region	Loamy sand	+10.0	+8.3	7.8	4.8	Uniform	–	98
Poltava region	Black earth	+16.0	+13.0	12.9	16.9	Non-uniform	0.2	280
Krasnodar Territory		+19.3	+15.8	18.2	17.31		0.5	250
Central Asia								
Tashkent	Loamy soil (saline)	+19.0	+18.3	22.4	19.3	Uniform	–	0.7–3.0
Samarkand	Loamy sand (saline)	+19.8	+21.1	22.9	18.7		–	0.5–2.5
Bukhara	Limestone-sandstone	+24.3	+22.0	25.6	16.9	Non-uniform	Up to 0.8	280–300
Kagan	Loamy sand	+26.0	+17.8	29.6	28.3		0.6–0.8	250–280
Urgench	Loamy soil (saline)	+28.4	+22.3	26.2	25.3	Uniform	–	1.5–2.8
	Loamy sand	+26.5	+21.4	28.3	24.8	Non-uniform	0.5–0.7	230–250

Note. 1. Temperatures in the Extreme North, Western and Eastern Siberia, given in the Table, were measured in summer, and those in Central Asia –– mostly in autumn. 2. Temperature and specific electrical resistance were measured when specimens were placed for testing, and when they were taken out. 3. In all the cases the specimens were taken out exactly in a year.

$$\overline{v}_s = 0.6 + 0.548T^{1.058} \text{ g / (dm}^2\text{·year)} \approx$$
$$\approx 0.0077 + 0.007T^{1.058} \text{ mm / year}, \quad (1)$$

where T is the temperature of the pipe wall ($0 \le T \le 60$ °C). At T = 40 °C, $\overline{v}_s$ = 0.354 mm / year.

Naturally, these values of $\overline{v}_s$ should be used for very large areas of thinning of the pipe walls detected in diagnostics, i.e. where the «uniform» corrosion mechanism takes place.

For pitting defects in the pipe wall, as noted above, the rate of corrosion through thickness equal to $\overline{v}_s \cong$ $\cong$ 2 mm / year is quite realistic. For defects of the type of groove-like thinning of the pipe wall, where selectivity of the corrosion process can hardly be excluded, it can be assumed with a certain degree of conservatism that $\overline{v}_s$ = 1 mm / year, as is reported in study [1]. Naturally, the above mean values of the rate of soil corrosion of the pipe wall may substantially differ from the real ones in a number of cases. Such probable

Table 2. Data on the rate of soil corrosion of pipeline steel depending upon the temperature in a range of 40–120 °C (60 % sand and 40 % clay) [5]

Temperature, °C	Steel	Humidity of corrosive environment, %	Corrosion of pipeline steel, g / (dm^2·year)	Mean value of corrosion over three specimens, g / (dm^2·year)	Depth of corrosion cavities, mm / year
40 ± 2	17G1S	21.3–15.8	24.8	25.6	0.7
	St3		25.9		
	Swedish		26.0		
60 ± 2	17G1S	29.7–17.0	46.9	44.5	0.9
	St3		41.6		
	German				
80 ± 2	17G1S	19.6–13.7	74.5	79.9	1.2
	St3		85.0		
	Japanese		80.3		
100 ± 2	17G1S	15.4–9.1	53.4	62.7	1.8
	St3		69.6		
	Swedish		65.2		
120 ± 2	17G1S*	23.7–1.0	20.4	19.7	2.6
	St3*		19.6		
	German		19.2		

Note. Steels 17G1S and St3 were domestically produced.

deviations can be allowed for to a certain extent by using the probability approaches to description of the risk of accident. In such a case, rate v_s should be regarded as a random quantity having certain distribution density φ_v. For example, as holds in the case of the truncated normal normalised law of distribution of value X (Figure 2)

$$\varphi_X = \frac{1}{S_X}\left[\frac{1}{\sqrt{2\pi}\xi_X}\exp\left[-\frac{1}{2}\left(\frac{X-\overline{X}}{\xi_X}\right)^2\right]\right], \quad (2)$$
$$A_X \le X \le B_X,$$

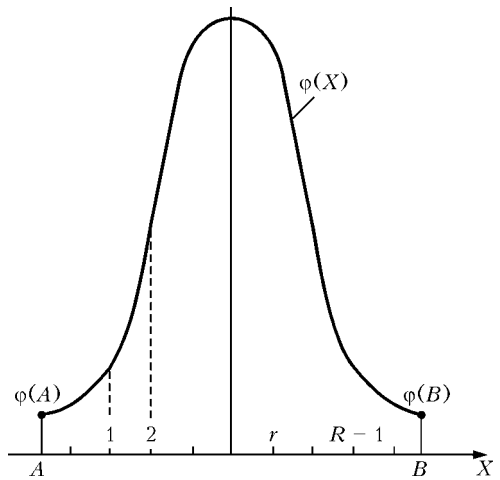

Figure 2. Density of distribution of X values corresponding to truncated normal distribution law

where $S_X = \int_{A_X}^{B_X} \frac{1}{\sqrt{2\pi}\xi_X}\exp\left[-\frac{1}{2}\left(\frac{X-\overline{X}}{\xi_X}\right)^2\right]dX$; A_X and B_X are the boundaries of truncation of the normal distribution law selected on the basis of really probable values of X, and ξ_X is the standard deviation of random quantity X.

Under conditions of limited information, it is convenient to relate the truncation boundaries to the ξ_X value. For example, $A_X = \overline{X} - k\xi_X$. Then, because of symmetry, $B_X = \overline{X} + k\xi_X$, where k is determined by the $0 < k \le 3$ condition, assuming that at $k = 0$ the X value is deterministic and equal to $\overline{X}$, and at $k > 3$ the density of distribution of the X value differs but very insignificantly from the normal law, where $A = -\infty$ and $B = +\infty$.

Therefore, $\xi_X = \frac{\overline{X} - A}{k}$, i.e. the mean values of soil corrosion rate $\overline{v}_s$ and approximate probable truncation boundary A (e.g. $A_{v_s} \ge 0$) being known, it is possible to plot an approximate curve of distribution density φ_{v_s}. The more the specific information on v_s is available, the more accurate is the distribution φ_{v_s}. Moreover, in this case it is not necessary to refer to the normal distribution law. Other descriptions of the random quantity of v_s are also possible, including in the form of plot of $\varphi_{v_s}(v_s)$, or in the form of a table of discrete values of $\Pi_{v_s}(v_s)$, i.e. relative frequencies of the v_s values, where

$$\Pi_{v_s}(v_s) = \varphi_{v_s}(v_s)\Delta v_s. \quad (3)$$

One of the dangerous manifestations of the process of soil corrosion of pipelines, especially in the zone of welded joints, is propagation of stress corrosion cracks. Under static loading, resistance to this type of fracture is characterised by the corresponding diagram of static corrosion crack resistance of the pipeline material under the effect of the corrosive environment with a specific composition and temperature (Figure 3).

As seen from Figure 3, the diagram of static corrosion resistance relates the rate of growth of sizes of a crack (in depth da / dt or in length dc / dt) to the corresponding values of stress intensity factor $K_I(G)$ or $K_I(D)$ at the crack apex. In a general case, such a diagram may have three regions, depending upon the values of K_I. Region *I* ($K_I < K_{ISCC}$) is the zone of crack propagation mostly by the mechanism of electrochemical corrosion, region *II* ($K_{ISCC} < K_I < K_{IC}$) is the zone of crack propagation by the mechanism of hydrogen-induced embrittlement, and region *III* ($K_I > K_{IC}$) is the zone corresponding to spontaneous growth of the crack.

It is of high practical interest to have such a diagram for each particular combination of the pipe material, composition and temperature of the corrosive environment [6], but this requires a large scope of experimental studies, which is time-consuming [7]. However, the most characteristic parameters are the value of K_{ISCC} and growth rate $v(K_I)$ in region *II* (Figure 3).

Experimental determination of dependence v–K_I in region *II* is much less time-consuming and allows using the in-process methods, one of which, developed at present by the E.O. Paton Electric Welding Institute, is described by Prof. Z.T. Nazarchuk, Academician of the NAS of Ukraine, in study [7]. The method makes it possible to use specimens of a relatively small section, as the operation of monitoring of the crack growth is based not on current measurements of linear sizes of the crack, but on registration of time intervals between the jumps of the crack growth using acoustic emission (Figure 4). For this the use is made of a fundamental assumption that at $K_I > K_{ISCC}$ the crack grows with time in a jump-like manner, i.e. in discrete steps equal to $\Delta l = \alpha K_I^2$, where α is the proportionality factor, which is approximately constant at $l_1 \le l \le \lambda_N$ (l_1 and λ_N are the initial and final sizes of the crack, respectively).

The following equations are employed to derive the required v–K_I dependence:

$$\left.\begin{array}{l} l_n = l_{n-1} + \Delta l \\ n = 1, 2, \ldots, N \end{array}\right\}, \quad (4)$$

$$\alpha = \frac{l_N - l_1}{\sum\limits_{n=1}^{N} K_I^2(l_n)}, \quad \Delta l_n = \alpha K_I^2(l_n), \quad (5)$$

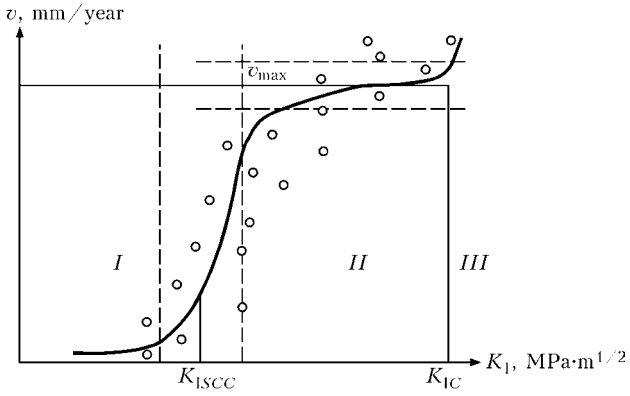

Figure 3. Diagram of static corrosion crack resistance (see designations in the text)

$$K_I(l_n) = \frac{6F_n\sqrt{l_n}}{B}\{1.93 - 3.07(l_n/W) + 14.53(l_n/W)^2 - 25.11(l_n/W)^3 + 25.8(l_n/W)^4\}, \quad (6)$$

where F is the load (Figure 4), W is the specimen thickness, and l_n is the length of the crack for the n-th condition.

The α values at measured l_1, l_N, Δl_n and $K_I(l_n)$ are determined from dependencies (4) through (6) by the method of successive approximations. Then, by using the experimental data on time intervals Δt_n, we determine the $K_I(l_n)$ dependence of $v_n = \Delta l_n / t_n$. The zone of a dramatic decrease in v_n determines the K_{ISCC} value.

Figure 5, *a* shows the results obtained by using the described procedure for a specimen of steel 17G1S in 3 % NaCl solution. Dependence v–K_I obtained in this way has a large scattering of the experimental data, as the real process of hydrogen-induced embrittlement at $\Delta l \approx 5$–10 μm strongly depends upon the geometrical and physical (microstructural) heterogeneities on the path of the crack growth, as well as upon the temperature.

This circumstance requires the use of statistic methods. The normal truncated law (2) can be applied for the crack growth rate at $K_I > K_{ISCC}$ (for $\log v = U$ in Figure 5, *a*):

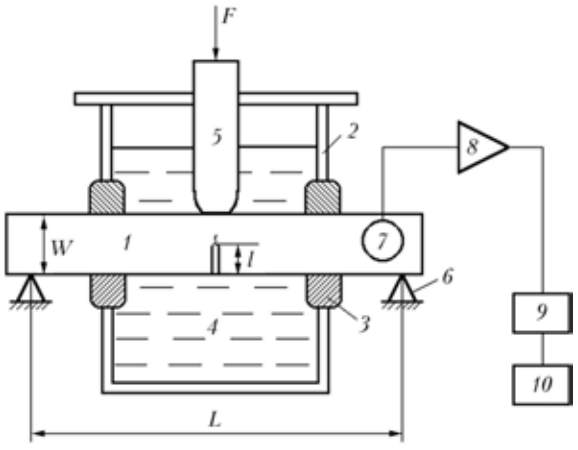

Figure 4. Flow diagram of experimental investigation of corrosion cracks: *1* — prismatic specimen; *2* — chamber; *3* — sealing; *4* — water; *5* — indenter; *6* — support; *7* — piezoelectric sensor; *8* — amplifier; *9* — acoustic emission source; *10* — recorder

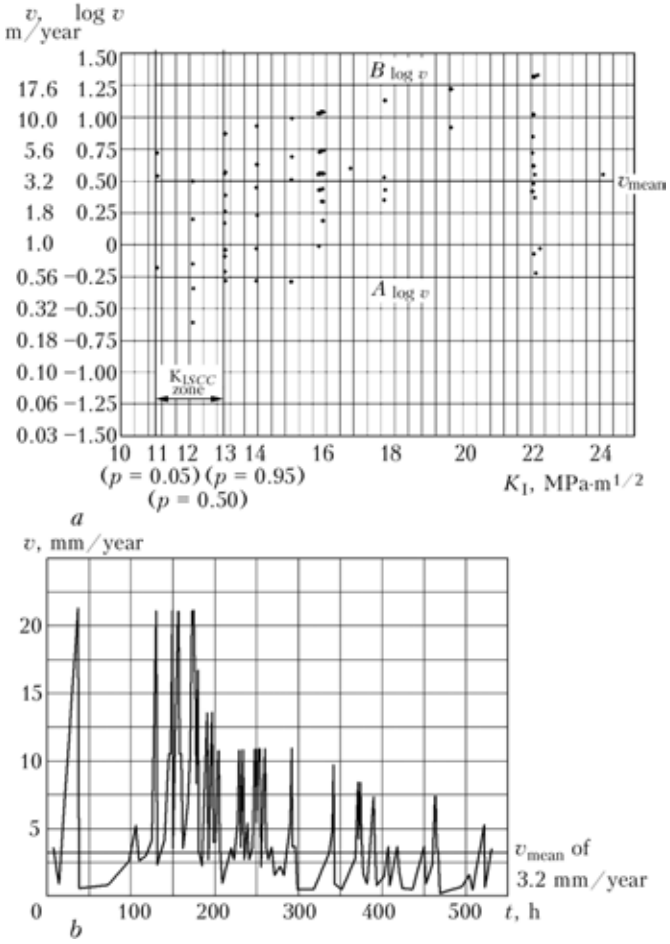

Figure 5. Diagram of static corrosion crack resistance for steel 17G1S at about 20 °C in 3 % NaCl solution (*a*), and diagram plotted on the basis of kinetics of testing the Charpy-type specimen containing a crack (*b*)

$$\overline{U} = \frac{1}{N}\sum_{n=1}^{N} U_n; \quad \xi_U = \left[\frac{1}{N}\sum_{n=1}^{N} (U_n - \overline{U})\right]^{0.5}; \qquad (7)$$
$$A_U = \overline{U} - 2\xi_U.$$

For the threshold value of stress intensity factor K_{ISCC}, it is more logical to employ the Weibull distribution with probability

$$p(K_I) = K_{ISSC} = 1 - \exp\left[-\left(\frac{K_I - K_0}{K_d - K_0}\right)^{\eta}\right], \qquad (8)$$

where parameters K_0, K_d and η are determined by processing the experimental values of K_I in a range of the probable values of K_{ISCC}, the mean value of K_{ISCC} is estimated at p = 0.5, the upper value ---- at p = 0.95, and the lower value ---- at p = 0.05 (Figure 5, *a*).

The following results were obtained for the data shown in Figure 5 by using the above procedure:

$$\overline{U} = 0.5, \quad \overline{v} = 3.2 \text{ mm / year}, \quad \xi_U = 0.25,$$
$$\text{therefore } A_U = 0, \quad B_U = 1.0, \qquad (9)$$
$$\text{or } A_v = 1 \text{ mm / year}, \quad B_v = 10 \text{ mm / year}.$$

Solving the equation for K_0 and K_d at η = 4.0 yields K_d = 12.2 MPa·m$^{1/2}$ and K_0 = 9.91 MPa·m$^{1/2}$, i.e.

$$K_{ISCC}(p) = 9.9 + 2.29[-\ln(1 - p)]^{0.25} \text{ (MPa·m}^{1/2}\text{)}. \qquad (10)$$

The above approach to estimation of characteristics of resistance of the pipeline material to corrosion fracture as a result of soil corrosion in the case of damage of the external corrosion protection can also be employed for the corrosion defects on the inside surface, naturally, in testing the pipe wall material under appropriate conditions, which are primarily determined by the composition and temperature of the corrosive environment.

Consider another group of characteristics of the steel pipeline material, which determine its resistance to a spontaneous growth of crack-line defects. At present, two-parameter criterion R6 has gained wide acceptance as a criterion that formulates the said probability under static loading of a tough-brittle material [8]. With this criterion, resistance of the material within the crack zone to tough fracture is expressed in terms of yield strength σ_y and tensile strength σ_t, while brittle fracture resistance, respectively, is expressed in terms of the critical value of stress intensity factor K_{IC} at a corresponding temperature, allowing for the probability of degradation of the material during many year's operation. The latter remark is highly topical, as main pipelines in many countries, including Ukraine, have been in operation for more than one decade. Moreover, it is a well-known fact that, despite a careful selection of pipe steels, the probability of degradation of their strength properties cannot be ruled out.

The experimental data from [9], shown in Figure 6, on the probability of ageing of pipe steels and degradation of their characteristics of the type of σ_y, σ_t, σ_y / σ_t and δ demonstrate this probability quite clearly, although mainly for the weld zones, where the possibility exists of preheating to a temperature of 250 °C and preliminary deformation tensioning to about 2 %.

The data from [9], shown in Figures 7 and 8, which compare the inventory pipe materials and those after 21 years of operation, are more realistic for the pipe metal. As follows from the data of Figures 6 and 7, characteristics σ_y and σ_t, which are responsible, according to criterion R6 [8], for development of the tough fracture mechanism within the zone of a crack-like defect, do not remain constant during operation, i.e. in long-time operation, e.g. after 15–20 years, it is recommended to check the real values of σ_y and σ_t by the appropriate diagnostics methods to compare them with the rated ones in the as-received state (Table 3).

It should be noted that there is always a certain scatter of the values of σ_y and σ_t, which fits the normal truncated distribution law (2) at $\xi_\sigma \approx 20$ MPa.

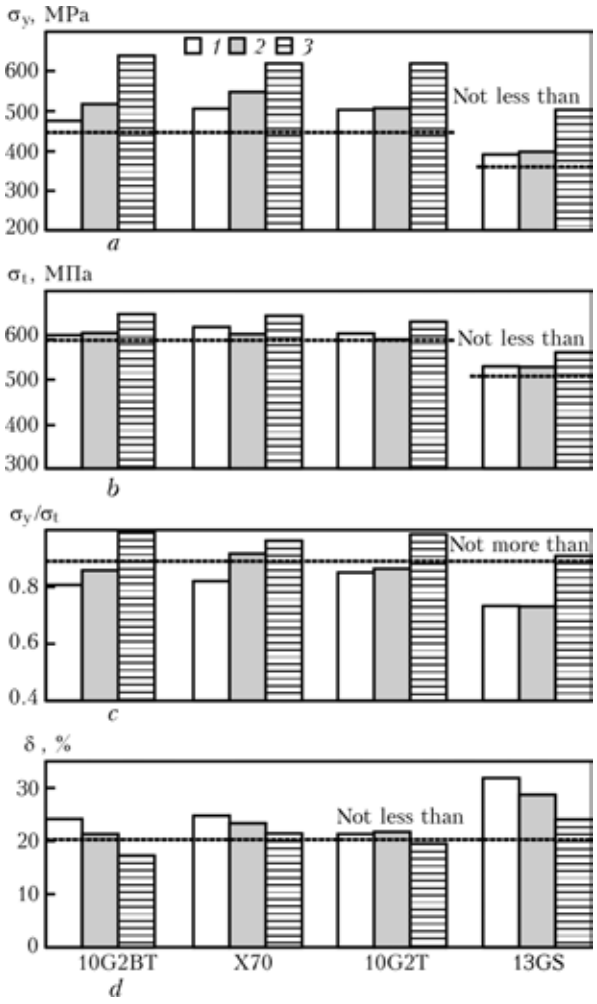

Figure 6. Diagrams of mechanical properties (*a*–*d*) of pipe metal from emergency stock in the as-received state (*1*), after ageing and heating to 250 °C (*2*), and after ageing with preliminary deformation to 2 % (*3*) (dotted line — standard)

The problem of in-process determination of values of K_{IC} within the zone of defects detected in the pipeline wall is more complicated for technical diagnostics, although plenty of investigation data are available for pipe steels, e.g. given in Table 4. Limited wall thicknesses (20–30 mm) do not allow using standard specimens directly from the pipe wall at characteristic ratios $(K_{IC} / \sigma_y)^2 > 50$ mm for pipe steels, as characteristic thickness B of a specimen should meet condition $B > m(K_{IC} / \sigma_y)^2$ with coefficient $m \approx 2.5$.

This circumstance leads to using indirect methods, which are based on an experiment related to measuring the material characteristic that correlates well with K_{IC} and does not require specimens with big cross sections. This is a critical value of J-integral J_C (MPa·m), where [12]

$$K_{IC} \cong \sqrt{\frac{EJ_C}{1-\nu^2}} \quad (\text{MPa}\cdot\text{m}^{1/2}), \qquad (11)$$

where E is the elasticity modulus of the material, and ν is the Poisson's ratio,

or critical normal tear crack opening displacement $\delta_C(m)$, where [10]

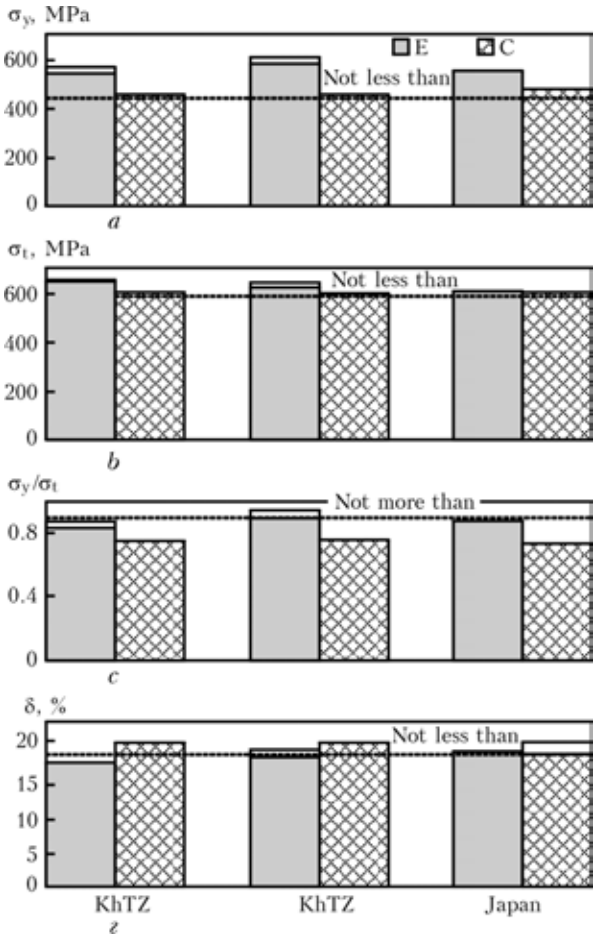

Figure 7. Diagram of mechanical properties (*a*–*d*) of material of pipelines 1420 mm in diameter, made from controlled-rolling steel X70 by different manufacturers: *E* — pipes after long-time operation (21 years); *C* — certificate data (dotted line — standard)

$$K_{IC} = \sqrt{\delta_C \sigma_y E} \quad (\text{MPa}\cdot\text{m}^{1/2}), \qquad (12)$$

or fracture energy of Charpy specimens at impact under appropriate conditions for ferritic steel, where

$$K_{IC} \approx 8.47(KCV)^{0.63} \ (\text{MPa}\cdot\text{m}^{1/2}), \qquad (13)$$

where KCV is the fracture energy (J / cm^2) for a standard Charpy specimen with a cross section of 10 × × 10 mm (see Table 3).

In the case of limited experimental information, the temperature dependence of K_{IC} for pipe steels can be written down by using the following relationship [12]:

$$K_{IC}(p) = 30 + 70 \exp\,[0.019(T - T_0)], \ p = 0.5, \qquad (14)$$

where T_0 is determined at known K_{IC} for any temperature T, e.g. at temperature T_{KCV} to determine KCV in (13), i.e.

$$T_0 \approx T_{KCV} - \frac{1}{0.019} \ln\left[\frac{8.47(KCV)^{0.63} - 30}{70}\right]. \qquad (15)$$

The mean value of K_{IC} ($p = 0.5$) for a service temperature (e.g. +40 °C — pipe wall temperature) being determined, it is possible to estimate K_d, according to [12], allowing for dependence (8) at K_0 =

Table 3. Rated values of mechanical characteristics of steel pipes in as-received state [10]

Steel grade / diameter; thickness, mm	σ_t, MPa	σ_y, MPa	δ, %	KCV, J / cm^2 (at temperature, °C)
10G2T, 10G2BT / 1420; 15.7	588	461	20	78.4 (–15)
10G2FB / 1420; 18.7	588	441	20	78.4 (–15)
X70 / 1420; 18.7	558.7	441	20	78.4 (–15)
09G2FB, 08G2FYu / 1420; 16.8	549.2	421	19	78.4 (–15)
17G1S-U / 1020, 1220; 9.6–15.2	510	360	20	29.4 (–5)
17GS / 530; 7–10	510	353	20	29.4 (0)
13GS / 1020; 11.1 1020; 9.5	510 539	363 402	20 20	29.4 (0) 29.4 (0)
17G1S-U / 1020; 9.6–14.9	510	363	20	39.6 (–40)
13G2AF / 1020; 9.2–14.3	530	363	20	29.4 (–60)
09G2FB, X70 / 1420; 15.7	588.7	441	20	78.4 (–15)
17G1S / 1220; 10.5–12.5 1220; 12	588.7 510	412 362	21	39.2 (–15) 39.2 (–15)

= 20 MPa·m$^{1/2}$ and η = 4 [10], and then calculate the values of K_{IC} for any p:

$$K_{IC}(p) = (K_d - 20)[-\ln(1 - p)]^{0.25} + 20 \quad (\text{MPa}\cdot\text{m}^{1/2}). \tag{16}$$

As a result, we obtain the comprehensive required information on resistance of the pipeline material to a spontaneous growth of cracks.

It can be seen from the above-said that it is possible to find the material characteristics that determine the risk of failure under corresponding service conditions in each particular case of a defect detected in a pipeline made from modern steels. Variations in these characteristics within the set ranges determine quantitatively the probability of failure, i.e. the wider the variation ranges, the higher the probability of failure at constant mean values.

Demonstrate this by an example of calculation of failure risk for the 17G1S steel pipe with diameter d = 1220 mm and wall thickness δ = 12.5 mm, under

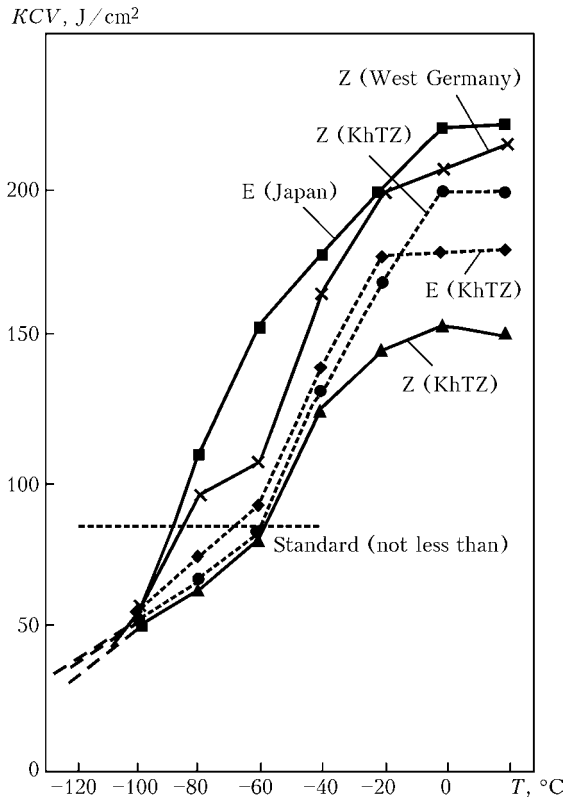

Figure 8. Impact toughness of metal of the 1420 mm diameter pipes made from steel X70 by different manufacturers: *Z* — emergency stock; *E* — after operation

Table 4. Results of investigation of fracture toughness K_{IC} for pipe steels at temperatures –30 °C ≤ T ≤ 20 °C [11]

Steel and investigation zone	T, °Ñ	K_{IC}, MPa·m$^{1/2}$
10G2FB, base metal	–30	230
	+20	240
10G2FB, weld metal	–30	146
	+20	206
10G2FB, HAZ	–30	182
	+20	240
06G2NAV, base metal	–30	150
	+20	130
06G2NAV, weld metal	–30	148
	+20	130
06G2NAV, HAZ	–30	130
	+20	130
VSt3kp (unkilled), base metal	–30	134
	+20	170
17GS	–30	126
	+20	136
17G1S	–30	186
	+20	164
X70	–30	300
	+20	300
10KhGNMAYu	–30	140
	+20	124

Table 5. Initial data for calculation of failure risk in the zone of detected surface cracks under corrosion conditions (steel 17G1S)

Crack number j	$a_0 \times 2c_0$, mm	Direction	σ_m, MPa	$\overline{\sigma}_y$, MPa	$\overline{\sigma}_t$, MPa	$À_{à}$, mm	ξ_a, mm	$À_{ñ}$, mm	$\xi_{ñ}$, mm
1	1.6 × 80	Along generating line	307.5	360	510	1.2	0.2	--	--
2	1.6 × 80	Same	307.5	412	588	1.2	0.2	--	--
3	1.6 × 80	»	263.5	360	510	1.2	0.2	--	--
4	1.6 × 80	»	263.5	412	588	1.2	0.2	--	--
5	1.6 × 200	Along circumference	154.0	360	510	–	--	90	5

Note. $K_{IC}(p) = 161.5[-\ln(1-p)]^{0.25} + 20$ (MPa·m$^{1/2}$); $K_{ISCC}(p)$ according to (10); $\overline{U} = 0.5$; $\xi_U = 0.25$; $A_U = 0$; $B_U = 1.0$; $\xi_\sigma = 20$ MPa; $A_\sigma = \overline{\sigma} - 2\xi_{sigmaÁÚ\ *KÀmsÇÙÄ\ >ÀÀ>\_ÇK).ÇtH-)ÇAb\ 2tÀ3xÇc7ÀsÁ}$; j = 1, 3, 5 without heat treatment; j = 2, 4 with heat treatment.

working pressure in the pipe equal to P_w = 5.4 MPa (membrane stresses σ_m = 263.5 MPa) and P_w = = 6.3 MPa (σ_m = 307.4 MPa), and at the initial rated values of mechanical properties, e.g. given Table 5, assumed with certain conservatism to be the mean values. Detected defects of the crack-like type can be described by a surface semi-elliptical crack with size $a_0 \times 2c_0$, located along the generating line j = 1--4, and along the circumference j = 5 (Table 5), on the external surface of a pipe.

It is assumed that damage of the insulation took place at time moment t = 0, and that the defects under consideration start growing with time at rate v, according to diagram v--K_I in Figure 5, *a*, at the values of its parameters (9) and (10) and pipe temperature of 40 °C (Table 5). The $K_I(j)$ values are calculated at the crack apex $j = G, D$ (Figure 9), from the dependencies given in [10] at different time moments t, starting from t = 0, successively at step Δt:

$$K_{Ij}(j) = \frac{\sqrt{\pi a}}{Q} F_j(\sigma_m + H_j\sigma_t), \quad j = D, G, \tag{17}$$

where

$$\begin{aligned}
Q &= 1 + 1.464(a/c)^{1.65};\\
F_j &= [M_1 + M_2(a/\delta)^2 + M_3(a/\delta)^4]g_j;\\
M_1 &= 1.11 + 0.09(a/c); \quad M_2 = -0.54 - \frac{0.89}{0.2 + a/c};\\
M_3 &= 0.5 - \frac{1}{0.65 + a/c} + 14(1 - a/c)^{24};\\
g_G &= 1; \quad g_D = [1 + (0.1 + 0.35)(a/\delta)^2]\sqrt{a/c};\\
H_G &= 1 - (1.22 + 0.12a/c)\frac{a}{\delta} +\\
&+ [0.55 - 1.05(a/c)^{0.75} + 0.47(a/c)^{1.5}](a/\delta)^2;\\
H_D &= 1 - 0.34(a/\delta) - 0.11(a/c)(a/\delta);\\
a(t) &= a(t - \Delta t) + v(K_{IG})\Delta t;\\
c(t) &= c(t - \Delta t) + v(K_{ID})\Delta t.
\end{aligned} \tag{18}$$

For σ_{ref} responsible for tough fracture within the crack zone in criterion R6 [8] only due to membrane stresses σ_m, the use is made of the dependencies described in studies [6, 12].

For cracks along the generating line

$$\sigma_{ref} = M_S\sigma_m, \quad M_S = \frac{1 - 0.85\, a/\delta\, \dfrac{1}{M_t}}{1 - 0.85a/\delta}, \tag{19}$$

$$M_t = \frac{1.0005 + 0.49001\lambda + 0.32409\lambda^2}{1.0 + 0.50144\lambda - 0.01106\lambda^2}, \quad \lambda = \frac{1.818a}{\sqrt{\delta\dfrac{d}{2}}}.$$

For cracks along the circumference

$$\begin{aligned}
\sigma_{ref} &= \sigma_m Z,\\
Z &= \left\{\frac{2\alpha}{\pi} - \frac{(a/\delta)\theta}{\pi}\left[\frac{2 - (2\cdot 2\delta/d) - 2a/d}{2 - 2\delta/d}\right]\right\}^{-1},\\
\theta &= \frac{2\pi c}{4d}, \quad \alpha = \arccos(A\sin\theta),\\
A &= \chi\,\frac{(1-\tau)(2 - 2\tau + \chi\tau) + (1 - \tau + \chi\tau)^2}{2[1 + (2 - \tau)(1 - \tau)]},\\
\chi &= \frac{a}{\delta}, \quad \tau = \frac{2\delta}{d}.
\end{aligned} \tag{20}$$

It follows from the results of calculations of the probability of failure shown in Figure 9 that this probability can be markedly decreased as a result of reduction of service time t at damaged corrosion insulation, and lowering of working pressure P_w. The use of steel 17G1S with increased σ_y and σ_t (after heat treatment) also contributes to these results.

The effect of scattering of the set values of the rate of corrosion growth of the crack considered is shown in Figure 10, where the calculated values of failure

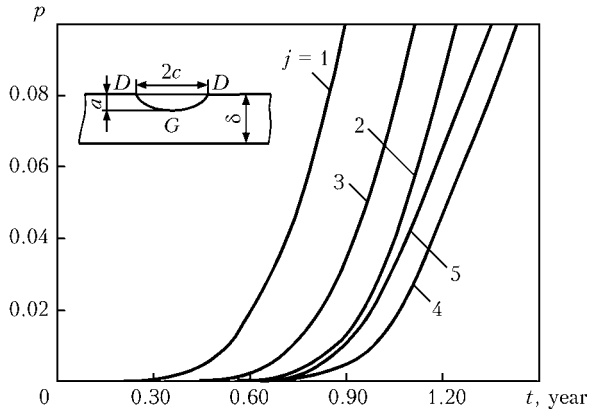

Figure 9. Kinetics of growth of failure risk with time t for corrosion cracks in wall of the 17G1S steel pipe measuring 1220 × 12.5 mm, according to Table 5

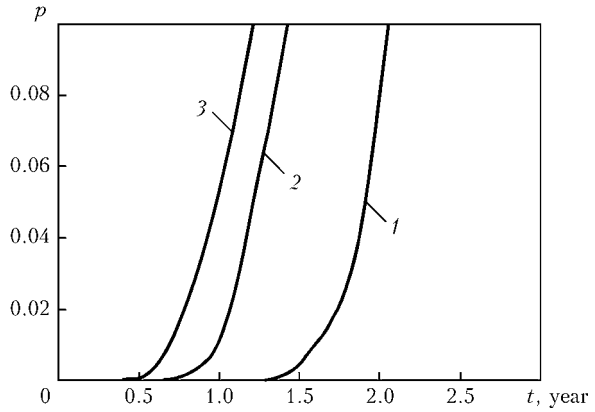

Figure 10. Results of calculation of failure risk for corrosion crack $j = 4$ from Table 5 for three variants of truncation of distribution of function $U = \log v$

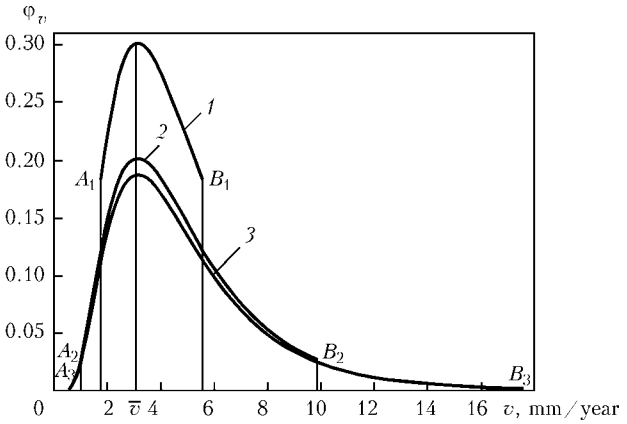

Figure 11. Normalised densities of distribution of values j_v for three variants of truncation of normal distribution of function $U = \log v$ at $\overline{v} = 3.2$ mm / year (see designations in the text)

probability p are given for corrosion crack $j = 4$, according to Table 5 and Figure 9, for three variants of truncation of the accepted normal law of distribution of function $U = \log v$, according to Figure 5: $\overline{U} = 0.5$, $\xi_U = 0.25$. Variant 1: $A_U = 0.25$ and $B_U = 0.75$, which corresponds to $A_v = 1.78$ mm / year and $B_v = 5.62$ mm / year (Figure 11, curve *1*). Variant 2: $A_U = 0$ and $B_U = 1.0$, which corresponds to $A_v = 1$ mm / year and $B_v = 10$ mm / year (Figure 11, curve *2*). Variant 3: $A_U = -0.25$ and $B_U = 1.25$, which corresponds to $A_v = 0.56$ mm / year and $B_v = 17.8$ mm / year (Figure 11, curve *3*).

It can be seen from the above data that substantial limitation of the range of scattering of the v values in transition from variant 3 to variant 1 leads to overestimation of the safe remaining life of the pipeline containing a very dangerous defect considered. And although this overestimation is not in excess of one year, nevertheless it shows the importance of allowance for «tails» in distributions φ_X for the initial data.

CONCLUSIONS

1. Modern approaches to estimation of the risk of failure in the zone of detected defects in the form of discontinuities of the pipeline materials under static loading require information on resistance of the material to corrosion fracture (various types of corrosion cracks), as well as to spontaneous growth of crack-like defects.

2. Available literature data on the rate of surface soil corrosion under natural conditions for specimens of pipe steels in different regions of the former Soviet Union show that temperature conditions exert the substantial effect on the rate of corrosion losses of metal.

The rate of uniform surface corrosion increases approximately 5–6 times with variations of the temperature in a range of 10–60 °C.

Based on analysis of the available experimental data on the rate of surface soil corrosion, it is possible to recommend the use of the truncated normal distribution law at the mean values of $\overline{v}_s$, which depend upon the temperature according to (1) for uniform corrosion, and then increase these values approximately 3 and 5 times, respectively, for the groove-like and pitting defects under the corrosion conditions.

3. Accumulation of the information on the rate of growth of stress corrosion cracks for pipe steels using modern approaches of fracture mechanics is of high practical interest, as such defects are most dangerous under conditions of corrosion damage of a pipeline.

4. Fracture toughness of the material determining its resistance to spontaneous growth of crack-like defects in pipe steels during long-time operation requires appropriate monitoring, which can be experimentally realised by using mostly indirect methods. Approaches based on the Weibull distribution combined with the master-curve (10) are worthy of special notice for description of stochasticity of the K_{IC} values.

1. Makhnenko, V.I., Velikoivanenko, E.A., Olejnik, O.I. (2008) Risk analysis as a method for formalizing decision making on unscheduled repair of welded structures. *The Paton Welding J.*, **5**, 2–7.
2. (2000) *ISO SD 16708 Standard*: Petroleum and natural gas industrials. Pipeline transportation systems. Reliability — Based Limit State Methods.
3. But, V.S., Olijnyk, O.I. (2006) Strategy of development of repair technologies for operating main pipelines. In: *Problems of remaining life and service safety of structures, installations and machines*. Ed. by B.E. Paton. Kiev: PWI.
4. *DSTU 4219–2003*: Main steel pipelines. General requirements to corrosion protection. Valid from 01.12.2003.
5. Marchenko, A.F. (1995) Soil corrosion of pipeline steel and main pipelines. *Stroitelstvo Truboprovodov*, **1**, 29–34.
6. Makhnenko, V.I. (2006) *Remaining safe service life of welded joints and connections of current structures*. Kiev: Naukova Dumka.
7. (2001) *Fracture mechanics and strength of materials*: Refer. Book. Vol. 5: Non-destructive testing and technical diagnostics. Ed. by Z.T. Nazarchuk. Lviv: G.V. Karpenko FMU.
8. Milne, L., Ainsworth, R.A., Dowling, A.R. et al. (1986) Assessment of the integrity of structures containing defects. *CEGB, Report R/H/R6, Revision 3*. April.
9. Rybakov, A.O., Semenov, S.E., Goncharenko, L.V. (2006) Evaluation of state and manifestations of strain ageing of gas pipeline metal in application of controlled rolling steel. In: *Problems of remaining life and service safety of structures, installations and machines*. Ed. by B.E. Paton. Kiev: PWI.
10. *VBN V.2.3-00018201.04–2000*: Calculations of strength of operating main pipelines with defects. Kiev: Gosneftegazprom.
11. Krasovsky, A.Ya., Krasiko, V.N. (1990) *Crack resistance of main pipeline steels*. Kiev: Naukova Dumka.
12. (2000) *Fitness-for-service*. American Petroleum Institute. Recommended practice 579.

THEORETICAL INVESTIGATION OF DYNAMIC BEHAVIOR OF MOLTEN POOL IN LASER AND HYBRID WELDING WITH DEEP PENETRATION

G. TURICHIN[1], **E. VALDAITSEVA**[1], **E. POZDEEVA**[1], **U. DILTHEY**[2] and **A. GUMENIUK**[2]
[1]St.-Petersburg State Polytechnic University, St.-Petersburg, Russia
[2]ISF — Welding and Joining Institute, Aachen University, Aachen, Germany

The article devoted to the simulation of dynamic phenomena of the laser welding process with deep penetration. The presented model is a future development of steady-state model of laser welding. It based on the approach of Lagrange mechanics and takes into account melt flow, wave motion on the cavity surface, melting viscosity, bubble pressure, recoil pressure and radiation parameters. The results of calculations describe self-oscillation nature of the cavity shape during welding. With the base of presented model a simulation of keyhole collapse, leading to defect formation, and a description of acoustic emission spectra from the cavity has been developed.

Keywords: laser welding, self-oscillation process, defects, mathematical model, monitoring

The processes of laser welding with deep penetration, as well as related processes of hybrid welding, are frequently accompanied by porosity appearance and spiking phenomena. The reason of these effects connected with self-oscillation nature of vapour cavity and melt pool in deep penetration welding. Results of experimental investigation of the laser welding prove that the process is not stationary even at stabilisation of all external effects on a weld pool. The experiments on high-speed filming of the laser welding of compound workpieces, consisting from metal and quartz glass [1], have shown a continuous change of the cavity shape, quasi-periodic moving of zones of the maximum brightness on its depth and also availability of such zones on a back wall. The plasma plume filming above the keyhole has shown its quasi-periodic fluctuations [2]. The comparative researches of the liquid metal movement on the weld pool surface and process of spike formation have shown conformity between spiking and a melt tipping out from the melt pool. The same results were obtained later after X-ray filming [3].

The analysis of self-oscillations at action of high intensity energy fluxes on materials is conducted in [4] on the basis of the linear theory of stability. The further development of this approach is submitted in [5]. The stability is investigated on the basis of the joint analysis of the development of temperature, hydro- and gas-dynamic perturbations with the account of relaxation processes and target surface shielding by products of evaporation. The attempts to take into account a real geometry of a cavity surface in laser welding were undertaken by the authors of [6], and in [7] the linear stability of the cavity shape has been investigated. The description of temporary dynamics of cavity radius on the basis of a problem reduction to one ordinary differential equation is indicated in [8]. The authors used the axial symmetry of model problem for reduction of hydrodynamic equations to one ordinary differential equation, but this model predicts only attenuation of fluctuations.

For detail understanding of the nature of dynamic processes in the melt pool during deep penetration welding, it is necessary to have a dynamic model of welding process, based on the clear physical picture of the laser welding process with deep penetration.

Because such model could be applied for the aim of prediction of welding defect appearance and for creation of reliable monitoring and control systems, it should answer the following obvious demands to be used simultaneously for welded joint quality prediction and in the on-line control systems:

- physical equivalence;
- work in real time mode;
- work on available computer technology in the industry.

These requirements don't allow construction the dynamic model of the laser welding process on the base of the direct solution of all total combination of connected physical problems describing the laser welding processes, as it was done for steady-state process model [9–11]. The possible way to develop such dynamic model is using of minimum variation principles and Lagrange (or Hamilton) mechanics formalism, which allow reducing the model to several ordinary differential equations.

Description of the model. To use formalism of the Lagrange mechanics to derive the active zone dynamics equations, it is necessary to take into account

*From Proc. of the 3rd Int. Conf. «Laser technologies in welding and materials processing» (29 May–1 June, 2007, vil. Katsieveli, Crimea, Ukraine), 131–135.

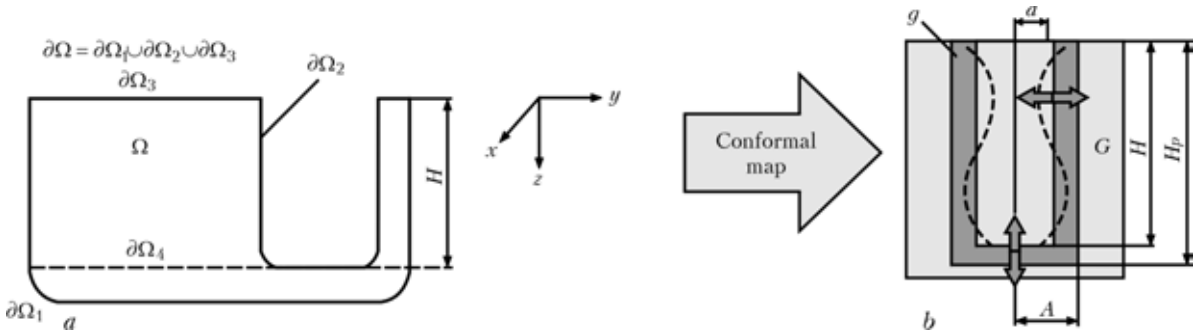

Figure 1. Dividing circuit of the molten pool (*a*) and its conformal map (*b*): Ω — melt zone; ∂Ω — melt zone boundaries; *A* and *a* — image radii of keyhole and fusion boundaries on the conformal map plane respectively; *H* — keyhole depth; H_p — penetration depth; *G* and *g* — images of surface of penetration and threshold cavities respectively

such phenomena as wave motion of the cavity surface, change of the shape and sizes of the weld pool in time and influence of the cavity motion as the whole on oscillations of its depth and radius. Besides the friction forces effect would be taken into account into the movement equations. We'll consider geometry of the model and its possible simplifications before deriving equations of motion by Lagrange formalism. For simplification let us apply that penetration depth $H_p >> a$, where *a* is the keyhole radius, and ignore inclination of the cavity and melt pool walls. Suitable model form of the active zone is show in Figure 1.

The melt flow is described by flow potential φ that answer Laplace equation $\Delta\varphi = 0$ and boundary conditions

$$\left.\frac{\partial\varphi}{\partial n}\right|_{\partial\Omega_1} = 0; \quad \left.\frac{\partial\varphi}{\partial n}\right|_{\partial\Omega_2} = f(\theta, t).$$

Here function f is determine by the cavity motion. It is impossible to get the analytic solution of task about the potential flow of the melt in the region shown in Figure 1, but it is possible to use a conform mapping to simplify the problem by transformation this task into determination of the melt velocity field in the region bounded by two co-axial cylinders with radii *A* and *a*. It is especially convenient to do it, if in the mapping space the energy is presented as function of the cavity section areas.

Taking into account the wave movement on the cavity surface and using Fourier expansion for cavity cross-section area $s(z) = s_0 + \sum_{n=1}^{\infty} s_n \cos\frac{\pi n z}{H}$ in the motionless (in respect to the target) coordinates system to describe the shape of surface, after using of the continuity equation one can obtain the following expression for the velocity v_z:

$$v_z = \frac{1}{S - s}\left(\dot{s}_0 z + s_0\dot{H} + \sum_{n=1}^{\infty}\frac{\dot{s}_n H}{\pi n}\sin\frac{\pi n z}{H}\right),$$

where *S* is the keyhole cross-section area.

For the melt between the target surface and parallel plane, passing through cavity bottom, after transformation it is possible to get

$$E = E_\perp + E_z,$$

where

$$E_\perp = \pi H a^2 \times$$
$$\times\left(\frac{\rho v_0^2}{2}\frac{A^2 + a^2}{A^2 - a^2} + \frac{\rho\dot{a}^2}{2}\frac{A^4}{(A^2 - a^2)^2}\left\{\ln\frac{A^2}{a^2} - 2\left(1 - \frac{1}{2}\frac{a^2}{A_2}\right)^2 + \frac{1}{2}\right\}\right);$$

$$E_z = \frac{\rho}{2(s - s_0)} \times$$
$$\times\left\{\dot{s}_0^2 H^2\left(\frac{1}{3} + \sum_{n=1}^{\infty}(-1)^n\frac{2s_n}{(\pi n)^2(S - s_0)}\right) + s_0^2\dot{H}^2 H + \sum_{n=1}^{\infty}\frac{H^3\dot{s}_n^2}{2(\pi n)^2} + \right.$$
$$+ s_0 H^2\dot{s}_0\dot{H}\left(1 + \sum_{n=1}^{\infty}\frac{2((-1)^n - 1)s_n}{(\pi n)^2(S - s_0)}\right) +$$
$$+ \sum_{n=1}^{\infty}\sum_{k=1}^{\infty}\frac{1}{2}\dot{s}_0\dot{s}_n(s_{n-k} - s_{n+k})\frac{H^3}{p^2 nk(S - s_0)} - \sum_{n=1}^{\infty}(-1)^n\dot{s}_0\dot{s}_n\frac{H^3}{\pi^2 n} \times$$
$$\times\left[\frac{2}{n} + \sum_{k=1}^{\infty}(-1)^k\frac{1}{\pi}\frac{s_k}{S - s_0}\left(\frac{1}{(n + k)^2} + \frac{1 - \delta_{nk}}{(n - k)^2}\right)\right] +$$
$$+ \sum_{n=1}^{\infty} s_0 H^2\dot{s}_n\dot{H}\frac{1}{\pi^2 n} \times$$
$$\left.\times\left[\frac{2(1 - (-1)^n)}{n} - \sum_{k=1}^{\infty}\frac{s_k}{S - s_0}\left(\frac{(-1)^{n+k} - 1}{n + k} + \frac{1 - \delta_{nk}}{n - k}\right)\right] - \right\}.$$

The bottom part kinetic energy E_b can be calculated by the same way:

$$E_b = \frac{\rho}{2}\dot{H}^2\frac{4\pi a^2 A^5}{(A^2 - a^2)^2}\frac{A}{L - H}\sum_{i=1}^{\infty} \times$$
$$\times\left(\frac{J_1\left(l_i\frac{a}{A}\right)}{l_i^4 J_0(l_i)} + \frac{J_1\left(l_i\frac{a}{A}\right)}{3l_i^2 J_0(l_i)}\left(\frac{L - H}{A}\right)^2\right),$$

where l_i is the root of the equation $J_1(l_i) = 0$; *L* is the penetration depth.

Since potential energy of the active zone is superficial energy, it is enough to calculate a free surface area and multiply it by the value of the specific surface energy equal to surface tension coefficient σ. Having left parts containing the small parameter s_n / s_0 out, one can get

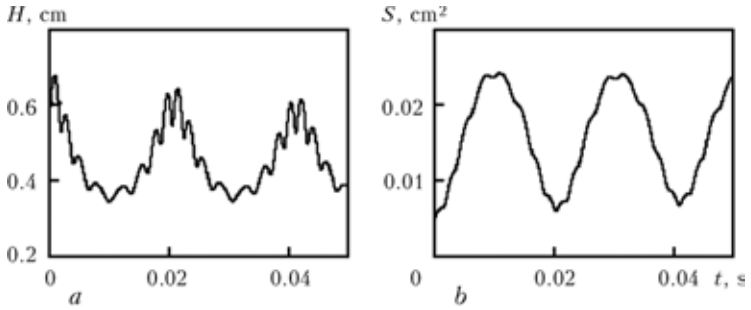

Figure 2. Temporal behavior of the cavity depth H (a) and its cross-section area S (b)

$$\Pi = \sigma \left\{ \pi A^2 + 2\pi aH + \frac{\sqrt{\pi}}{4} \sum_{n=1}^{\infty} \frac{n^2 s_n^2}{H\sqrt{s_0}} + 2H_1(A + a) \right\}.$$

It is easy to get the expressions for generalised forces Q_i that corresponds to chosen generalised coordinates (s_0, s_n, H) by using definition $Q_i = \delta A_i / \delta q_i$, where δA_i is the virtual work on the virtual displacement δq_i. For Q_H it is easy to get $Q_H = (p - p_0)s_0$, where p is the vapour pressure inside the cavity; p_0 is the external pressure.

Taking into account the vapour jet reactive force, we have finally

$$Q_H = (p - p_0 + \rho_0 v_0^2)s_0,$$

where ρ_0 and v_0 is the density and the velocity of vapour jet in the workpiece surface plane, respectively.

Let us evaluate Q_s. After several transformations, neglecting the small parts we have

$$Q_{s_0} = (p(s_0) - p_0)H - \frac{1}{3}\frac{\sigma}{a}H + (-1)^n \frac{2}{\pi^2}\frac{\sigma}{a}\frac{s_n}{s_0}H_n^2;$$

$$Q_{s_n} = H\left[\left.\frac{\partial p}{\partial s}\right|_{s=s_0} \frac{s_n}{s_0} + \frac{\sigma}{a}\frac{s_n}{s_0}(-1)^n \frac{1}{\pi^2 n^2} + \frac{2}{\pi^2}\frac{\sigma}{a}\sum_{\substack{k=1 \\ k\neq n}}^{\infty} \frac{s_k}{s_0}(-1)^{n+k}\frac{n^2+k^2}{(n^2-k^2)^2}\right].$$

To determine $p(s_0)$ and $\left.\frac{\partial p}{\partial s}\right|_{s=s_0}$ the non-stationary heat transfer problem has been solved analytically. Let us consider generalised viscous forces according to Lagrange mechanics formalism, having determined the dissipative function $D = \frac{dE}{dt}$, and the generalised friction force $R_i = \frac{1}{2}\frac{\partial D}{\partial Q_i}$. Solving task about the melt flow in the boundary layer at the melting front gives following expression for the dissipative function:

$$D_1 = -\rho L\sqrt{\frac{\nu}{\pi}} \int_{-\infty}^{t} \frac{d\tau}{\sqrt{t-\tau}} \int_0^H \frac{dv_0}{d\tau} v_0(t)dz,$$

where $L = 2\pi A$ is the melting front perimeter.

Now we can get Lagrange equation (dynamic model one) imagined as

$$\frac{d}{dT}\frac{\partial L}{\partial \dot{q}_i} - \frac{\partial L}{\partial q_i} = Q_i + R_i,$$

where q_i assumes H, s_0, s_1, ... s_n, ..., consecutively.

Modeling results and discussion. To fulfil calculates the system was «cut» in s_2, and the system obtained from four ordinary differential equations of second order was solved numerically by standard 6th order Runge–Kutt algorithm. The test calculations was made for welding of mild steel in the power range of 1–10 kW and welding speed from 0.3 till 5.0 cm / s. Examples of calculation results are shown in Figures 2 and 3 for radiation power Q = 3 kW, welding speed v = 1 cm / s, intensity distribution of the radiation corresponding to TEM_{00} mode with beam radius 0.015 in the focus (86 % of the full power inside), focus distance 20 cm and surface focusing. The initial conditions are taken from the calculation results of the stationary model of laser welding [10].

Analysis of the calculation results shows that when excess pressure inside the cavity and the capillary pressure being equal, force parts of the equations are zero. This condition is unstable balance point. Dense occupation of the limited regions on the phase portraits by the phase trajectories says about turbulent character of the cavity oscillations. It explains the calculation results independence upon initial conditions (when the initial point gets into the attractor). Sizes

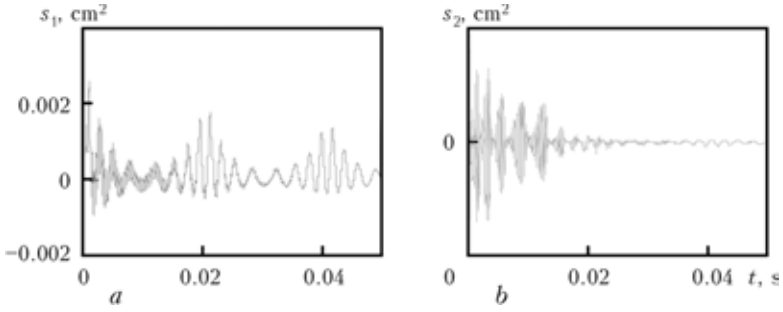

Figure 3. Temporal behavior of the first (a) and second (b) order waves on the cavity surface

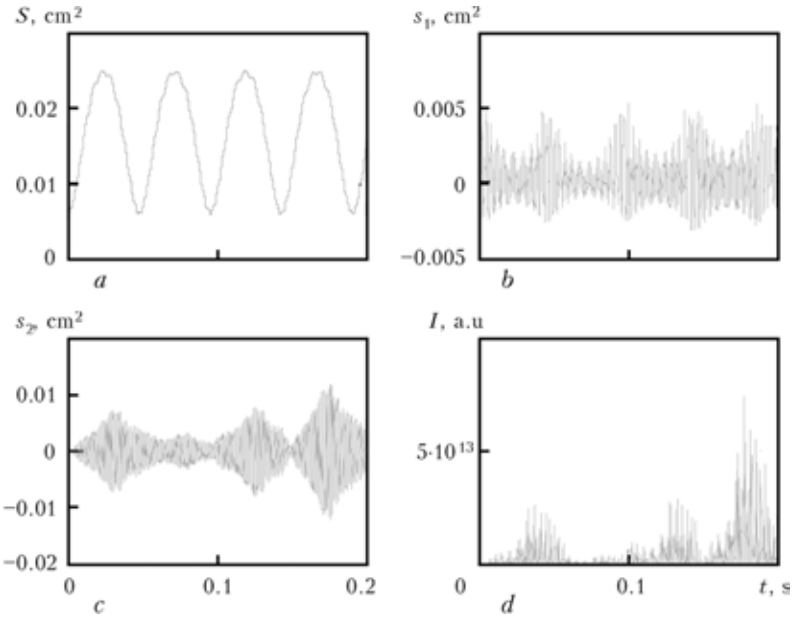

Figure 4. Temporal behavior of cavity area of cavity cross-section (*a*), amplitudes of waves on the cavity surface (*b*, *c*) and acoustic emission intensity (*d*)

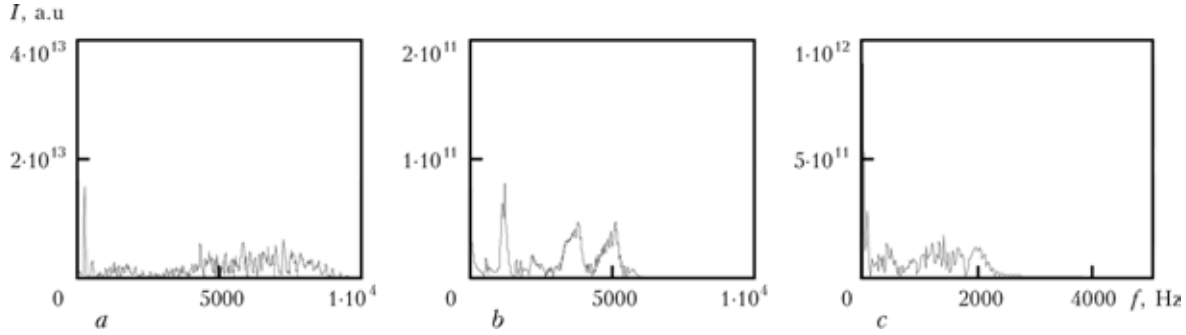

Figure 5. Frequency spectra of acoustic emission at welding speed 5 cm / s and penetration depth ≈ 0.25 cm (*a*), 3 cm / s and ≈ 0.42 cm (*b*), 1 cm / s and ≈ 1.1 cm (*c*)

and shape of the attractor are determined by welding mode parameters.

Modelling show that different generalised coordinates have the different oscillations spectra. The lowest frequencies (less than 500 Hz) are typical for cavity radius oscillations. The amount of high frequency components in the spectra of the cavity depth oscillation is more than the same components in the spectra of the radius oscillation. The first s_1 and second s_2 order waves have the highest frequency spectra (up to 10 kHz). These spectra are also depending on the cavity depth. The feeding velocity increasing also decreases the low-frequency oscillations. Because of this model describes the non-linear cavity oscillation, amplitudes of which are not very small, it allows looking more precisely on the hydrodynamic stability of the cavity shape, as it was investigated in [8]. Accordingly [8], increase of the beam radius leads to increase of the wave amplitudes on the cavity surface.

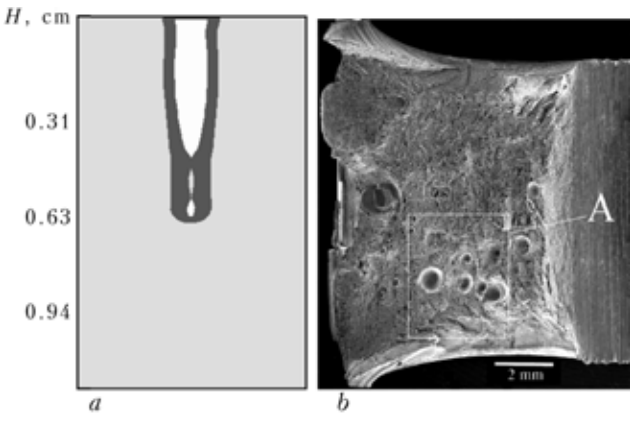

Figure 6. Simulation of porosity formation due to cavity collapse (*a*), and results of experimental observation of pores formed by this effect (*b*) during laser welding of pipe steel

To illustrate a dependence between the dynamics of cavity depth H, the area of cavity cross-section S and the amplitudes of waves on the cavity surface s_1 and s_2 from one side and acoustic emission parameters, the example of temporal behavior of this values and their frequently spectra are shown in Figure 4. The temporal dynamics of acoustic emission is more close to dynamics of banding around of the cavity generalised coordinate with highest frequency s_2, but frequency spectra lie in the region of lesser frequency.

The increases of power and, thus, increases of penetration depth lead to shift of spectra to direction of smaller frequencies that correlated with behavior of spectra of all generalised coordinates of cavity dynamic model. The changes of welding speed (Figure 5)

lead to the same changes of spectra of acoustic emission, so the cavity depth is a value that in general determined a situation here.

The developed mathematical formalism has been implemented in CAE system LaserCAD. With this feature it is possible to use LaserCAD for dynamical analysis of porosity formation and spiking phenomena (Figure 6).

CONCLUSION

In this article, the dynamic model of the laser welding process with deep penetration based on the variation principles, is presented. The model takes into account melting flow, wave motion on the cavity surface, melting viscosity, bubble pressure, recoil pressure and radiation parameters. The model allows the welding process to be analysed both for continuous and for temporally modulated radiation. The model predicts self-oscillation character of the cavity behavior in welding, moreover the cavity oscillations are look like stochastic in general case.

1. Bashenko, V.V., Mitkevich, E.A., Lopota, V.A. (1983) Peculiarities of heat and mass transfer in welding using high energy density power sources. In: *Proc. of 3rd Int. Coll. on EBW* (Lion, 1983), 61–70.
2. Lopota, V.S. et al. (1989) State of material and its parameters in the beam interaction zone in laser welding with deep penetration. *Fizika i Khimiya Obrab. Materialov*, **2**, 104–115.
3. Matsunawa, A., Kim, J.-D., Seto, N. et al. (1998) Dynamics of keyhole and molten pool in laser welding. *J. Laser Appl.*, 10(**6**), 247–254.
4. Zuev, S.V., Selischev, V.I. et al. (1980) Self-oscillations under action of high density energy source on materials. *Fizika i Khimiya Obrab. Materialov*, **6**, 3–7.
5. Arutunyan, V.Yu., Baranov, E.P. et al. (1985) *Laws of pulse-periodic modes of deep penetration of metals*: Preprint IAE 4137 / 16. Moscow.
6. Uglov, S.V., Selischev, V.I. (1988). *Self-oscillations in action of high density energy fluxes on materials*. Moscow: Nauka.
7. Mirzoev, F.Kh. (1994) Vaporisation-capillary instability in deep gas-vapour keyholes. *Kvant. Elektronika*, 21(**2**), 147–150.
8. Turichin, A. (1996) Hydrodynamic aspects of cavity stability in beam welding. *Fizika i Khimiya Obrab. Materialov*, **4**, 74–82.
9. Kaplan, W. (1994) A model of deep penetration laser welding based on calculation of the keyhole profile. *J. Phys. D: Appl. Phys.*, **27**, 1805–1814.
10. Beyer, E., Dahmen, M., Fuerst, B. et al. (1995) A tool for efficient laser processing. In: *Proc. of ICALEO* (San Diego, USA), 1035–1039.
11. Schulz, B., Fuerst, S., Kaierly, G. et al. (1996) Powerful features for LBW including theoretical aspects. In: *Proc. of ICALEO* (Detroit, USA), 1–9.

STRUCTURE OF DEPOSITED METAL OF THE TYPE OF GRAPHITISED HYPEREUTECTOID STEELS

I.A. KONDRATIEV, I.A. RYABTSEV, I.L. BOGAJCHUK and **D.P. NOVIKOVA**
E.O. Paton Electric Welding Institute, NASU, Kiev, Ukraine

Studied was structure of the deposited metal of the type of graphitised hypereutectoid steels and influence on the graphitisation process by different cladding techniques. It was established that tempering at 400 °C with holding for 2 h and delayed cooling with the furnace should be applied immediately after cladding for graphitisation of the deposited metal containing not less than 1.5 wt.% C and 1.1 wt.% S. Modification of the deposited metal by aluminium and calcium allows activation of the graphitisation process.

Keywords: arc cladding, cladding consumables, flux-cored wires, structure of deposited metal, graphitised steels

Graphitised iron-carbon alloys, i.e. alloys with free graphite inclusions of different shapes contained in their structure, include not only cast irons, but also hypereutectoid steels containing 1.3–2.0 % C [1]. Application of such steels is one of the methods providing substantial improvement in tribotechnical characteristics of the components of friction pairs, graphite inclusions in the steels acting as solid lubrication.

Traditionally, graphitised steel is produced by a method similar to that employed to produce malleable cast iron, by using high-temperature annealing to form graphite inclusions in the steel structure as a result of decomposition of cementite formed in solidification of the steel. To increase competitiveness of such steels, it holds promise to develop the technologies providing formation of graphite inclusions and prevention of formation of structurally free cementite directly during the solidification process without the use of high-temperature annealing. Utilisation of modifiers combined with optimisation of chemical composition of the steel can be one of the ways of solving this problem [2].

These studies were aimed at the development of such electrode materials and cladding technology, which could provide metal of the type of graphitised steel with free graphite inclusions directly during the cladding process in a cladding thermal cycle using certain techniques (preheating, tempering and delayed cooling after cladding) and modifying additions.

At the first stage, investigations were conducted to study deposited metal with a composition close to that of commercial grades of graphitised steel. Flux-cored wires of different compositions were manufactured for this purpose. They were used to perform multilayer submerged-arc cladding of specimens under a layer of flux AN-26. Chemical composition of the deposited metal and its hardness are given in the Table.

Chemical composition of deposited metal

Experimental flux-cored wire	Chemical composition, wt.%			*HV*	
	Ñ	Si	Mn	After cladding	After annealing*
PP-Op-1	0.94	1.00	1.27	45	25
PP-Op-2	0.95	1.40	0.50	40	26
PP-Op-3	1.40	0.86	1.19	47	30
PP-Op-4	1.50	1.15	0.60	43	26
PP-Op-5	1.60	2.00	0.55	43	20
PP-Op-6	1.80	1.46	0.58	49	20

*Graphitising annealing at 680 °C for 6 h.

It was established that immediately after cladding the finely dispersed graphite inclusions were contained in the metal deposited with experimental wire PP-Op-5 and containing 1.6 wt. C and 2.0 wt.% Si. Structure of this metal consisted of martensite (microhardness *HV*0.05 412–441), troostite (*HV*0.05 362–383), and cementite precipitates with the graphite formed inside them (Figure 1).

It turned out that after annealing at 680 °C, holding for 6 h and cooling with the furnace (the most extensively used method for annealing graphitised steels), graphite inclusions were found in metal of two more types, deposited with flux-cored wires PP-Op-4 and PP-Op-6. Therefore, the effect of graphitisation of the deposited metal takes place only at the carbon and silicon contents of the metal equal to not less than 1.50 and 1.15 wt.%, respectively, and to a still higher degree ---- with increase in the weight content of these elements. Structure of the metal deposited with wires PP-Op-4 and PP-Op-6 in the as-deposited state consisted of bainite-martensite mixture and troostite (Figure 2, *a*, *c*), and structure of the same metal after annealing consisted of temper sorbite, the hardness of which grew with increase in the carbon content (hardness *HV*0.05 185 and 303, respectively), and graphite inclusions (Figure 2, *b*, *d*).

Because the metal deposited with wires PP-Op-5 and PP-Op-6 exhibited increased sensitivity to formation of solidification cracks, which was caused by the increased carbon and silicon contents, metal 150SG deposited with flux-cored wire PP-Op-4 was chosen for further investigations. This wire turned out to be most efficient, as it provided good formation of the deposited metal and good detachability of the slag crust.

Experiments were conducted to determine the effect of cladding parameters, as well as auxiliary technological operations (preheating, tempering and delayed cooling after cladding), on the processes of graphitisation of deposited metal 150SG.

The effect of submerged-arc cladding parameters using flux-cored wire PP-Op-4 on structure of the as-deposited metal and the deposited metal after annealing was investigated. Cladding was performed under conditions that provided current density of 55 and 100 A / mm^2. It was found that the cladding parameters had no substantial effect on the graphitisation processes. However, increase in the current density led to coarsening of structure of the deposited metal.

As reported in technical literature, graphite precipitates in cast graphitised steels may form not only as a result of special graphitising annealing, but also as a result of partial graphitisation in slow cooling of castings [3].

It is a known fact that cladding of the majority of parts is performed with preheating and tempering or delayed cooling after cladding in the furnaces or thermostats. A clad part is held in the furnace for some time at a certain temperature, and then it slowly cools down, whereas the thermostats provide slow cooling without holding at a certain temperature [4]. Therefore, the graphitisation process can be combined with the auxiliary cladding operations.

Two tempering temperatures were chosen for investigations ---- 400 and 500 °C. The specimens were held at these temperatures for 2, 4 or 6 h, and then cooled with the furnace. Graphite inclusions in the deposited metal appeared as early as in holding for 2 h, their volume content and size insignificantly changing with further increase in the holding time and temperature. Structure of the deposited metal consisted of sorbite (hardness *HV*0.05 341–362), cementite (*HV*0.05 700–705) located along the grain boundaries, and graphite inclusions formed inside cementite (Figure 3).

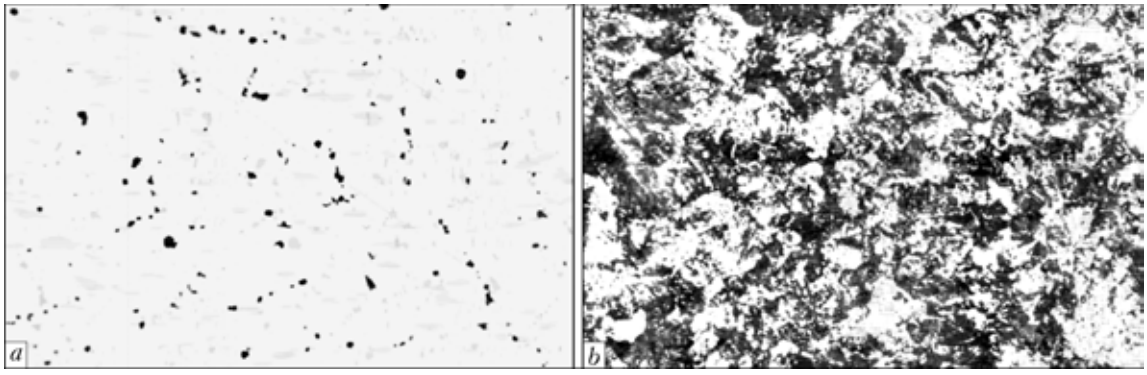

Figure 1. Microstructure of metal with 1.6 wt.% C and 2.0 wt.% Si immediately after cladding without (*a*) and with etching in nitric acid (*b*) (×400)

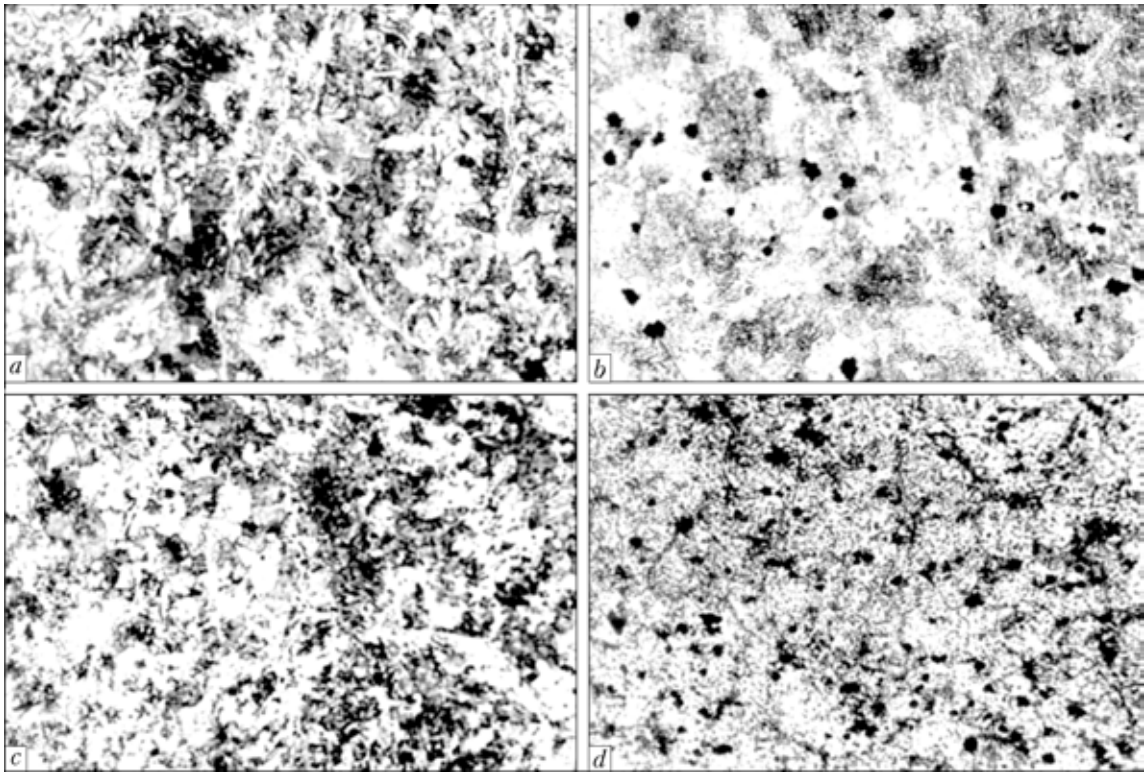

Figure 2. Microstructure of metal with 1.50 wt.% C and 1.15 wt.% Si (*a*, *b*), and 1.80 wt.% C and 1.46 wt.% Si (*c*, *d*) after cladding (*a*, *c*) and annealing at 680 °C for 2 h (*b*, *d*) with etching in nitric acid (×400)

Therefore, it was established that tempering after cladding at 400 °C for 2 h and subsequent slow cooling provided graphitisation of the deposited metal of the type of hypereutectoid steel 150SG.

As noted above, formation of graphite inclusions in structure of hypereutectoid steels during solidification can also be achieved due to modification. Aluminium and calcium are widely applied for this purpose [3, 5–8]. By combining nitrogen and sulphur to form stable chemical compounds, these modifying elements do not only facilitate nucleation of graphite, but also create favourable conditions for acceleration of diffusion of carbon. The effect of modifying additions on the process of graphitisation of steel and cast iron can also be explained by decrease in stability of cementite, formation of dispersed non-metallic inclusions, and increase of the content of carbon in austenite or ferrite due to decrease in its solubility in solid solution [3]. The effect of aluminium on the process of graphitisation of hypereutectoid steel shows up even at its content of 0.1 wt.%, the volume content and size of the graphite inclusions growing with increase in the aluminium content. The content of calcium in graphitised steel may amount to 0.05 wt.% [9].

Modifiers in the form of powders of aluminium and silicocalcium of the SK30 grade were added to charge of the experimental flux-cored wires in an amount not in excess of 4 % of mass of a flux-cored wire. Chemical composition of the resulting deposited metal was as follows, wt.%: 1.5 C, 1.4 Si, 0.5 Mn. The total content of aluminium and calcium was 0.21 wt.%. Hardness of the as-deposited metal was *HRC* 42–43, and that after tempering at 400 °C for 2 h was *HRC* 38–39.

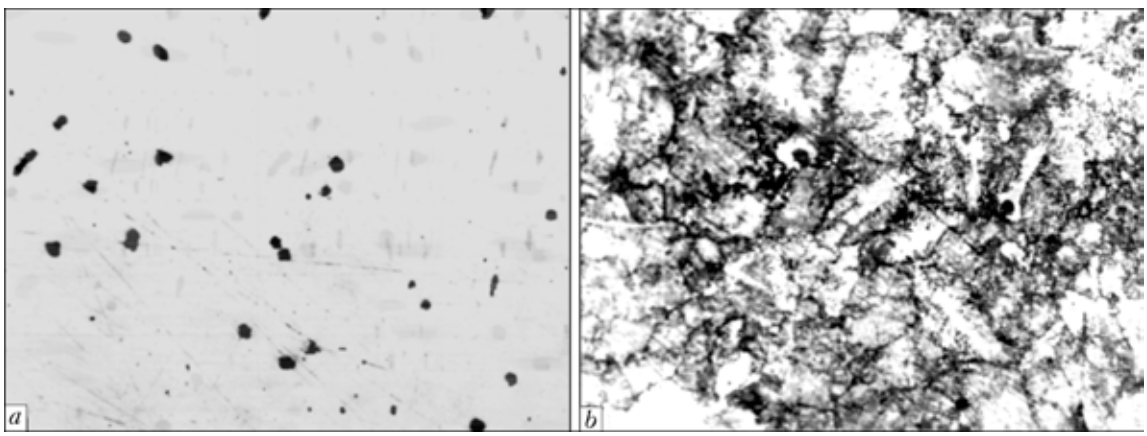

Figure 3. Microstructure of metal with 1.50 wt.% C and 1.15 wt.% Si after tempering at 400 °C for 2 h without (*a*) and with etching in nitric acid (*b*) (×400)

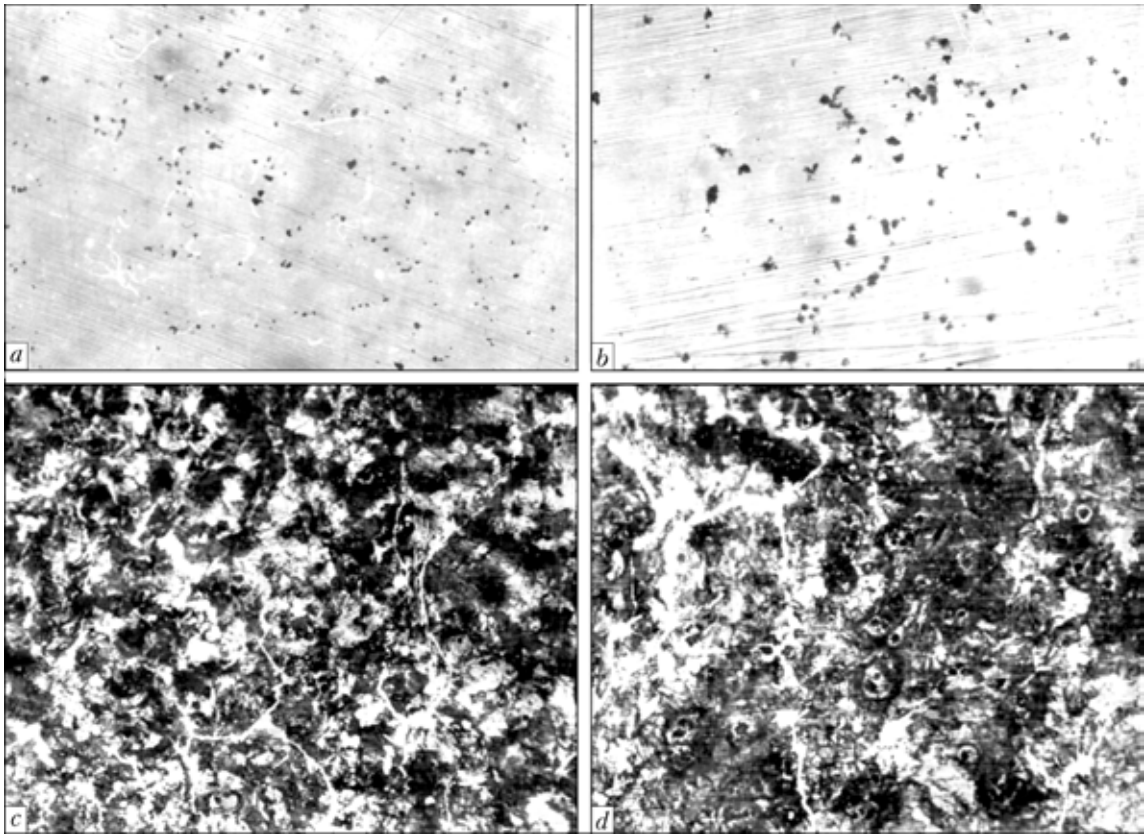

Figure 4. Microstructure of metal with 1.50 wt.% C and 1.15 wt.% Si, modified by aluminium and calcium immediately after cladding (*a*, *c*) and after tempering at 400 °C for 2 h (*b*, *d*): *a*, *b* — without etching; *c*, *d* — etching in nitric acid (×400)

With modification of the deposited metal by aluminium and calcium in the initial state, graphite precipitates detected on the section surface were mostly of a globular shape (Figure 4, *a*). The volume content of the graphite inclusions amounted to 0.7 %. After tempering at 400 °C for 2 h, the deposited metal of this type contained also the flaky graphite inclusions, in addition to the globular ones (Figure 4, *b*), their volume content growing to 1.28 %. Structure of the metal consisted of troostite (*HV*0.05 349–386) with thin cementite precipitates along the grain boundaries and small pearlite islands (*HV*0.05 286–290) (Figure 4, *c*). After tempering, structure of the deposited metal consisted of troostite (*HV*0.05 321–325), pearlite (*HV*0.05 281–286) and small cementite precipitates (Figure 4, *d*). Graphite inclusions were found in all structural components.

CONCLUSIONS

1. Graphite inclusions are formed in deposited metal of the type of hypereutectoid steel containing not less than 1.6 % C and 2.0 % Si after submerged-arc cladding using flux-cored wires.

2. For graphitisation of deposited metal containing not less than 1.5 wt.% C and 1.1 wt.% Si, it is recommended to use the following heat treatment instead of high-temperature annealing: immediately after cladding a part should be placed into a furnace at 400 °C, and after holding for 2 h it should be subjected to slow cooling. Modification of the deposited metal by aluminium and calcium allows activation of the graphitisation process.

1. Todorov, R.P., Nikolov, M.P. (1976) *Structure and properties of cast products of graphitized steel*. Moscow: Metallurgiya.
2. Bublikov, V.P. (2002) Modified hypereutectoid steel with globular graphite. *Protsessy Litia*, **2**, 22–27.
3. Bunin, K.P., Baranov, A.A., Pogrebnoj, E.N. (1961) *Graphitisation of steel*. Kiev: AN Ukr. SSR.
4. Ryabtsev, I.A., Kondratiev, I.A. (1999) *Mechanised arc cladding of metallurgical equipment parts*. Kiev: Ekotekhnologiya.
5. Bublikov, V.B., Kozak, D.S., Zelyonaya, L.A. et al. (2003) Influence of modification by ferrosilicium, silicobarium and silicocalcium on structure formation of cast graphitised steel. *Protsessy Litia*, **4**, 29–35.
6. Todorov, R.P. (1981) *Graphitized iron-carbon alloys*. Moscow: Metallurgiya.
7. Chernovol, A.V., Gerashchenko, N.Ya. (1998) About graphitising modification of magnesium cast iron. *Metally i Litio Ukrainy*, **3 / 4**, 24–28.
8. Kimstach, G.M. (1992) About modification of low-silicon graphitised Fe–C alloys. *Litejnoe Proizvodstvo*, **8**, 5.
9. Sitnik, N.M., Nesvit, P.M., Gartsunov, Yu.F. et al. (1973) Production of cart iron with globular graphite in deposited metal. *Ibid.*, **7**, 20–21.

EFFECT OF ZIRCONIA ON PROPERTIES OF SLAG IN FLUX-CORED WIRE SUBMERGED-ARC SURFACING USING FLUX AN-348A

V.E. SOKOLSKY[1], A.S. ROIK[1], V.P. KAZIMIROV[1], I.I. RYABTSEV[2], D.D. MISHCHENKO[2], I.A. RYABTSEV[2], A.S. KOTELCHUK[2] and V.S. TOKAREV[2]

[1]Taras Shevchenko Kiev National University, Kiev, Ukraine

[2]E.O. Paton Electric Welding Institute, NASU, Kiev, Ukraine

Effect of zirconia on slag properties in submerged-arc surfacing using low-alloy flux-cored wire PP-Np-20KhGS and flux AN-348A was investigated. It is established that, when depositing the first layers, zirconia is contained in the surface layer of the slag crust adjacent to the deposited metal in the form of individual inclusions of predominantly monoclinic shape. Formation of zirconia induces substantial microstresses in the slag crust and leads to its cracking, thus preventing chemical bonding of the crust and deposited metal through an interlayer of oxides and improving detachability of the slag crust.

Keywords: arc surfacing, submerged-arc surfacing, flux-cored wire, zirconia, detachability of slag crust, X-ray examinations

Submerged-arc surfacing with preheating, or surfacing in several layers over large areas, leads to increase of up to 400 °C or more in temperature of a workpiece, which makes removal of the slag crust much more difficult and decreases the quality and productivity of the surfacing process [1].

Numerous experimental data relating poor detachability of the slag crust to chemical bonding of the slag and deposited metal through an oxide interlayer present on its surface have been accumulated up to now [2–5]. Detachability of the slag crust can be improved by changing the oxidation potential of the slag in such a way that the formation of the oxide interlayer is avoided or its epitaxial coalescence with the weld surface is eliminated [4]. Detachability of the slag crust also depends upon the temperature of solidification of the slag [6] and difference in thermal expansion coefficients (TEC) between the slag crust and deposited metal [7].

It is a known fact that ZrO_2 has a strong effect on the oxidation potential and physical-chemical properties of the slag [8, 9]. As shown by experiments, adding zirconium concentrate $ZrSiO_4$ to the flux-cored wire charge improves detachability of the slag crust in submerged-arc surfacing using flux AN-348A [10].

This study is dedicated to investigation of the effect of zirconia on oxidising ability, solidification temperature and TEC of the slag. In addition, it gives results of X-ray examinations of the slag crust in submerged-arc surfacing using low-alloy flux-cored wires PP-Np-20KhGS and flux AN-348A. The examinations were carried out to reveal causes of the positive effect of zirconia on detachability of the slag crust of the above flux.

Six experimental flux-cored wires of the PP-Np-20KhGS type, which provided different ZrO_2 contents of the slag (Table), were made for the examinations. Experimental flux-cored wires 2 mm in diameter were used for continuous multilayer deposition of individual beads 150–180 mm long on plates measuring 20×50×200 mm. Parameters of deposition of all the layers were kept constant: current 230–250 A, voltage 24–26 V, and surfacing speed 20 m / h. When using wires 1–4, detachability of the slag crust deteriorated in deposition of the third and fourth layers. Wires 5 and 6 provided excellent detachability of the slag crust in deposition of the fifth layer. However, it decreased with overheating of a specimen.

The effect of zirconia on reactivity of oxygen in the slag, i.e. oxidising ability of the slag (Figure 1), viscosity (Figure 2) and TEC of deposited metal 20KhGS and slag crusts (Figure 3) was investigated.

Reactivity of oxygen in slags was measured by the procedure [11] based on the method of measuring EMF of the slag melt using oxygen sensor with solid yttrium-stabilised zirconia electrolyte.

Viscosity of the slag melts was determined with the rotary viscosimeter developed by the E.O. Paton

Results of chemical analysis of slag crust and metal deposited by using flux AN-348A and experimental wires of the PP-Np-20KhGS type containing zirconia in their charge

No.	Experimental flux-cored wire	ZrO_2 content of slag crust, wt.%	Content of chemical elements in deposited metal, wt.%				
			C	Si	Mn	Cr	Zr
1	PP-Op-1	–	0.09	0.32	1.15	0.56	–
2	PP-Op-2	0.21	0.14	0.33	1.20	0.60	0.03
3	PP-Op-3	0.63	0.11	0.29	1.18	0.69	0.02
4	PP-Op-4	0.90	0.10	0.33	1.20	0.68	0.03
5	PP-Op-5	1.62	0.12	0.25	1.19	0.46	0.03
6	PP-Op-6	3.63	0.13	0.40	1.25	0.59	0.04

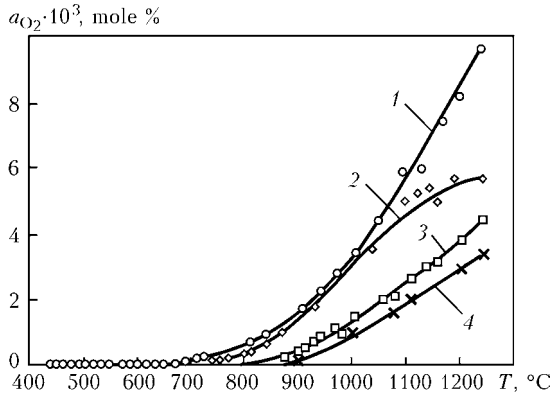

Figure 1. Reactivity of oxygen in slag AN-348A with different ZrO_2 contents: *1* — 3.63; *2* — 1.62; *3* — 0.90 wt.%; *4* — without ZrO_2

Electric Welding Institute [12]. The method is based on the relationship between viscosity of a fluid and moment of torsion of a working medium suspended in it, with uniform rotation of the crucible with the fluid or the medium proper.

The values of TEC of an intact slag crust as removed from the deposited bead and deposited metal 20KhGS was found by using thermomechanical analyser Du Pont 943.

As seen from Figure 1, ZrO_2 increases reactivity of oxygen in the slag and, therefore, its oxidising ability. This effect shows up to the maximal degree at a more than 1.6 wt.% content of ZrO_2 in the slag, the reactivity of oxygen increases in this case 1.5–2 times.

Measuring viscosity of the slags (Figure 2) shows that the viscosity of the slag and its solidification temperature grow at a ZrO_2 content as low as 0.90 wt.%. The viscosity values tend to growth with an increase of up to 3.63 wt.% in the ZrO_2 content of the slag.

Investigations of variations in the TEC values of deposited metal 20KhGS and slag crusts of flux AN-348A at a different ZrO_2 content show that with increase in the weight content of ZrO_2 in the slag the difference in TEC between the deposited metal and slag crust grows and remains so almost over the entire

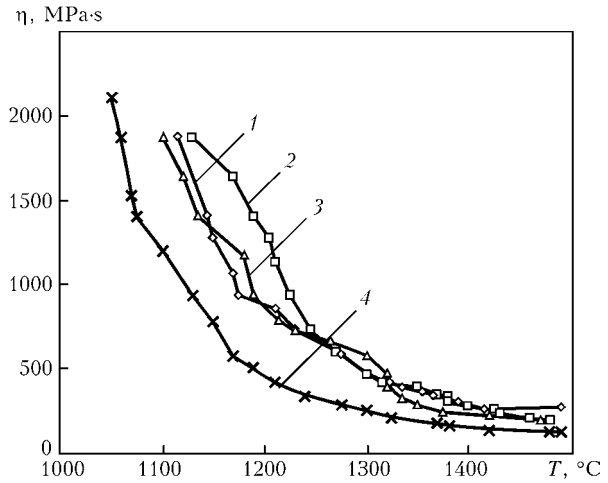

Figure 2. Viscosity η of slag AN-348A with different ZrO_2 contents: *1* — 0.90; *2* — 1.62; *3* — 3.63 wt.%; *4* — without ZrO_2

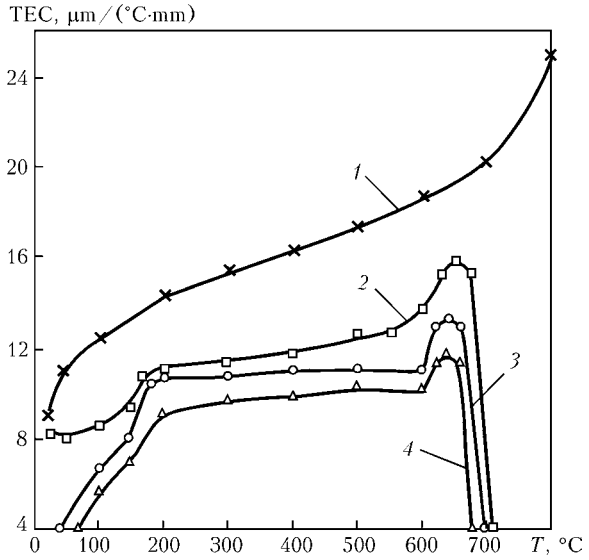

Figure 3. TEC of deposited metal 20KhGS (*1*) and slag crusts of flux AN-348A (*2*), as well as of flux with an addition of 0.90 (*3*) and 3.63 % (*4*) ZrO_2

temperature range, up to a slag softening temperature (Figure 3).

X-ray examinations were conducted to study the charge of one of the experimental wires PP-Np-20KhGS (wire 5, Table), flux AN-348A and material of the surface layer of its slag crusts on the side of the deposited metal after surfacing using this wire. The experimental data were checked using software «PowderCell» (PCW), which is disseminated free of charge in the Internet [13, 14].

The X-ray pattern of a mineral component of the charge of experimental wire PP-Np-20KhGS, containing zirconium concentrate, is in full agreement with the X-ray pattern of a pure zirconium concentrate, which is identified as $ZrSiO_4$, i.e. no transformations take place in it during the wire manufacturing process (Figure 4).

Material for X-ray examinations of the surface layer of the slag crust was scraped off using a special diamond tool. X-ray patterns of the specimens taken from deeper layers of the crust show decrease in intensity I of the diffraction maxima with increase in thickness of the slag crust. The intensity of the diffraction lines is but slightly different from the background in a region of half-thickness of the crust. Weak crystalline peaks in a range of 20–25° of X-ray scattering angle 2θ were seen both in the first and second curves with almost identical intensity.

Investigations of material of the surface layer of the slag crust of flux AN-348A (CuK_α-radiation in air at room temperature) after deposition of the first layer with good detachability of the slag crust and deposition of the fifth layer with decreased detachability of the slag crust showed the intensive crystalline peaks present in the X-ray pattern in the first case (Figure 5, curve *3*), and crystalline peaks hardly differing from the background in the second case (Figure 5, curve *2*). No crystalline peaks were seen in the X-ray pattern of flux AN-348A (Figure 5, curve *1*).

Specimen of the slag crust after deposition of the first layer contains crystalline phases that do not correspond to the probable components of flux AN-348A and their combinations. They are identified as a mixture of monoclinic, tetragonal and orthorhombic zirconium dioxides (Figure 5, curve *3*). No cubic ZrO_2 with lattice of the CaF_2 type was revealed. Therefore, in one-layer surfacing zirconia does not combine with any compound to form other components of slag AN-348A, and is contained in the slag crust in the form of individual inclusions of three different modifications.

Specimen of the slag crust after deposition of the fifth layer (Figure 5, curve *2*) contains no crystalline inclusions of zirconia. This is indicative of the absence of its free inclusions.

According to the constitutional diagram, one compound, i.e. zircon $ZrSiO_4$, is present in the ZrO_2–SiO_2 system. As reposted in early studies, its melting temperature is not less than 2700 K. However, the later experiments showed that zircon decomposes in solid phase at 1949 K, and that the assumption that it melts to form two types of the melts is unjustified [15].

Results of our investigations show that $ZrSiO_4$ decomposes during welding (surfacing) into zirconium and silicon dioxides:

$$Zr_2SiO_4 \underset{1976\ K}{\rightarrow} ZrO_2\ (tetr.) + SiO_2. \qquad (1)$$

This is proved by the presence of $ZrSiO_4$ in the non-magnetic component of the welding wire before the surfacing process (Figure 4, curve *2*), and by its full absence in the surface layer after surfacing (Figure 5). As only various modifications of ZrO_2 can be identified in the zircon decomposition products, it can be assumed that silica partially melted and dissolved in the molten slag, and ZrO_2 did not dissolve and, probably, did not even melt in the slag melt. Weak crystalline peaks in a range of 20–25° of 2θ, which can be related with a certain degree of caution to the amorphous silica phase at the initial stage of solidification, indicate to a probability of only partial dissolution of SiO_2. An indirect proof of dissolution of SiO_2 is the fact that at $T > 800$ K

$$K_f > K_d, \qquad (2)$$

where K_f and K_d are the constants of formation and decomposition of zircon, respectively.

Therefore, the constant of synthesis of zircon is higher than the rate of its decomposition. However, a detailed study of conditions of thermal decomposition showed that it takes place only with removal of silica from the reaction sphere [15], in this case in its dissolution in the slag melt.

Crystalline ZrO_2 in its pure form is present under normal pressure over the entire temperature range in three modifications: monoclinic (low-temperature), tetragonal and cubic (stable at high temperatures). Zirconia has a monoclinic lattice at a temperature of approximately up to 1273 K. Density of monoclinic

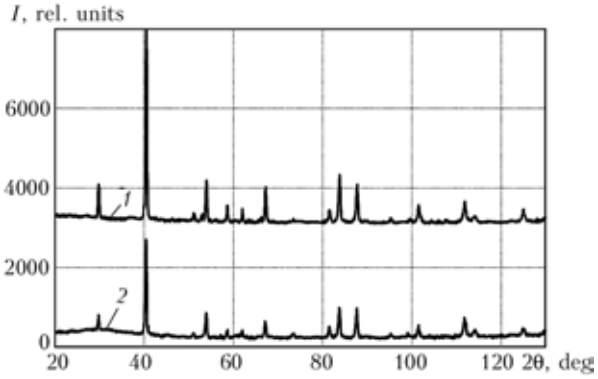

Figure 4. X-ray patterns of zirconium concentrate (*1*) and mineral component of charge of experimental wire PP-Op-2 (*2*) obtained in CuK_α-radiation

ZrO_2 is 5.68 g / cm^3. In heating to above 1273 K, monoclinic zirconia starts transforming in a diffusion-free manner (martensitic type) into the tetragonal one, and the transformation ends at a temperature of about 1450 K. The tetragonal modification exists to a temperature of 2645 K, after which it transforms into the face-centred cubic modification. Melting of cubic ZrO_2 occurs at 2673 K [15]. Orthorhombic zirconia forms under a higher pressure and at high temperature [15].

Hysteresis of transformation of ZrO_2 takes place in the case of cooling. The monoclinic form appears at 1240 K, and the tetragonal one disappears at 1023 K. The range of transformation of ZrO_2 decreases with increase in its purity [15]. The transformation of monoclinic (stable) ZrO_2 into the tetragonal modification and vice versa is accompanied by a 7 % change in volume of ZrO_2, this leading to cracking of the ZrO_2 material. A bigger change in volume is observed in transformation of the orthorhombic modification into the monoclinic one. To prevent cracking, ZrO_2 is stabilised at a temperature from 1973 K to the melting point by adding oxides CaO, MgO and V_2O_3. And although CaO and MgO are components of welding flux AN-348A, saturation of ZrO_2 with stabilising additions due to the flux is unlikely, as it requires portioned supply of additions and a long time of annealing, which is impossible to achieve during the welding process.

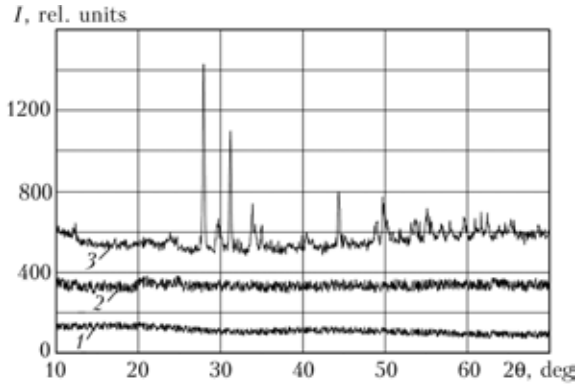

Figure 5. X-ray patterns (CuK_α-radiation) of flux AN-348A (*1*) and slag produced by surfacing using this flux with poor (*2*) and good (*3*) detachability of the slag crust

To check X-ray patterns of the slag resulting from submerged-arc surfacing using flux-cored wire PP-Np-20KhGS and flux AN-348A (Figure 5, curve *3*), the background was first subtracted from the experimental curves using software PCW, and then the profile of the experimental X-ray pattern was specified using the sum of theoretical curves calculated for the expected modifications of ZrO_2 (Rietveld method) [13, 14]. The calculated curves plotted with allowance for the volume content of each modification of ZrO_2 are shown in Figure 6. Parameters of an elementary cell and volume content of crystalline phases in a specimen were used as the main values to be checked. It was established that the crystalline phase consisted mostly (88.1 vol.%) of monoclinic zirconium dioxide with cell parameters a = 5.18 (5.17) Å, b = 5.24 (5.23) Å, c = 5.341 (5.360) Å, β = 99.18 (99.25)°, cell volume ---- 142.6 (143.1) Å^3, and X-ray density ---- 5.74 (5.72) g / cm^3 (here and below the values given in brackets are parameters of the elementary cell of the initial phase before checking using software PCW). Tetragonal ZrO_2 (9.27 vol.%) has the following lattice parameters: a ---- 3.63 (3.63) Å, c ---- 5.19 (5.20) Å, cell volume ---- 68.4 (68.4) Å^3 and X-ray density ---- 5.99 (5.99) g / cm^3. Orthorhombic ZrO_2 (2.66 vol.%) has the following lattice parameters: a ---- 5.64 (5.59) Å, b ---- 6.43 (6.48) Å, c = 3.33 (3.33) Å, cell volume ---- 120.9 (120.8) Å^3, and X-ray density ---- 6.77 (6.77) g / cm^3.

As seen from the above data, because of the high rate of the welding process, transition of the tetragonal form into the monoclinic one is not completed, and crystalline ZrO_2 is concentrated at the metal–slag interface in the form of the monoclinic phase (basic), as well as small amounts of the tetragonal and, probably, orthorhombic phases. At first sight, the presence of the orthorhombic phase, which can be produced only at a high temperature and pressure, is unlikely. However, fine inclusions of crystalline ZrO_2 in matrix

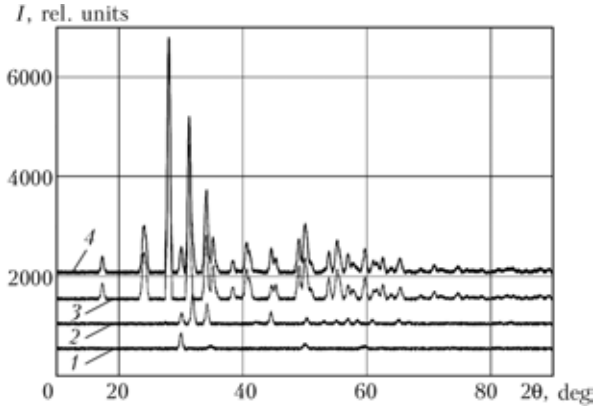

Figure 6. Theoretical X-ray patterns of different modifications of ZrO_2 allowing for their volume content: *1* — orthorhombic zirconium dioxide; *2* — tetragonal zirconium dioxide; *3* — monoclinic zirconium dioxide; *4* — general X-ray pattern of specimen with good slag crust detachability, checked by PCW (Figure 5, curve *3*) and produced by additive summation of X-ray patterns *1–3*

of the basic phase of the slag crust may experience substantial compressive forces, which are higher than a pressure of $40 \cdot 10^3$ MPa, at which the orthorhombic phase is formed. A limited volume of the already solidified slag cavity, where a spot-like inclusion of the tetragonal phase of ZrO_2 was located, prevents formation of a lower-density monoclinic phase, thus increasing the probability of formation of a small volume content of the orthorhombic phase, which is densest among all the crystalline modifications of ZrO_2.

Therefore, according to the constitutional diagram, after decomposition of zirconium concentrate at a sufficiently high temperature, the following phase transformations with participation of ZrO_2 may take place within the arc zone:
in heating

$$ZrO_2\ (\text{tetr.}) \underset{2645\ \text{K}}{\rightarrow} ZrO_2\ (\text{cub.}) \underset{2973\ \text{K}}{\rightarrow} \underset{2973\ \text{K}}{\rightarrow} ZrO_2\ (\text{melt.}); \quad (3)$$

in cooling

$$ZrO_2\ (\text{melt.}) \underset{2973\ \text{K}}{\rightarrow} ZrO_2\ (\text{cub.}) \underset{2645\ \text{K}}{\rightarrow} \underset{2645\ \text{K}}{\rightarrow} ZrO_2\ (\text{tetr.}) \underset{1240–2645\text{K}}{\rightarrow} ZrO_2\ (\text{monocl.}). \quad (4)$$

The molten droplet together with mineral additions passes through the highest-temperature arc zone within fractions of a second. Even if the temperature of the arc is much higher than 2973 K, each phase transition should be accompanied by structural transformations and energy expenditures, which require a certain time for re-dislocation of atoms in formation of a new crystalline phase or long-range fracture in melting, i.e. complete realisation of several phase transitions take place, including melting, solidification and a few stages of re-crystallisation, which is unlikely during such a relatively short period of time.

Time limitation in passage of the molten droplet of wire through the arc zone prevents formation of cubic ZrO_2 and melting of ZrO_2. It is probable that ZrO_2 is overheated in this case to a temperature above the point of formation of zircon (1976 K) by ΔT, but restructuring has no time to occur, i.e. no phase transitions occur during the heating process

$$ZrO_2\ (\text{tetr.}) \underset{\Delta T}{\rightarrow} ZrO_2\ (\text{tetr.}), \quad (5)$$

then follows the cooling cycle

$$ZrO_2\ (\text{tetr.}) \underset{1240–2973\ \text{K}}{\rightarrow} ZrO_2\ (\text{monocl.}). \quad (6)$$

When the droplet gets into the zone of contact with the molten pool metal, zirconium dioxide turns out to be on the pool surface and enter into contact with the molten slag. This leads to the fact that the ZrO_2 content within the metal–slag contact zone is higher than in a total volume of the molten slag. Spot-type inclusions of zirconium dioxide are formed

because of a relatively small volume content of the slag phase in the matrix. In the case of cooling at a temperature of 1240–1023 K (when the slag has already solidified), the tetragonal form of ZrO_2 transforms mostly into the monoclinic form, which is stable at a low temperature, and has the maximal density and maximal volume among all other modifications of ZrO_2. Increase of its volume in phase transition (6) leads to substantial microstresses inside the slag crust, especially at the slag–metal interface, as the content of zirconium dioxide is maximal in this region. As a result, the slag crust cracks at the slag–metal interface, which leads to improvement in its detachability.

In multilayer surfacing without interruptions for cooling of a workpiece, the base metal becomes heavily overheated. This causes increase in the time of dwelling of the slag at a high temperature, and slag components interact with each other more intensively and for a longer time. In this case, ZrO_2 does not precipitate in the slag crust in the form of individual inclusions, but forms complex oxide systems with other components of the slag, having different types of chemical bonds and different physical transformations, thus leading to volumetric changes during cooling. Therefore, at a substantial increase in temperature of a workpiece, the positive effect of ZrO_2 on detachability of the slag crust of flux AN-348A diminishes.

CONCLUSIONS

1. Addition of ZrO_2 to charge of an experimental wire of the 20KhGS type leads to increase in the oxidising ability of the slag, difference in TEC between the deposited metal and slag crust, as well as temperature of solidification of the latter during submerged-arc surfacing using this wire and flux AN-348A.

2. It was established by X-ray examinations of the slag crust of flux AN-348A that zircon contained in the flux-cored wire charge during surfacing decomposes into dioxides by reaction $ZrSiO_4 \rightarrow ZrO_2 + SiO_2$. In deposition of the first layers, in the case of a relatively low temperature of a workpiece, ZrO_2 is contained in the surface layer of the slag crust adjacent to the deposited metal in the form of individual inclusions primarily of the monoclinic shape. In multilayer surfacing with interruptions for cooling, zirconium dioxide melts and forms complex oxide systems with other components of the slag.

3. Formation of ZrO_2 of the monoclinic form, having a maximal volume, induces substantial microstresses in the slag crust and its cracking. Moreover, difference in TEC between the slag crust and deposited metal grows with increase in the content of ZrO_2. All this improves detachability of the slag crust of flux AN-348A with increase of its ZrO_2 content. In continuous multilayer surfacing, no free inclusions of ZrO_2 are formed, and the positive effect of ZrO_2 on detachability of the slag crust of flux AN-348A diminishes.

1. Frumin, I.I. (1961) *Automatic arc surfacing*. Kharkov: Metallurgizdat.
2. Podgaetsky, V.V. (1952) *Some peculiarities of metallurgical processes in submerged-arc welding of steel*: Syn. of Thesis for Cand. of Techn. Sci. Degree. Kiev.
3. Pokhodnya, I.K., Yavdoshchin, I.R., Karmanov, V.I. et al. (1974) Mechanism of cohesion between slag crust and weld surface. *Avtomatich. Svarka*, **5**, 5–9.
4. Pokhodnya, I.K., Karmanov, V.I., Vojtkevich, V.G. (1976) Investigation of peculiarities of cohesion mechanism between slag crust and weld metal alloyed with titanium and vanadium. *Ibid*., **6**, 1–4.
5. Pokhodnya, I.K., Demchenko, L.I., Yavdoshchin, I.P. et al. (1977) Kinetics of formation of intermediate layer between weld metal and slag crust. *Ibid*., **2**, 1–4.
6. Podgaetsky, V.V., Kuzmenko, V.G. (1988) *Welding slags*. Kiev: Naukova Dumka.
7. Volobuev, O.S., Potapov, N.N., Volobuev, Yu.S. et al. (1989) To the problem of influence of linear expansion coefficient on slag crust detachability. *Svarochn. Proizvodstvo*, **8**, 37–39.
8. Bobrikov, Yu.V., Potapov, N.N., Starchenko, E.G. (1983) Peculiarities of metal oxidation by zirconium dioxide in submerged-arc surfacing. *Ibid*., **9**, 6–7.
9. Potapov, N.N. (1985) *Oxidation of metals in fusion welding*. Moscow: Mashinostroenie.
10. Ryabtsev, I.I. (2005) Improvement of slag crust detachability at higher temperatures in flux-cored wire submerged-arc surfacing. In: *Proc. of Sci.-Techn. Conf. of Junior Scientists on Welding and Related Technologies* (Kiev, 25–27 May, 2005). Kiev: PWI, 59–60.
11. Bondarenko, T.P., Rimsky, S.T., Zalevsky, A.V. et al. (1991) Procedure of measurement of reactivity and pressure of oxygen in fluxes. In: *Welding consumables for mechanized arc welding of steels*. Kiev: PWI.
12. Kolisnyk, V.N., Shono, S.A., Saginov, I.A. *Rotational viscometer*. USSR author's cert. 667867. Int. Cl. G 01 11 / 14. Publ. 15.06.79.
13. Rietveld, H.M. (1969) A profile refinement method for nuclear and magnetic structures. *J. Appl. Cryst*., **2**, 65–71.
14. Kovba, L.M. (1991) *Radiography in inorganic chemistry*: Manual. Moscow: MGU.
15. Berezhnoj, A.S. (1970) *Multicomponent systems of oxides*. Kiev: Naukova Dumka.

NATURE OF FRACTURE OF WELDED JOINTS OF 10Kh13G18D + 09G2S STEELS AT VIBRATION LOADS

A.I. GEDROVICH[1], **A.N. TKACHENKO**[2], **S.N. TKACHENKO**[2] and **V.P. ELAGIN**[3]
[1]V. Dal East-Ukrainian University, Lugansk, Ukraine
[2]OJSC «HC Luganskteplovoz», Lugansk, Ukraine
[3]E.O. Paton Electric Welding Institute, NASU, Kiev, Ukraine

Peculiarities of fracture of welded joints between austenitic steel 10Kh13G18D and pearlitic steel 09G2S under vibration loads were investigated. The investigation results allowed identification of the mechanism of impact by technological factors in welding on service crack resistance of the above joints.

Keywords: arc welding, dissimilar joints, cracks, vibration loads, structural and mechanical inhomogeneity, fusion zone, α-phase precipitation, deformation ageing, welding technology

An important factor influencing the fatigue life, reliability and quality of diesel and electric trains (Figure 1) is ensuring the strength of bodies subjected to alternating loads and their atmospheric corrosion resistance. One of the promising directions for solving these problems in OJSC «HC «Luganskteplovoz» when manufacturing the body frame sheeting is application of austenitic steel of 10Kh13G18D type, featuring a high strength and corrosion resistance. This allows reducing the sheeting thickness to 1.5 mm, increasing the body strength and length, its seating capacity, reducing the painting costs in manufacturing and service [1]. However, during running trials of diesel and electric trains, cracks were found in welded joints of body sheeting of 10Kh13G18D steel with the main frame of pearlitic steel 09G2S, which lower the water-tightness of the frame and lead to development of corrosion in these sections (Figure 2).

It was noted earlier [2–4] that the welded joints of 10Kh13G18D steel with 09G2S steel are characterized by a developed structural, chemical and mechanical inhomogeneity in the fusion zone from the side of both austenitic and pearlitic steel. This results in lowering of the strength and ductility properties of welded joints with fracture running in the fusion zone from the side of austenitic 10Kh13G18D steel at testing of tensile samples. This is caused by formation of sections of α-phase there.

It is of interest to study the features of fracture of samples at alternating loading with parameters close to sheeting loads in carriage service. For this purpose mock-up samples (Figure 3) of the welded joint of the body sheeting with the underframe were made by welding sheets of 10Kh13G18D steel of 1.5 × 300 × × 300 mm size with 65 mm overlap, to tubes of 09G2S steel of a rectangular cross-section of 180 × 75 mm with 7 mm wall thickness and of 300 mm length. Mechanized gas-shielded arc welding with austenitic wire of Sv-08Kh20N9G7T grade of 1.2 mm diameter was performed by the technological variants given in the Table. Samples were tested in a special facility for vibration testing of railway carriage assemblies at the following parameters: oscillation frequency of 25 Hz, amplitude of displacement of the sheeting cantilever of 2.0–2.5 mm. Testing was followed by metallographic and durometric studies of the fracture zone and comparative evaluation of the structural and mechanical inhomogeneity of the metal. The structure was studied using «Neophot-32» microscope after electrolytic etching of microsections in 5 % H_2SO_4 solution. The quantity of the ferritic phase was determined using Ferritqehaltmesser 1.53″ ferritometer, micro-

Figure 1. Diesel train DEL-02

Figure 2. View of the carriage with weld defects developing during its service

Variants of technology and results of vibration testing

Variant #	Welding technology	Heat input, J / cm	Magnetic component, vol.%	Number of cycles to sample fracture·10^{-7}
1	Mechanized welding in CO_2	3350	2.5--5.0	0.95
2	Same + technological bead made by non-consumable electrode argon-arc welding along the line of metal fusion with 10Kh13G18D steel from the weld face	3350	0.7--7.0	>1.45 (no fracture)
3	Automatic consumable electrode pulsed argon-arc welding	1190	0.1--0.5	1.4
4	Automatic consumable electrode CO_2 «cold» welding (CMT-process)	1320	0.1--0.8	1.5

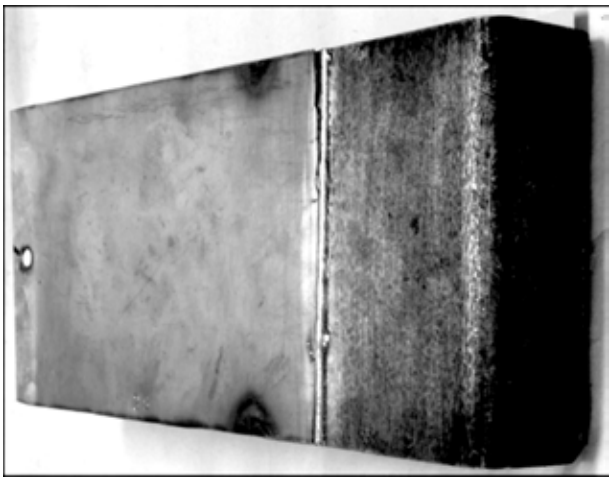

Figure 3. Tested mock-up sample of the joint of the side wall sheeting with the frame of the diesel train main frame

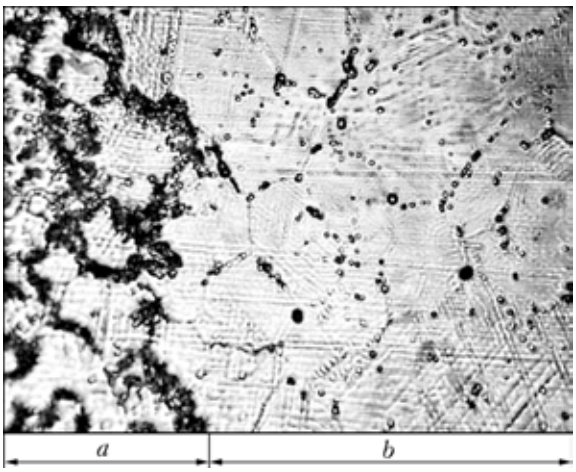

Figure 5. Microstructure of the zone of fusion (*a*) and austenitization (*b*) of the HAZ from the side of steel 10Kh13G18D of 09G2S + 10Kh13G18D welded joint (×320)

hardness was measured by PMT-3A instrument at 0.02 and 0.2 kg loads. Results of testing welded joints are given in the Table.

The smallest number of cycles to fracture is found for joints of welding variant #1 with a high heat input. Additional treatment of these joints by the welding arc in argon with a non-consumable electrode with technological bead deposition in the zone of weld fusion with 10Kh13G18D steel prevented sample fracture (variant #2). Improvement of fatigue strength of welded joints was further promoted by lowering of the heat input in welding by variants #3 and #4. Application of the technological bead in the fusion zone after welding (variant #2) promotes an increase of the quantity of α-phase, and heat input reduction promotes its lowering.

All the tested samples failed in the fusion zone or the HAZ from the side of 10Kh13G18D steel (Figure 4). The section, pertaining to the fusion zone (section *a* in Figure 5) is characterized by structural and mechanical inhomogeneity, which is manifested in precipitation of δ-ferrite in it and an abrupt lowering of hardness (Figure 6). Section *b* in Figure 5 has no δ-ferrite, it has less nonuniform hardness distribution, coarser grains and worse structure etchability compared to section *a* and base metal. Increased hardness and presence of slip bands oriented at dif-

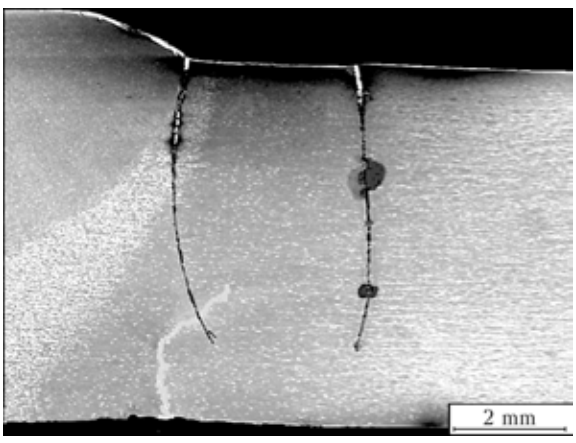

Figure 4. Macrosection of the welded joint with cracks after testing

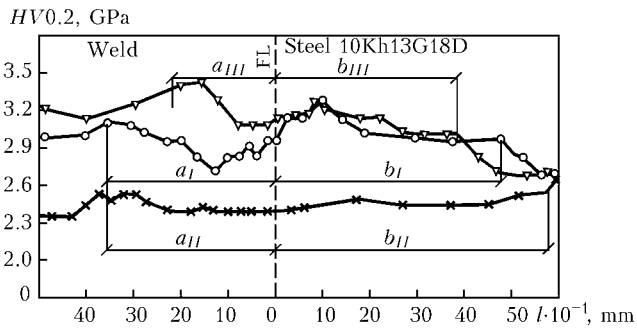

Figure 6. Hardness distribution in the section of weld–10Kh13G18D steel in 09G2S+10Kh13G18D welded joints made by different technologies (see the Table): *I* — variant 1; *II* — 2; *III* — 4; *a* — sections with precipitations of δ-ferrite; *b* — austenitization section

ferent angles within each grain are indicative of deformation localizing there and strain ageing of the metal. This is confirmed by microhardness lowering from 2700–3200 to 2300–2660 MPa at welded joint soaking, increase of the heat input, or repeated metal heating in these zones when making the technological bead. At heat input lowering the width of sections *a* and *b*, as well as softening of section *a*, become smaller. After technological bead deposition the hardness of sections *a* and *b* became much smaller (Figure 6). This promoted lowering of mechanical inhomogeneity, improvement of ductile properties of the metal and more uniform distribution of deformations in the welded joint.

Thus, improvement of fatigue strength of welded joints made at a lower welding heat input, is due to narrowing and softening of sections of structural inhomogeneity in the zone of fusion of the weld with steel 10Kh13G18D, and that of sections made with the technological bead is due to lowering of the degree of mechanical inhomogeneity, improvement of metal ductility in these sections and more uniform distribution of deformation.

In conclusion it should be noted that the most prone to cracking in dissimilar welded joints of body sheeting of austenitic steel 10Kh13G18D and underframe of carriage frame of pearlitic steel 09G2S of diesel and electric trains in their service are the zone of fusion of the weld with 10Kh13G18D steel and its HAZ.

The cause for cracking in the zone of fusion with the weld of 10Kh13G18D steel in welded joints with 09G2S steel at vibration loads is formation of the structural and mechanical inhomogeneity accompanied by softening and lowering of the metal ductile properties under the influence of the thermodeformational cycle of welding and localization of plastic deformation in it, and in the HAZ –– deformation strengthening and lowering of metal ductility in the coarse-grain zone.

Lowering of specific heat input in welding or deposition of a technological bead after welding from the side of the fusion zone of 10Kh13G18D steel promote an improvement of welded joint resistance to fracture at vibration loads.

1. Tkachenko, A.G., Gedrovich, A.I., Galtsov, I.A. (2002) Application of metastable corrosion-resistant steel 10Kh13G18DU as sheeting of electric and diesel trains. In: *Proc. of Int. Conf. on Welding and Related Technologies* (Kiev, 22–26 Apr., 2002). Kiev: PWI, 56–57.
2. Gedrovich, A.I., Galtsov, I.A., Zhidkov, A.B. et al. (2002) Welding of austenitic steel 10Kh13G18DU in production of diesel and electric trains on «HC Luganskteplovoz» enterprise. *Svarshchik*, 28(**6**), 10–11.
3. Gedrovich, A.I., Tkachenko, A.N., Tkachenko, S.A. et al. (2007) Peculiarities of structure and properties formation in 10Kh13G18D steel fusion zone. *The Paton Welding J.*, **4**, 20–24.
4. Gedrovich, A.T., Tkachenko, A.N., Tkachenko, S.A. (2006) Structure and properties of a joint of 10Kh13G18D + 09G2S steels. *Ibid.*, **12**, 37–39.

CHANGE OF MECHANICAL PROPERTIES OF WELDED JOINTS OF CARBON AND LOW-ALLOYED STEELS AT ELECTROMAGNETIC IMPACT

A.K. TSARYUK[1], **V.Yu. SKULSKY**[1], **S.I. MORAVETSKY**[1] and **V.A. SOKIRKO**[2]
[1]E.O. Paton Electric Welding Institute, NASU, Kiev, Ukraine
[2]SPC «DS Ltd.», Nikolaev, Ukraine

The paper deals with published results of investigations of the impact of high density electric current pulses on impact toughness of St3 steel. It is noted that the electromagnetic impact mechanism suggested by the authors can only be manifested in a narrow layer near the metal sample surface. Results of experimental investigations are given, which demonstrate that passing electric current of a comparatively low density through the metal of steel welded joints also leads to a marked change of its impact toughness.

Keywords: steel, welded joints, heat treatment, electromagnetic impact, electrophysical treatment, deformation, mechanical properties

The interest to application of energy of the electromagnetic field and electric current to make an impact on micro- and submicrostructure of structural alloys and their welded joints has been growing lately. In this connection it is becoming urgent to obtain new experimental data on the influence of electromagnetic impact (EMI) on mechanical properties and stressed state of welded joint metal of the modern structural materials [1–4].

At present there is no generally accepted terminology for designation of the methods allowing a purposeful change of the mechanical properties and stressed state of metallic materials using EMI. Designations for them are accepted by various authors depending on their own idea of the kind and mechanism of the impact. Names of the methods involving passing electric current directly through the item being treated can contain such terms as electrically stimulated (rolling), electric, electric-pulse, electric-discharge, electrodynamic, electromechanical (treatment), etc. The names of the methods requiring product exposure in the magnetic field, induced, for instance, using a solenoid, may include such notions as thermomagnetic, magnetic-pulse, magnetoabrasive (treatment), etc.

Unlike heat treatment, structural transformations at realization of the above processes result from interaction of the external electromagnetic field (electric current) with the electromagnetic field of the actual crystalline lattice of both the magnetic and non-magnetic materials. Mechanisms of this phenomenon are not quite clear now. This is related to the fact that EMI is a comprehensive impact, including:

- magnetodynamic related to back magnetization of the ferromagnetic in the magnetic field of flowing electric current. Magnetoelastic interaction with the dislocation structure of the ferromagnetic occurs at shifting of interdomain boundaries;
- electrodynamic, related to appearance of pinch-effect (static or dynamic) generating elastic mechanical stresses in the material;
- thermal (Joulean heat, eddy current, etc.), which is accompanied by a thermofluctuation change of the material structure, and in a number of cases development of internal thermoelastic stresses and deformations;
- interaction of conductivity electrons with the field of dislocation elastic deformations, which lower the force of electron braking of the dislocation and magnitude of potential barriers leading to non-thermal transformation of the dislocation structure of the metal with lowering of dislocation density.

The noted impacts on the material structure are characteristic for a wide class of treatment methods called electrophysical methods [5]. Therefore, in our studies we believe it is expedient to use the general term of «electrophysical treatment» (EPhT) with indication of its kind and parameters. The latter allows differentiation of such treatment by the principle of the impact and kind of applied energy among the kinds of treatment widely applied for welded structures (heat and mechanical treatment). With the insufficiently known mechanisms and determining factors of EMI (electric current or electromagnetic field) EPhT detalization in the names of the methods is only possible proceeding from the secondary technological features of EMI realization, this leading to excess diversity of terminology.

In [4] it is shown that EPhT of low-carbon steel of St3 grade by high-density pulsed currents led to a many time increase of its impact toughness without any essential change of material hardness. In this case material heating as a result of EPhT was equal to several degrees. Light microscopy did not reveal any changes in the steel microstructure. The results are another confirmation of the real possibility of development of highly efficient energy-saving processes of

treatment of steels (and their welded joints) to obtain the specified mechanical properties. For successful application of such processes it is highly important to know the essence and features of the mechanisms of EMI influence on material structure.

The earlier expressed opinion of the authors of [4] on the mechanism of EMI influence is based on the ability of electric current to concentrate in the vicinity of microscopic inhomogeneities of the metal structure (cracks, pores, non-metallic inclusions, grain boundaries), causing considerable local heating there. The spatially discrete (mosaic) nature of heat evolution creates a thermally elastic field, in which the compressive microstress peaks coincide with temperature maximums, and the latter, in their turn, are localized near the structure imperfections. Such an impact of current leads to intensive plastic deformation and subsequent recrystallization of microvolumes associated with defects, «healing» of the latter and, ultimately, to a change of the residual mechanical properties of the metal. A condition for such thermal impact is dissipation in the metal of a certain amount of electromagnetic energy applied by the pulse in a time shorter than that required for the temperature field reaching a steady-state mode [6].

The following can be added to the above-said for discussion purposes. It is obvious that the mechanism of the «mosaic» temperature field, «healing» microscopic fracture sites as a result of concentration of electric current on structural inhomogeneities, implies that the current is distributed through the entire treated section. Pulsed current density can be regarded as uniform, if there is no driving of current to the surface (skin-effect). Current pulse duration determines the frequency of the electromagnetic field and its critical value, at which metal thickness is equal to the depth of the skin-layer: $f_{cr} = (\pi\mu_0\mu\gamma\delta^2)^{-1}$, where f_{cr} is the critical frequency above which the skin-effect develops, Hz; γ is the specific conductivity of steel, S / m; μ_0 is the magnetic permeability of vacuum, H / m; μ is the relative magnetic permeability of steel; δ is the material thickness, m [7–9].

A capacitor bank of 600 mF × 5 kV was used as the current source [4]. By our estimate, the discharge current of the above bank can be not less that 100 kA at pulse duration of 10^{-3} – 10^{-5} s, this corresponding to the frequency of the electromagnetic field of 1–100 kHz. For a sample of St3 steel of 10 × 10 mm cross-section (assuming that μ_n = 200, γ = $= 8 \cdot 10^6$ S / m) critical frequency $f_{cr} \approx 1.5$ Hz, so that the skin-effect always develops at EPhT with 1 kHz and higher frequency of the electromagnetic field. Calculation showed that the depth of the skin-layer can be $(0.04–0.40) \cdot 10^{-3}$ m.

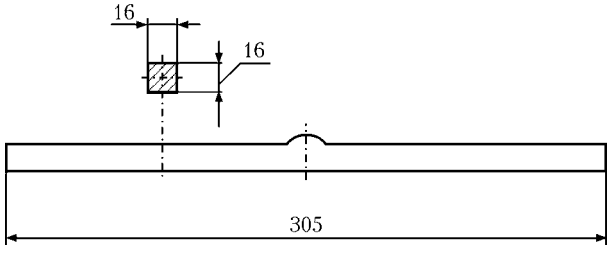

Figure 1. Schematic of a template cut out across the welded joint

Thus, the above mechanism of the impact can be manifested in a quite narrow layer near the sample surface. However, the actual value of the tough component fraction in sample fracture after EPhT [4] was close to 100 %. The above-noted contradiction, in our opinion, can be eliminated, if we assume that the electrodynamic (force) impact of powerful pulses of electric current ---- dynamic pinch-effect, due to strong surface effect, can have a dominant role in structural transformations. Here elastic mechanical stresses of a vibratory nature were generated [10], the action of which on the material inner regions was similar to that of ultrasound, which can essentially affect the metal microstructure [11, 12]. However, it is also necessary to take into account the high value of discharge current, and the fact that the above calculated depth of the skin-layer is the distance over which the current density drops e times (e = 2.7182818...). In this case it can be assumed that despite the strong skin-effect the section layers removed from the surface were also subjected to the impact of electric current of a comparatively low density. Therefore, at interpretation of the mechanism of the impact of powerful current pulses on the steel structure, it is interesting to make a calculation or experimental estimation of current densities in the central part of the treated section and allow for the impact mechanisms characteristic of low density current.

We believe that for development of the concepts of the mechanism of EMI on ferromagnetic materials it will be appropriate to give a more detailed description of the results of our own studies of the influence of EPhT by low-density electric current on the mechanical properties of the metal of steel welded joints, which were the subject of a paper at some time [13].

Composition of steels 20 (GOST 1050–88) and 09G2S (GOST 19282–73) selected for investigations, is given in Table 1. Butt joints of plates of the above steels 16 mm thick were welded by manual arc multipass welding into a V-shaped edge preparation with UONI-13 / 55 electrodes of 4 mm diameter at welding current of 120–130 A. Weld metal composition is given in Table 1. Welded joints were cut up into transverse templates (Figure 1), which were separated into three groups. Templates of the first group were heat-treated (heating up to 650 °C, soaking for 1 h, cooling with the furnace), those of the second group were subjected to EPhT, and those of the third group were left in as-welded condition.

EPhT of the samples was performed in DS10D unit (Patent of Ukraine 43290A) with up to 10 kA working current at up to 30 V voltage. The set law of current variation was supported by the system of automatic control of the unit. EPhT was performed (Figure 2) by passing electric current pulses along the template (across the weld) with the following parameters: trapezoidal pulse shape, alternating pulse polar-

Table 1. Composition of welded joint metal, wt.%

Object of control	Ñ	Si	Mn	S	P
Steel 20 welded joints					
Weld	0.102	0.400	1.09	0.019	0.020
BM	0.193	0.180	0.50	0.018	0.011
Steel 09G2S welded joints					
Weld	0.086	0.31	0.97	0.016	0.018
BM	0.107	0.61	1.42	0.026	0.029

ity, current amplitude of 4–10 kA, duration of amplitude value of current of 1.5–2.0 s, duration of the leading and rear front of 0.5–1.0 s, duration of the pause between the pulses of 5–10 s, number of pulses in EPhT cycle —– up to 100. Selected EPhT parameters corresponded to the frequency of electromagnetic field of 0.25–0.40 Hz, which is below the critical value $f_{cr} \approx \approx 0.6$ Hz for templates of 16 mm thickness. Therefore, the possibility of skin-effect development at EPhT was eliminated.

EPhT had a thermal impact, for minimization of which the template was immersed into a tank of a dielectric material with water, which allowed indirect control of metal heating temperature. It is believed to be improbable that the temperature of the treated metal was higher than 100–150 °C, as no indications of water boiling by the end of EPhT cycle of each template were observed.

Cylindrical samples (type II) for static tensile testing of welded joint metal and Charpy samples (type IX) for impact bend testing of welded joint metal to GOST 6996–66 were cut out of the templates. In the cylindrical samples the fusion line runs through the middle of the sample working part (Figure 3, *a*). In order to determine the impact toughness of the metal in the area of the fusion zone and adjacent overheating region the sharp notch in Charpy samples was made so that its tip was on the fusion line (Figure 3, *b*).

Optical microscopy did not reveal any fundamental differences in the microstructure of welded joint metal in as-welded condition, after heat treatment and after EPhT. Results of mechanical testing of welded joint metal are given in Table 2.

Impact bend testing demonstrates an essential influence of EPhT on the metal properties. It cannot be attributed to phenomena characteristic for the heat treatment conditions. Neither the theory of dynamic heating with the phenomenon of concentration of electromagnetic fields in the vicinity of structural microdefects and inhomogeneities, nor the theory of electrodynamic impact, are suitable. At present we are finding the following explanation for the found influence, which is based on published data.

It is known that plastic deformation runs in the entire deformed volume in an extremely non-uniform manner. In this connection, the material deformability is limited by using the ductility of individual microvolumes, which results in fracture sites initiation in

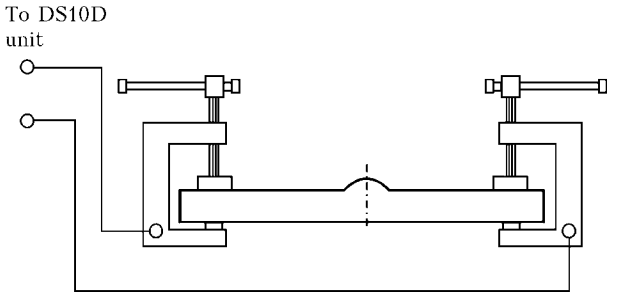

Figure 2. Schematic of a sample connection to the unit when performing EPhT of welded joint metal

them. Metal microvolumes adjacent to the above ones, are only slightly deformed. Also known is the role of dislocation clusters in fracture site formation [14].

Deformation of work-hardened metal without fracture is possible only after recrsytallization annealing. The thermal energy (imparted to the entire metal volume) leads to weakening of interatomic bonds and loss of elastic properties of the metal, which enables structural transformations of a relaxation nature owing to potential elastic energy accumulated at plastic deformation, these transformations being, in principle, reduced to dislocation structure transformation.

Variable magnetic field induced by current pulses in the ferromagnetic material volume, causes the processes of shifting of interdomain boundaries (Bloch walls) and rotation of domain magnetization vectors [15]. Magnetoelastic interaction of Bloch walls with dislocations can cause dislocation motion in ferromagnetic crystals at magnetization [16, 17]. In addition, the weak magnetic field affects the state of the electrons, ensuring a covalent bond between the atoms forming a dislocation–stop complex. In a number of cases, this lowers the height of potential barriers, facilitates dislocation stripping from the stops, and reduces the quantity of impurities capable of becoming effective stops [18]. The processes of rotation of domain magnetization vectors lead to appearance of active stresses of the II kind between the adjacent metal microvolumes [15], which also promotes structural transformations.

Interaction of conductivity electrons with the material dislocation structure lowers the force of electron braking of dislocations (influence of «electron wind») and value of potential barriers [19–21]. This interaction runs primarily on the head dislocations in non-

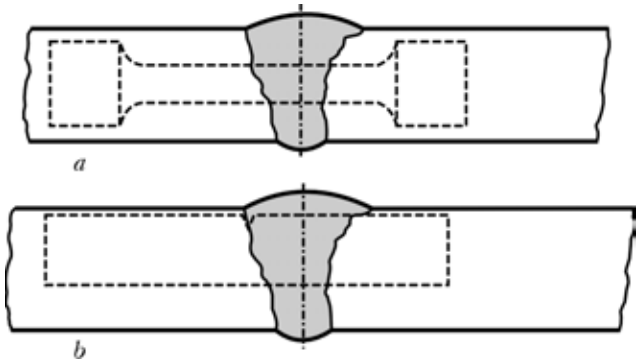

Figure 3. Schematic of cutting out samples of type II (*a*) and IX (*b*) from welded joint templates for mechanical testing

Table 2. Dependence of mechanical properties of welded joint metal on the kind of post-weld treatment

Steel	Kind of metal treatment	Ultimate resistance at tensile testing σ_t, MPa	Impact toughness *KVC*, J / cm^2, at testing temperature, °C	
			+20	–20
20	Without treatment	459.3–467.8 / 463.6	78.7–115.7–66.3 / 86.9	48.2–18.0–27.8 / 31.3
	Heat treatment	455.8–445.4 / 450.6	111.3–118.6–158.6 / 129.5	50.1–68.6–97.7 / 72.1
	EPhT	468.3–463.2 / 465.8	204.5–230.5–120.5 / 185.2	191.1–82.3–184.5 / 152.6
09G2S	Without treatment	499.3–521.9 / 510.6	354.6–291.4–253.6 / 299.9	236.2–50.7–57.6 / 114.8
	Heat treatment	483.9–478.7 / 481.3	296.8–300.5–287.4 / 294.9	237.8–343.9–233.1 / 271.6
	EPhT	520.3–497.7 / 509.0	344.7–336.7–232.8 / 335.1	37.2–325.2–325.7 / 229.4

Note. σ_t values are averaged by the data of two tensile tests, *KCV* values ---- by the results of three impact bending tests.

equilibrium dislocation groups (in the clusters), which are on the verge of stripping from the stop. The current pulse initiates their relaxation, which is accompanied by microplastic deformation, and is implemented due to the energy of internal stresses accumulated during the preliminary plastic deformation. Therefore, the current pulse can be minor as to the level of equivalent action. For instance, the influence on material creep is found already at current density of 0.15 A / mm^2 [22].

The above physical processes involving an electromagnetic field and low-density electric current apparently, lead to non-thermal transformation of the dislocation structure, which is accompanied by lowering of dislocation density in the clusters and improvement of structurally-sensitive characteristics of the metal. In the case of EPhT with a pronounced skin-effect, the influence of the considered processes on the material structure and properties is, probably, also found alongside the dynamic pinch-effect.

1. Loskutov, S.V., Levitin, V.V. (2002) Effect of electric pulse treatment on structure and service life of titanium alloys. *Zhurnal Tekhn. Fiziki*, 72(**4**), 133–135.
2. Valeev, I.Sh., Barykin, N.P., Trifonov, V.G. (2003) Variation of structure and mechanical properties of aluminium alloy AMg6 under the action of powerful current pulses. *Fiz. Met. i Metallovedenie*, 96(**4**), 85–89.
3. Lobanov, L.M., Pashchin, N.A., Skulsky, V.Yu., et al. (2006) Influence of electrodynamic treatment on the stress-strain state of heat-resistant steels. *The Paton Welding J.*, **5**, 8–11.
4. Babutsky, A.I., Chizhik, G.V., Pakhotnikh, A.P. (2007) Influence of pulse electric current treatment on impact toughness of steel. *Metaloznavstvo ta Obrobka Metaliv*, **2**, 19–23.
5. Arenkov, A.B. (1967) Treatment of materials by energy of pulse magnetic field. In: *Principles of electrophysical methods of treatment of materials*. Ed. by A.V. Donskoj. Leningrad: Mashinostroenie.
6. Beklemishev, N.N., Gorbunov, N.M., Koryagin, N.I. et al. (1989) *Ductility and strength of metallic materials under pulse action of high power electromagnetic field*. Moscow: IPM.
7. Dashuk, P.N., Zajenets, S.L., Komelkov, V.S. et al. (1970) *Technique of high pulse currents and magnetic fields*. Moscow: Atomizdat.
8. Kajdalov, A.A., Sokirko, V.A. (2005) Demagnetization of products before welding. *Svarshchik*, **5**, 21–23.
9. Koshkin, N.I., Shirkevich, M.G. (1962) *Reference book on elementary physics*. Moscow: Fizmatgiz.
10. Belova, M.M., Protsenko, S.S., Ivanov, A.V. (1987) Dynamics of elastic-plastic layer deformation in pulse energy release. *Problemy Prochnosti*, **12**, 87–91.
11. Belikov, A.M., Makarov, V.V., Roshchupkin, A.M. (1989) Variation of structure and kinetic peculiarities of polycrystalline aluminium behavior at ultrasonic impact. *Fiz. Met. i Metallovedenie*, **67**, Issue 6, 1209–1214.
12. Polotsky, I.G., Nedoseka, A.Ya., Prokopenko, G.I. et al. (1974) Lowering welding residual stresses by ultrasonic treatment. *Avtomatich. Svarka*, **5**, 74–75.
13. Moravetsky, S.I. (2003) Influence of post-weld electrophysical treatment on mechanical properties of carbon and low-alloy steel welded joints. In: *Abstr. of Pap. of 2nd All-Ukr. Sci.-Techn. Conf. of Junior Scientists and Specialists on Welding and Related Technologies* (Vorzel, 25–27 June, 2003). Kiev: PWI, 31.
14. Vladimirov, V.I. (1984) *Physical nature of metal fracture*. Moscow: Metallurgiya.
15. Livshits, B.G., Kraposhin, V.S., Linetsky, Ya.L. (1980) *Physical properties of metals and alloys*. Moscow: Metallurgiya.
16. Chebotkevich, L.A., Urusovskaya, A.A., Veter, V.V. (1965) Movement of dislocations under the impact of the magnetic field. *Kristallografiya*, 10(**5**), 688–691.
17. Chebotkevich, L.A., Urusovskaya, A.A., Veter, V.V. et al. (1967) Interaction of Bloch walls with dislocations in weak magnetic fields. *Fizika Tv. Tela*, 9(**4**), 1093–1097.
18. Golovin, Yu.I. (2004) Magnetoplasticity of solids. *Ibid*., 46(**5**), 769–803.
19. Bataronov, I.L. (1999) Mechanisms of electroplasticity. *Sorosovsky Obrazovat. Zhurnal*, **10**, 93–99.
20. Fiks, V.B. (1981) Entrainment and retardation of mobile defects in metals by conductivity electrons. *Zhurnal Eksp. i Teor. Fiziki*, 80(**4**), 1539–1542.
21. Fiks, V.B. (1981) About interaction of conductivity electrons with isolated dislocation in metals. *Ibid*., 80(**6**), 2313–2316.
22. Kishkin, S.T., Klypin, A.A. (1973) Effects of electric and magnetic actions on creep of metals and alloys. *Doklady AN SSSR*, 211(**2**), 325–327.

FRENCH INSTITUTE OF WELDING TODAY*

V.N. BERNADSKY
E.O. Paton Electric Welding Institute, NASU, Kiev, Ukraine

The paper gives information about the modern structure and forms of scientific-technical activity of the French Institute of Welding. The main research areas and forms of their realization in industry are highlighted. The role of informational support of all structures of the «French Institute of Welding» group is shown.

Keywords: France, Institute of Welding, structure, directions of activity, welding technologies, reliability, nondestructive testing, training and certification of personnel

The French Institute of Welding (IW) is one the leading and the eldest welding institutes in Europe. It was founded in 1930 in Paris in boulevard de la Chapelle as Institute of Autogenous Welding. Today IW is a prominent center in the sphere of welding and allied technologies that has modern scientific-experimental and laboratory-testing base, as well as highly professional scientific-engineering potential. By the end of 2006 the number of the employees exceeded 720 persons that is 1.5 times more than in 1996; the areas of its experimental and technological base exceeds 8,000 m^2 at present.

In 2005 the management of the Institute took the decision about serious reorganization of general structure and management of the «French Institute of Welding» associative group. As a result the Institute turned from vertical structure and control system to horizontal-regional already in 2006. Such approach foresaw the transfer of IW main activity for the sake of industry to the regional IW representative offices in all Departments of France and to the foreign branches with delegation of definite rights and duties to their heads. The appropriate plan of IW technical and commercial activity was designed under new conditions and, first of all, was directed to maximum approach to their direct partners and customers, and the main ---- on widening the circle of partners and to the growth of orders volume. Considerable broadening of scientific-technical services is foreseen simultaneously in regional and foreign departments of IW: by diagnostics of welded structures and nondestructive testing of welded joints; training, retraining and certification of workers, scientific-engineering examination when designing, manufacturing and maintenance of welded structures and constructions.

Complex of the enterprises of the French Institute of Welding, when all organizational changes, preserved traditional orientation of its activity on welding production of such prospects and hightech branches as petroleum chemistry, gas transport systems, power engineering, including nuclear, aircraft industry as well as industrial construction.

The most serious structural change in the process of the Institute of Welding reorganization was the conversion of big «Services» complex subdivision, founded in 1948 on the rights a the branch, into the «Institute of Welding ---- industry» with rather wide autonomy and with its own logotype rather different from the principal one. Subdivisions and specialists, connected with diagnostics and nondestructive testing, welding and technical inspection and working personnel certification, technological maintenance, examination and other types of engineering and technical services in the sphere of welding manufacturing of industrial enterprises and constructions of France and other EU countries, were included into the structure «IW ---- industry».

Institute of Welding, when the given reorganization, left the right for itself to carry out scientific researches and technological developments of innovation nature, laboratory-analytical researches, training structures of higher (ESSA) and secondary (EAPS) professional education and to give the graduates the qualification of «international welder-engineer», «international welder-technician» and other, certification of personnel on welding and nondestructive testing, the system of information ensuring of scientific and production-commercial activity of the whole complex, as well as to issue «Soudage et Techniques Connexes» journal and «Infos Members. Bull'Doc» bulletin, and lately «Welding and Cutting» journal together with DVS and TWI.

IW regional system, that was available before, was expanded in the frame of a new structure; 36 technical representative offices and 12 centers for professional training and certification of welder workers in all eight departments in France are included into it at present. Regional directors head IW group of technical offices and training centers in each department.

The new step in IW activity development is implementation of its developments and its specialists' activity at the enterprises in actively developing regions of the world. IW opened three permanent branches in Morocco, Quatar and Iran in 2006 with this purpose. The establishment of new branches is supposed in the nearest future in Asia. Foreign branches quickly justified their technical and economi-

*The author expresses his gratitude to Nina Khomenko (E.O. Paton EWI) for participation in the article preparation and Catherine Levy (IW) for provided materials.

cal expediency. Permanently present in appropriate regions, they gained access to new interested customers, increased the afflux of orders. Besides, IW mobile groups work from time to time by contracts as experts, technologists and flow detector specialists at enterprises in more than 30 countries of the world. Such active form of IW activity on serving foreign partners provided in 2006 about 15.2 % of the Institute total turnover and the growth of these earnings increased by 40 % in 2006, if to compare with 2005.

As a result of purposeful activity of all subdivisions, included into the «French Institute of Welding» association group, the total turnover of the Institute made EUR 65.5 mln in 2006, that is almost 2 times exceeded its amount of financing in 1996. It is also possible to judge about IW work efficiency by net profit at the amount of EUR 1.57 mln by the end of 2006, which growth in comparison with 2005 increased by 11 %. The share of subdivisions into the total fund of IW financing for 2006 in the context of the main directions of its activity looks in the following way:

- researches and developments for the sake of industry ---- 7.9 %;
- diagnostics, inspection and nondestructive testing of welded structures and constructions ---- 69.4 %;
- calculations, designing, examinations and consultations ---- 3.6 %;
- professional training and certification of welding personnel of all levels ---- 13,7 %;
- other engineering and technical services and commercial operations ---- 5.4 %.

In the process of reorganization the management of the Institute together with the managers of its subdivisions foresaw separately the increase of attention to the work with labour collective, directed to the increase of personal initiative and responsibility, the improvement of labour conditions, skill to work in varying staff of project collaborators, efficiency, when carrying out the tasks and the most important ---- on the development of creative approach to innovations. Such forms of activity as working meetings by subjects, collective discussions of the results, individual discussions and revised system of benefits were included here.

Figure 1. Laboratory building of Technological Center in Yuts

The rise of importance and level of scientific and technical examination in modern hightech production found its repulse in IW organizational measures. So, in 2006 the goal program «Fellow» was adopted, its task was strengthening of IW representative offices. In accordance with it permanent acting group of IW experts was organized, it was directed to highly professional evaluation and selection of the most progressive technologies and other technical solutions in the interests of customers. Four experts of international level of competence were included into the staff of the group; they carry out independent scientific work and have the rank of IW deputy directors and also 26 expert-engineers. The sphere of their activity covers all regional offices in the country and foreign offices on the following four themes directions: «Materials and methods of joining», «Structures, estimation, examination», «Diagnostics and nondestructive testing», «Technological supervision, standard acts and standardization».

Applied scientific topics in the sphere of traditional welding technologies and welding consumables for mass application are connected, as a rule, with exceptionally concrete tasks, appeared in industry. Such develops allow active use of scientific and technological potential and IW innovation possibilities, as well as to assist in rising of national welding production technical level and competitive ability of manufactured welded production.

The peculiarity of IW original scientific researches and developments is that they, as a rule, are directed on investigation of new, more progressive technologies of joining and methods of testing. At present IW researches are concentrated on the study of technical possibilities of joining different materials applying friction stir welding, electron beam, laser and laser-hybrid welding, fusion welding by K-TIG method and brazing. Researches of new steels and alloys weldability, including their dissimilar combinations, are widely spread.

These works are carried out by the Department of technological researches and developments, it is one of the main departments in IW; its laboratory-experimental base (Figure 1) is located in Yuts (Mozel Department) and in fact it is IW Research-Technological Center. The Center square is 6,000 m^2, 75 engineers and technicians who are included into the staff of beam processes laboratories, fusion welding technique and technology, researches of strength and mechanics of welded structures destruction, corrosion and nondestructive method of testing and other work in it. The Center is equipped with modern laboratory, testing and technological equipment that permits IW to participate rather widely in large scale research programs including those in the frame of EU.

Programs on technological researches of laser and laser-hybrid welding processes occupy important place in the Center at present. The workshop is equipped with six laser sources of more than 1.0–1.2 kW power each. The following can serve as an example of applied

researches on concrete orders: creation of industrial welding technology of chrome-molybdenum and high-carbon steels of wide range thicknesses, as well as evaluation of technological availability and rational spheres of industrial application of cast irons laser welding-brazing. Complex researches on comparative evaluation of the up to day welding methods of thin sheet carbon steels, coated steels, stainless steel, steels of high strength, titanium and aluminium alloys were started in the frame of all European partner (seven co-participants) of SOFI program in 2006. The aim of the research is to obtain technological recommendations on optimal use of concrete methods of joining applicable in car and boiler manufacturing.

Specialists of the Center take part in «Hipo-TIG» European project on study technological features of new K-TIG process that combines high efficiency and good quality of joining (Figure 2). The process is designed for one pass butt welding of metal up to 12–15 mm thickness with through «keyhole» penetration. Application of high welding current values (500–1000 A) and electrode dipping into forming through hole of weld is typical for K-TIG process. Experiments were carried out on 12 mm thickness stainless steel, nickel and titanium alloys specimens. The influence of process parameters on maintenance of «keyhole» penetration and formation of the qualitative weld were determined. The results showed considerable (up to 10 times) increase of productivity with good quality of the joint, decrees of spattering and gas-dust evolution (in comparison with usual TIG process).

Friction stir welding (FSW) is studied in details and processed for concrete spheres of application in the IW second specialized technological Center in Mets as one of advanced innovation technologies. The Center is also included into the structure of IW Department of industrial researches and developments; 7 engineers and 3 technicians work in it and its laboratory-experimental workshop, which area of 1,300 m^2 is equipped with two 10 tons traveling crane, it has metallography laboratory and workshop CAD / CAM system with Cartia-V5 software. Two modern installations (Figure 3) with digital control and tables of 12 and 19 m length for FSW of extended welds as for flat elements (in two coordinates) and as for three dimensional units or structure fragments of height up to 4.5 m (in three coordinates) were installed in the laboratory building. Final cycle of FSW-process in the frame of «EuroSTIR» was carried out here in 2006; 40 partners from EU countries, including 6 French, took part in it. Final researches proved technological advantages of FSW-process in weldability in comparison with arc and beam processes. Participants of the project issued fundamental recommendations for industrial enterprises about rational branches of application of this process for joining alloys of aluminium, copper, magnesium, zinc and such dissimilar combinations as Al–Cu and Al–steel. Such technical recommendations also met the main task of «EuroSTIR» project, namely, promotion of

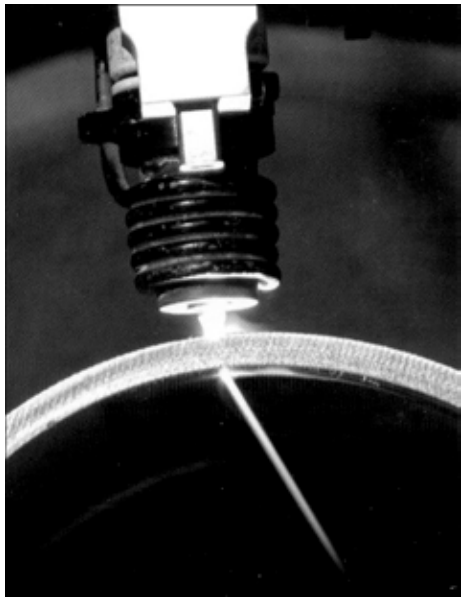

Figure 2. K-TIG welding of the pipe position butt joint 13 mm thick

FSW into European transport machine building (ship, aircraft, car manufacturing, railway rolling stock) and construction.

Another IW important development in the sphere of FSW-technologies is realization of «Wel Air» contract project. Perfection of industrial technology of friction stir welding-on of panels up to 12 × 2.4 m with different curve to the frames and timbers of aircraft structures, technologies of spot welding, slot and butt welds on aircraft aluminium alloys of 1–30 mm thickness is foreseen by the project. Industrial FSW-technology of three dimensional and three dimensional-mounting joints in automatic condition is directed on its further application in industry with the use of welding robots-manipulators by welding instruments including special, with double shoulder.

It should be mentioned that IW technological Centers in Mets and Yuts towns carry out not only research and experimental-industrial development of joint technology but also carry out minor orders of several enterprises on welded details and units manufacturing with applying of advanced welding methods on modern equipment.

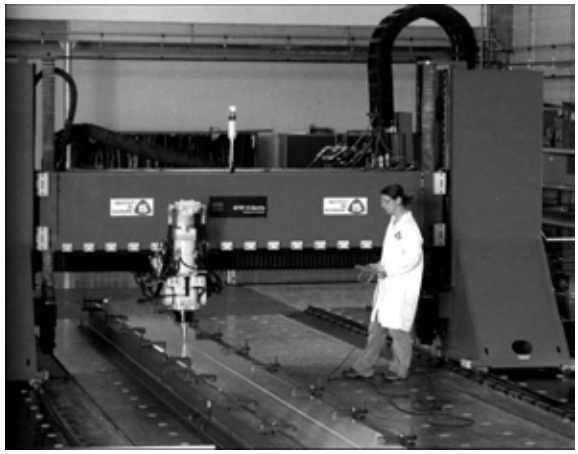

Figure 3. Installation for friction stir welding (14 m weld length) in Mets Center

Figure 4. «Laser Megajoule» welded spherical chamber for complex of thermonuclear researches: *a* — welding process and monitoring in the workshop; *b* — the chamber is prepared for transportation

Two more directions in IW general activity are of great importance: diagnostics, inspection and testing of welded structures and constructions with the aim of evaluation and prolongation of their operational capability as well as the work directly at the enterprises where important welded structures are manufactured, i.e. highly qualified technological maintenance and inspection at all the steps of structures manufacturing (blanking operations, assembling, welding, testing). The example of such activity can be participation of IW specialists in all stages of unique «Laser Megajoule» spherical chamber manufacturing, its mass is about 100 t and the diameter is 11 m, for French Thermonuclear Center (Figure 4).

Short-time program (for 5 years) on priority subjects of technological researches and developments in the sphere of welding and allied technologies is of interest and is adopted in IW; it is directed for the sake of industrial enterprises and branches. The program includes:

- development of methods for nondestructive testing of welded (stationary and board) containers and tanks for hydrogen storage;
- origination of monitoring method for aging process of welded structures and evaluation of their damage in the process of operation;
- development of industrial technologies for welding new structural materials: alloyed steels with high elastic limit, high-strength aluminium alloys and multi-materials for hybrid structures;
- raise of productivity and automation level of welding processes by the way of application of broadening volumes of self-adapted and hybrid welding as well as intensive robotization of welding industry;
- development of digital modeling of welding technologies and surfacing methods including those that eliminate further heat treatment.

According to the IW General Director Mr. Alain Houdart, the Institute, in the nearest future, remains faithful to its traditions in respect of permanent increase of researches innovation level, active transfer of progressive technologies and other innovations into industry, further development of IW net of foreign representative offices, establishment of new and strengthening of established business relations with customers of the leading French branches with which they have common vision on modern development of welding and allied technologies.

Permanently improving powerful system of information provision in the main spheres of IW activity is directed on providing these tasks. 34 out of 36 regional representative offices and foreign branches are already included into home institute system; the whole system is corresponded with the Institute website (www.isgroup.com). Actualization of application program base packet (EXP) of system control, that has a number of DBn subjects, was done in 2006. First of all the system allows accumulating and analyzing all information about IW available and potential customers including the first contacts, concrete demands, claims for contracts estimated costs, list of long-range tasks and services and other. More than 8,000 partner-customers are recorded in IW information system DBn, the considerable part of which make so-called IW full members — big industrial unions, concerns and companies of France, Belgium, Germany and other countries. DVS and TIW are associative members of the French Institute of Welding.

IW full members from industry have privileged access to a number of services from the part of the Institute subdivisions, in particular:

- open telephone access to bibliographical database that contains more than 14,000 annotations of international technical publications in the sphere of welding, welded structures and nondestructive testing;
- use of systematically actualized database of standard acts, technical recommendations, standards

and other national and international standard documentations;

• effective provision of technological consultations or recommendations and quarterly receiving of current technological documentation set in the form of a bulletin «Infos Members, Bull'Doc»;

• the possibility to familiarize with the results of some research works, done by IW by the contracts with industrial enterprises and constructions;

• the invitation to take part in ten research seminars, subject discussions and demonstrations, carried out during the year;

• free place reservation (Web-units of enterprises) on the IW Web-site.

The above stated illustrates new information approaches of IW to the work with partners and customers ---- industrial enterprises and constructions of EU countries, as well as modern management of IW activity on national and international markets of welding technologies and services. The main motto-task of the Institute for today is «to suggest to the customer the best solution wherever it stays».

By the materials of «Institut de Soudure. Rapport Annuel-2005», «Institut de Soudure. Rapport Annuel-2006» and «Soudaqe et Techniques Connexes».

REPAIR SURFACING OF GAS TURBINE BLADES MADE FROM HIGH-NICKEL ALLOYS

In the process of service of gas turbines the wear of seal strips is occurred, that decreases greatly the efficiency factor of the turbine. To restore the geometric sizes of strips, the technology of plasma-powder multilayer surfacing with a subsequent mechanical treatment has been developed. As a filler material, powders of dispersion-hardening nickel alloys of JS type with a strengthening γ′-phase, providing the preset level of wear resistance, are used.

Conditions of surfacing and consumption of filler material are selected depending on the geometry of the blades being restored.

Purpose and application. The offered technology can find application in repair of body of different-purpose blades, and also restoration of seal strips of gas turbines. Taking into account the decreased weldability of blade alloys and wide range of their compositions, technology of restoration repair of blades in each definite case is defined by the developer.

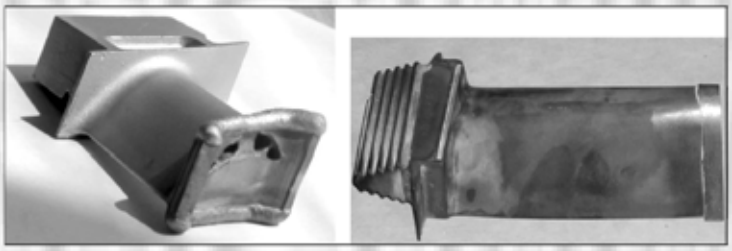

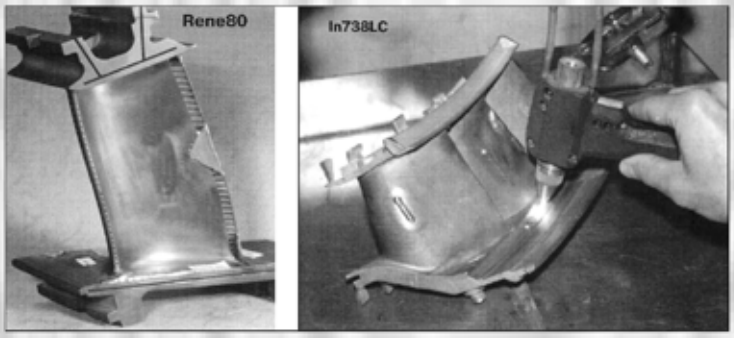

Status and level of development. It is recommended to use the technology at the customer facility. Equipment and materials are delivered.

Main developers and performers: Prof. Yushchenko K.A., Prof. Savchenko V.S., Res. Ass. Chervyakova L.V., Group Head Nakonechny A.A.

Contacts: Prof. Yushchenko K.A.
Tel./fax: (38044) 289 2202

FROM HISTORY OF WELDING

DEVELOPMENT AND PROGRESS OF ARC WELDING IN ACTIVE GASES

A.P. LITVINOV
Priazovsky State Technical University, Mariupol, Ukraine

Analyzed is the history of emergence and development of arc welding in active gases. It is noted that this welding method was developed on the basis of progress in metallurgical and electrodynamic components of the process. Maximum effect of its application was achieved at pulsed control of electrode melting, as well as by using special compositions of electrode wires and shielding gas.

Keywords: welding fabrication, arc welding, power source, MAG welding, CO_2 welding, welding metallurgy, electrode wire, engineering history

Consumable electrode CO_2 welding has now become widely applied in fabrication of steel metal structures. Starting from the first years of development of commercial technology it became an important means of mechanization of assembly-welding operations, pressing on manual arc welding and semi-automatic hose submerged-arc welding applied in ship-building, car- and carriage construction and in a number of other industries first in the USSR, and then also in other countries. However, analysis of development of this welding process has not been performed up to now. In collections and monographs, including those devoted to the history of welding, inaccuracies of a technological nature are found, concerning rod electrode welding in gas mixtures, wire compositions, metals being welded; the fundamental engineering solutions are not emphasized, system analysis of emergence and development of CO_2 welding technologies is not made, and the sequence of development of this welding process is not given [1–4]. Known are the works, dealing with the advantages of gas-shielded consumable electrode arc welding, limitations, main characteristics, possibilities of automation and robotization, method of controlling metal transfer, recommendations on selection of welding wire and welding modes [5].

The most recent work [6] devoted to achievements and problems of AC welding mentions the features of the processes of electrode wire melting, also in CO_2, and designs of power sources. However, analysis of development of this welding process has not been performed so far.

The purpose of this work is systematizing and establishment of the sequence of development of the main MAG welding processes, as well as the history of widening of its technological capabilities.

CO_2 carbon electrode welding. In the first arc welding process developed by N.N. Benardos, carbon ions participated in reactions with oxygen and ousted the air from the welding zone, preventing metal oxidation and nitriding of metal [7]. Work on improvement of the quality, versatility of application and improvement of the welding process efficiency was deployed at the start of the XX century. Acetylene-oxygen welding and stick coated metal electrode welding were developed. However, under the stationary conditions the steel, cast iron and copper products continued to be welded and repaired by Benardos method [8]: water solutions of fluorine and chlorine salts were applied on the edges for carbon-arc welding of aluminium and its alloys. In 1920s attempts were made in the USA to apply CO_2 as a shielding medium in welding (E. Tompson, General Electric Company), but it was not possible to obtain any positive results, as pores formed in welding. Starting from the middle of 1920s, intensive studies were performed in Germany and a number of other countries of the problem of arc welding automation, carbon electrode welding being considered as one of the most promising technologies [9]. E.O. Paton noted that carbon electrode welding found wide application abroad [9]. In 1936 N.G. Ostapenko, EWI staff member, developed the method of carbon electrode arc welding in a CO_2 jet and atmosphere of burning paper cord [8]. Such shielding allows changing the process polarity and improving heat input control. By 1938 EWI improved the semi-automatic and automatic carbon-electrode welding [10]. CO_2 carbon electrode welding continued to be applied in 1940–1950s as a mechanized technology of batch-production of a number of steel products [11]. N.G. Ostapenko wrote: «A CO_2 jet, while blowing over the carbon electrode, forms carbon oxide, which is not an oxidizer, and, therefore, can be used as a shielding atmosphere protecting the molten metal in the welding zone from ambient air…» [12, p. 7]. Steel products welded by the carbon arc in CO_2 (canisters, electric capacitors, alkaline accumulator boxes, thin-walled tanks, pipes, etc.) met the requirements of strength and air tightness made of the vessels, operating at normal pressure [12, 13]. At the same time,

EWI attempted to develop the technology of consumable-electrode CO_2 welding; however, no positive result could be achieved [1].

Development of consumable electrode CO_2 welding metallurgy. By the end of 1930s automatic submerged-arc welding of iron and steel was developed in the USA (Linde Company) and in the USSR (at EWI under the guidance of E.O. Paton) [8]. At EWI the high metal quality was achieved owing to application of electrode silicon-manganese wires, made at «Serp i Molot» and «Krasny Profintern» plants [14, p. 28]. On February 14, 1941, GOST 178–41 for welding wires, wt.%: up to 0.16 C; 0.8–1.1 Mn; 0.6–0.9 Si, not more than 0.04 S, not more than 0.04 P [14, p. 34], was approved. E.O. Paton noted that «flux or electrode wire should contain more manganese than it is necessary to have in the weld metal» [14, p. 38]. Increased content of silicon and manganese compared to these elements content in regular structural steels was introduced exactly with the purpose of deoxidizing. The idea of application of silicon-manganese wires was also used by K.V. Lyubavsky at the Central Research Institute of Mechanical Engineering Technology in the Welding Department, which was co-headed by E.O. Paton, in development of new flux compositions [15].

In 1952 K.V. Lyubavsky and N.M. Novozhilov demonstrated the possibility of consumable electrode welding of steels using CO_2 as shielding (USSR Author's Certificate #104283 of Febr. 2, 1952). They welded low-carbon steels and 30KhGSA steel using the known electrode wires (composition to GOST 2246–51) with deoxidizers ---- manganese and silicon [16]. However, in welding Kh18N9T steel, despite the application of special wires, the alloying impurities burnt out [16, p. 6]. Electrode wire melting ran in an unstable manner, and was accompanied by fan-like spattering. The authors noted that in view of «high potential capabilities for utilization of this process for automatic and semi-automatic welding, further investigation of this process is rational with development of the necessary electrode wires and special equipment» [16, p. 8]. They attributed the strong spattering of the electrode metal and unsatisfactory weld formation primarily to intensive constriction of the arc column as a result of energy consumption for dissociation and ionization of molecular gases on the column periphery [17]. Achievement of a stable running of the process became one of the most important tasks in development of commercial technology and equipment. On the other hand, it is known that the nature of drop transfer depends on the simultaneous action of electrode melting, arc pressure, forces of liquid metal surface tension, gravity and electrodynamic forces, values and directions of which change during formation or separation of the drop [18, 19].

Further development of CO_2 welding followed two paths, which may be called metallurgical and magnetoelectrodynamic, which eventually led to development of modern technologies ---- adjustment of electrophysical parameters. Substances changing the ionization potential of the arc discharge, began to be added to the welding zone. In 1960–1970s the electrode wire compositions were intensively developed, and mode parameters were determined; later on the search for shielding gas compositions was started (N.E. Bauman MHTÑ, E.O. Paton Electric Welding Institute, Rostov Institute of Agricultural Machinery (RIAM), etc.). Purpose-oriented change of the electrode metal composition became the main metallurgical direction, as a means of adjustment of metal melting and transfer, mainly due to addition of elements with a low ionization potential into the welding zone (salts of alkali, alkali-earth elements) and various alloying elements. Application of flux-cored wire was recognized to be the most practicable and effective. In 1957 I.K. Pokhodnya developed the compositions of electrode wires for CO_2 surfacing (E.O. Paton Electric Welding Institute) [20]. Flux-cored wire continued to be improved, the range of its application extended to CO_2 welding of alloyed and thermally stable steels, higher strength steels, as well as surfacing [21, 22].

Deposition of a thin layer of activators on Sv-08G2S wire, addition of rare-earth metals (0.03–0.07 %) to the consumable electrode composition allowed improvement of the technological properties of the process and arcing stability, lowering metal losses for spattering and nitrogen and hydrogen content in the weld metal. When water solution of cesium and sodium carbonates was used as activator, it was possible to achieve a stable spray transfer of the metal. It is established that at electrode activation at current supercritical for standard silicon-manganese wire the arc in CO_2 gas becomes spatially stable. At pulsed-arc welding with intermittent-spay transfer of electrode metal its losses for spattering dropped to 3–5 % [23–26]. To ensure high mechanical properties of weld metal V.I. Ulianov and other PWI specialists suggested alloying Sv-08G2S wire by aluminium (up to 0.01 %) [27]. In 2000 composite welding wires were developed based on a unified matrix with a core, consisting of microalloying modifying or fluxing additives in a state unbound with impurities in an insulating shell [28].

In 1974 PWI proved that in welding in CO_2 with oxygen addition (up to 30 %) the wire should contain an increased weight fraction of silicon or should be additionally alloyed by titanium and aluminium [29]. To reduce spattering and eliminate formation of the oxide film on the weld surface in welding of acid-resistant steels, a combined gas shielding of the welding zone was proposed with feeding of Ar and CO_2 from individual nozzles [30]. Development of gas composition and improvement of the quality of welding zone shielding were performed also when solving other problems. Thus, welding in Ar + O_2 + CO_2 mixture, compared to CO_2 and submerged-arc welding ensures a higher resistance of weld metal to crack initiation [17, 31, 32]. Over the last decade the attention was focused on improvement of welding efficiency due to

application of gas mixtures of CO_2 + 25–30 % He, this greatly increasing the wire feed rate and ensuring the process stability [33].

Invesitgation of electrophysical phenomena and development of power sources. In order to widen the applications of CO_2 welding it was necessary to develop the methods of controlling the electrode metal melting and transfer. Pulsed-arc processes related to variation of the electrical parameters of the mode, were regarded to be the most promising. During the 1940–1950s PWI accumulated extensive experience of investigation of the processes and introduction of submerged-arc thin wire welding. B.E. Paton, when studying the electric energy characteristics of arc welding processes, determined the conditions of welding with self-regulation of electrode wire melting and the requirements to welding circuit elements [34, 35]. PWI established the possibility of controlling the electrode metal melting and transfer, as well as other characteristics of the process due to current pulses or programming the variation of instantaneous power. Inert-gas pulsed-arc welding with a constant electrode feed rate and forced short-circuiting was performed for the first time in 1953 by A.V. Petrov at the Research Institute of Aviation Technologies (RIAT) [36].

In 1956 PWI and RIAT developed the process of CO_2 welding with thin wire of 0.6–1.2 mm diameter running with forced short-circuiting of the arc gap [37, 38]. After starting investigation of the new process, B.E. Paton established the following: «The welding arc in CO_2 is more contracted than in argon, it has a rising volt-amplere characteristic and the property of self-regulation; in CO_2 it is rational to apply DC power sources with a flat or rising external characteristic. Of great interest is application of semi-conductor welding rectifiers, the schematic of which is fitted with the necessary feedbacks...». B.E. Paton noted that «...the solution for application of alternating current for powering the arc in CO_2 should be sought in activation of electrode wire, as well as application of special welding transformers with feedbacks and pulsed arc ignition» [39, p. 6].

PWI proved that at increase of current density in the melting electrode the stability of the welding process can be achieved in the case of using a DC generator with a flat characteristic as the power source. Pulsed-arc welding with a constant electrode feed rate was developed at PWI in 1956 [38]. During the following years development of pulsed-arc welding processes was carried on in a number of other countries [40, 41]. By the start of 1970s the main kinds of pulsed-arc welding were formed, namely with continuous arcing, with forced short-circuiting of the discharge gap, also with forced arc breaking up [42–45]. Welding with continuous arcing is usually conducted with superposition of current pulses with the same parameters or of a group of pulses with different parameters. The process with forced short-circuiting is achieved, as a rule, by current programming in thin-wire CO_2 welding [46, 47].

The main goal of equipment improvement which was addressed by PWI, RIAM, Lincoln Electric (USA) and other companies, was control of the process of electrode metal mass transfer using not the traditional formation of pulses, separating the electrode metal drops and thus realizing welding without short-circuiting («pulse» mode), but forced formation of the short-circuits by controlling the arc current and voltage. PWI developed a process, at which the forced short-circuiting of the arc gap by electrode metal drops occur under the action of short-time current pulses. For stabilization of the welding process, particularly, for lowering the spatter, optimum relationships were found between the voltage and current, and power sources were developed with the respective dynamic properties. A relationship has been established between the metal transfer parameters and such power source characteristics as circuit inductance, short-circuiting resistance, etc. Feed mechanisms and mode control systems were optimized, semi-automatic machines were developed, also for two-mode welding [48–51]. In 1971 automatic AC welding in CO_2 was conducted for the first time [52]. In the following years this technology was improved on a new technical basis; arcing stabilizers with dual control were developed [53, 54].

Both the directions of improvement of CO_2 welding were used to develop the technology of welding specific metals and products. Many problems were solved through the use of pulsed control of current and arc power with programmable shielding gas feed (CO_2 and gas mixtures with Ar) into the welding zone. With this purpose, equipment for automatic and semi-automatic welding was developed: specialized power sources, blocks of modulation of the kind of shielding gases with different physico-chemical processes and devices for their feed synchronizing. The problem of welding different steels of low, medium and great thickness at welding current of 8 to 300 A was solved [55].

Starting from 1930s, vibroarc surfacing and welding were developed and widely accepted in the USSR. In these processes the AC electromagnet induces electrode vibrations, alternatively bringing it closer to the workpiece and moving it away from the workpiece; the arc can be powered both by direct and by alternating current [56]. Forced oscillations of the electrode continuously cause arc short-circuiting and ignition. The principle of vibration is combined with pulsed powering of the arc process in CO_2 welding. In the last decade of the previous century Fronius Company (Austria) developed equipment, allowing realization not only of the processes of MIG and MAG welding and surfacing by a steady and pulsed arc, but also controlling the welding process by dynamic adjustment of the wire feed rate. At the moment of short-circuiting the wire is withdrawn abruptly, the metal transfer occurring under the impact of the forces of inertia. Owing to a low short-circuiting current, the welding process runs practically without spatter-

ing and with minimum heating of the base metal. The technology was called «Cold Metal Transfer» [57]. A digital controllable microprocessor and welding current inverter source controllable in the digital mode with an integrated functional package were developed; the equipment is suitable for operation with robots with different control principles.

Development of CO_2 welding technique and its introduction. Developed in 1940s carbon-arc welding in CO_2 atmosphere, owing to its high efficiency and low cost, started ousting oxy-acetylene welding in manufacturing products from thin-walled steel (0.5–3.0 mm). The holder with the carbon electrode and nozzle can be easily moved manually or can be fixed on a carriage with precise tracing of the weld contour and automatic feeding of the carbon electrode as it burns. For mass production of small items specialized machine tools were designed, which perform assembly and displacement of blanks. The scope of operations performed manually was reduced, and intermediate operations were eliminated [12].

Commercial samples of equipment for mechanized consumable electrode welding were developed rather quickly. The experience of B.E. Paton's designing long flexible hoses, feed mechanisms, holders and other elements of equipment for semi-automatic (hose) submerged-arc welding turned out to be useful [58]. Welding heads of pilot units were made at PWI on the basis of feed mechanism of PSh-5 semi-automatic machine. In 1957 PWI developed a production sample of such a semi-automatic machine, and in 1958 specialized automatic machine tools for CO_2 welding were designed. In particular, the problem of automation of welding small-sized parts, sheet structures, vertical and overhead welds was solved.

It should be noted that, while the physico-chemical processes, technology and materials continued to be improved, the mechanical part of the equipment was designed in the most rational manner. At first thin-wire welding was performed with power supply from a welding generator with a flat characteristic. To ensure stable welding processes and lower the spattering, welding was conducted at certain voltage and current ratios. External characteristics of the source were formed by changing the magnetic flux of generator demagnetization and by other processes.

Improvement of power sources was conducted in keeping with the technology requirements (primarily, allowing for control of the nature of electrode melting) using new components as new generations of electronic devices were created [47, 49, 59]. Various following systems and computers were used to control the welding process. The opto-electronic system of following the welded joint, coupled with a microcomputer, ensures high-precision control in automatic gas-shielded metal-arc welding [60]. At the end of 1990s PWI developed an all-purpose technology complex for automatic and mechanized consumable electrode arc welding, including a specialized power source, block of modulation of the kind of shielding gases (Ar, CO_2 and gas mixtures) and devices for synchronization of the kind of welding current with the kind of welding gas [53].

Papers about the work performed in the USSR on development of consumable electrode CO_2 welding in 1950s were re-printed abroad and soon the US, Swedish and British companies were manufacturing equipment for this process.

CONCLUSIONS

1. Consumable electrode CO_2 arc welding was developed using the half a century experience of application of carbon-arc welding for steel product fabrication and silicon-manganese wire developed for submerged-arc welding.

2. Improvement of the technologies of CO_2 welding was following the path of improvement of the thermophysical parameters of the process by addition to the welding zone of substances changing the ionization potential of the arc discharge, and development of the methods of controlling the electrode metal melting and transfer by pulsed variation of mode electrical parameters.

3. The greatest effect was achieved at pulsed control of current and power of the arc with programmable feed of shielding gases (CO_2 and gas mixtures) into the welding zone.

1. Potapievsky, A.G., Petrov, A.V., Suptel, A.M. et al. (1982) Gas-shielded arc welding. Vacuum arc welding. In: *Welding in the USSR*. Vol. 1. Moscow: Nauka.
2. Simonson, R.D. (1969) *The history of welding*. Illinois: Morton Grove.
3. Manna, F. (1979) Storia della saldatura. *Napoli: Edizioni Scientifiche Italiane*, **1**, 539; **2**, 469.
4. Potapievsky, A.G. (1974) *Gas metal-arc welding*. Moscow: Mashinostroenie.
5. Sadler, N. (1999) A look at the fundamentals of gas welding. *Welding J.*, 78(**5**), 45-49.
6. Paton, B.E., Zaruba, I.I., Dymenko, V.V. et al. (2007) *Welding power sources with pulse stabilization of arc burning*. Kiev: Ekotekhnologiya.
7. Benardos, N.N. (1982) *Scientific-technical inventions and projects*: Coll. Kiev: Naukova Dumka.
8. Chekanov, A.A. (1963) *History of automatic electric welding*. Moscow: AN SSSR.
9. Paton, E.O. (1937) Works in electric welding field. *Visti AN URSR*, **6**, 11–27.
10. (1937) *Transactions of Electric Welding Institute of the Academy of Sciences of Ukr. SSR*. Ed. by E.O. Paton. Kiev: AN URSR.
11. Ostapenko, N.G. (1951) Automatic carbon-electrode CO_2 welding of side welds. In: *Jubilee proceedings dedicated to 80th anniversary of E.O. Paton*. Kiev: AN Urk. SSR.
12. Ostapenko, N.G. (1951) Automatic welding of side welds by carbon arc stabilized with carbon gas jet. *Avtogen. Delo*, **5**, 5–9.
13. Kirdo, I.V., Lebedev, V.K., Berzin, A.I. (1957) Carbon-electrode position welding of thin-walled pipes in carbon-dioxide gas atmosphere. *Avtomatich. Svarka*, **3**, 44–50.
14. Paton, E.O. (1961) *High-speed automatic submerged-arc welding*: Coll. Vol. 3. Kiev: AN Ukr. SSR.
15. Lyubavsky, K.V. (1941) Development of fluxes for high-speed welding of steels St2 and St3 with standard electrode wire. *Avtogen. Delo*, **6**, 25–31.
16. Lyubavsky, K.V., Novozhilov, N.M. (1953) Consumable electrode shielded-gas welding. *Ibid.*, **1**, 4–8.
17. Novozhilov, N.M. (1979) *Fundamentals of metallurgy of gas-shielded arc welding*. Moscow: Mashinostroenie.
18. Dyatlov, V.I. (1964) Elements of theory of electrode metal transfer in electric arc welding. In: *New problems of welding engineering*. Kiev: Tekhnika.

19. Ronsky, L.M. (1960) Metal transfer in CO_2 welding. *Avtomatich. Svarka*, **10**, 28–35.
20. Pokhodnya, I.K. (1957) Wire for CO_2 surfacing of wear-resistant steels. *Ibid.*, **3**, 51–54.
21. Pokhodnya, I.K., Golovko, V.N. (1974) High-efficient flux-cored wire for CO_2 welding. *Ibid.*, **7**, 66–68.
22. Pokhodnya, I.K., Shlepakov, V.N., Suprun, S.A. (1982) Welding flux-cored wire of E60 type for CO_2 welding. In: *Proc. of All-Union Conf. on Welding Consumables*. Kiev: Naukova Dumka.
23. Budnik, N.M., Evchenko, V.M., Belousov, Yu.G. et al. (1971) Peculiarities of metal transfer in activated wire CO_2 welding at straight polarity current. *Svarochn. Proizvodstvo*, **7**, 28–31.
24. Paton, B.E., Shejko, P.P. (1967) Automatic control of consumable-electrode pulse-arc welding process. *Avtomatich. Svarka*, **1**, 3–8.
25. Asnis, A.E., Slutskaya, T.M. (1982) Possibilities of decrease in manganese content of electrode wires for active-gas shielded welding. *Ibid.*, **8**, 71–72.
26. Dyurgerov, N.G., Shchekin, V.A., Nebylitsyn, L.E. (1975) Activated-electrode pulsed-arc CO_2 welding. *Svarochn. Proizvodstvo*, **10**, 22–23.
27. Ulianov, V.I., Litvinchuk, S.M., Vysotsky, G.A. (1972) Influence of aluminium on technological properties of Sv-08G2S type welding wire. *Avtomatich. Svarka*, **1**, 8–9.
28. Panin, V.N. (2000) New approaches in quality improvement of known welding consumables and in development of new consumables. In: *Current problems and achievements in the field of welding and related technologies and equipment on the threshold of the 21st century*. St.-Petersburg.
29. Slutskaya, T.M., Asnis, A.E., Tyurin, A.Ya. et al. (1974) Transition of impurity elements from wire to deposited metal in CO_2-oxygen mixture welding. *Avtomatich. Svarka*, **11**, 68.
30. Lavrishchev, V.Ya. (1970) Automatic welding of steel with double gas shielding. *Ibid.*, **2**, 41–43.
31. Paton, B.E., Potapievsky, A.G. *Method of pulse-arc welding*. USSR author's cert. 247430. Int. Cl. H 05 B. Publ. 04.07.69.
32. Asnis, A.E., Gutman, L.M., Poklady, V.R. et al. (1982) *Welding in active gas mixture*. Kiev: Naukova Dumka.
33. Miller, N.A., Salter, G.R. (1964) Effects of nitrogen in CO_2 welding. *British Welding J.*, **1**, 25–28.
34. Paton, B.E. (1947) *Welding heads and their current supply*. Kiev: AN Ukr. SSR.
35. Paton, B.E. (1954) Pulse arc ignition with the purpose of a considerable decrease of welding transformer voltage. *Avtomatich. Svarka*, **4**, 46–52.
36. Petrov, A.V. (1954) Consumable-electrode inert-gas shielded arc welding of stainless steels. *Vestnik Mashinostroeniya*, **9**, 68–70.
37. Zaruba, I.I., Kasatkin, B.S., Kakhovsky, N.I. et al. (1960) *CO_2 welding*. Kiev: Gostekhizdat Ukr. SSR.
38. Zaruba, I.I. (1957) Semi-automatic consumable-electrode welding of thin steel. *Avtomatich. Svarka*, **3**, 9–21.
39. Paton, B.E. (1957) Gas electric welding and rational fields of its application. *Ibid.*, **3**, 1–8.
40. Erdman-Jesnitzer, F. (1959) Beitrag zur Veranderung des Abschmelzcharakter von ummantelten Elektroden durch den elektrischen Anschlusskreis. *Schweissen und Schneiden*, **12**, 447–454.
41. Wilson, R.A. (1961) Vapor-shielded arc welding at 200 ipm. *Welding J.*, **1**, 13–17.
42. Paton, B.E., Potapievsky, A.G., Podola, N.V. (1964) Consumable-electrode pulse-arc welding with programmed control of the process. *Avtomatich. Svarka*, **1**, 1–6.
43. Paton, B.E., Potapievsky, A.G. (1973) Types of shielded-gas welding processes with stationary and pulse arc. *Ibid.*, **9**, 1–8.
44. Paton, B.E., Voropaj, N.M., Buchinsky, V.N. et al. (1977) Control of arc welding process with programming of electrode wire feed rate. *Ibid.*, **1**, 1–5, 15.
45. Zaruba, I.I., Saraev, Yu.N., Knyazkov, A.F. et al. *Method of arc welding with short-circuiting of arc gap and device for its realization*. USSR author's cert. 1313140. Int. Cl. B 23 K 9 / 18. Publ. 15.01.87.
46. Potapievsky, A.G., Lapchinsky, V.F. (1963) Dynamic properties of current sources for CO_2 welding. *Avtomatich. Svarka*, **9**, 42–47.
47. Lebedev, V.K., Medvedenko, N.F. (1968) Study of influence of transient processes on metal spattering in CO_2 welding. *Ibid.*, **5**, 11–14.
48. Belousov, Yu.G., Mikhajlov, A.N., Evchenko, V.M. et al. (1969) Two-mode semi-automatic machine for welding with thin electrode wire at higher current density. *Svarochn. Proizvodstvo*, **4**, 47–48.
49. Medvedenko, N.F., Zaruba, I.I., Sidorenko, M.N. et al. (1970) Improvement of typical power sources for CO_2 welding. *Avtomatich. Svarka*, **6**, 53–56.
50. Zaruba, I.I., Dymenko, V.V., Bargamen, V.P. (1973) Alternative current CO_2 welding. *Ibid.*, **10**, 64–68.
51. Buchinsky, V.N. (1980) Pulse-arc welding with discharge gap short-circuiting. *Ibid.*, **11**, 64–66.
52. Zaruba, I.I., Dymenko, V.V. (1982) Stabilizers of AC arc burning with double control. *Ibid.*, **5**, 43–46.
53. Shejko, P.P., Zhernosekov, A.M. (2003) Technology and equipment for consumable-electrode welding with programmable variation of gas shielding and welding current modulation. *Svarshchik*, **4**, 4.
54. Paton, B.E., Lebedev, V.K., Shejko, P.P. et al. *Method of consumable-electrode shielded gas arc welding*. Pat. 43424 Ukraine. Int. Cl. B 23 K 9 / 167. Publ. 17.12.2004.
55. Shejko, P.P., Pavshuk, V.M., Puzanenko, V.E. et al. (2003) Multipurpose power source for consumable-electrode arc welding methods. *Avtomatich. Svarka*, **4**, 56–57.
56. Khrenov, K.K. (1970) *Welding, cutting and brazing of metals*. Moscow: Mashinostroenie.
57. Bondarenko, V.L. (2004) Arc welding with pulse feed of electrode wire: the CMT process proposed by Fronius Society. *Avtomatich. Svarka*, **12**, 55–58.
58. Paton, B.E. (1945) Submerged-arc welding with flexible long electrode. *Avtogen. Delo*, **1**, 1–2.
59. Bykhovsky, O.G., Skomorokhov, V.M. (1973) Calculation of current and voltage in CO_2 welding arc. *Avtomatich. Svarka*, **11**, 72.
60. Kuhne, A.N., Frassek, B., Starke, G. (1984) Components for the automated GMAW process. *Welding J.*, **1**, 31–34.

ANALYSIS OF THE CAUSES OF FRACTURE OF BLADES IN AXIAL-FLOW COMPRESSOR OF UNIT GTK-25I

K.A. YUSHCHENKO[1], **V.S. SAVCHENKO**[1], **L.V. CHERVYAKOVA**[1], **V.I. IZBASH**[2] and **V.G. SOLYANIK**[2]
[1]E.O. Paton Electric Welding Institute, NASU, Kiev, Ukraine
[2]National Joint Stock Company «Neftegaz Ukrainy», Ukrtransgaz, Kiev, Ukraine

The causes of fracture of martensitic-ferritic steel blades in inlet rotary distributor of axial-flow compressor of the gas-pumping unit were studied. Fracture of the blades occurs in several stages: formation of corrosion sites, initiation and propagation of cracks within the zone of corrosion damage under cyclic loading, and fracture. At the initial stage, corrosion damage takes place at the martensite–ferrite interface, after which it develops from intergranular into intragranular corrosion fracture along the martensite needles, and then into fatigue fracture through the bulk of grain.

Keywords: gas turbine units, blades, high-alloy steel, fatigue-corrosion damage

Gas-turbine units GTK-25I, which are widely applied for transportation of gas, comprise the axial flow compressor with an inlet rotary distributor, which is fitted with variable-incidence stationary blades made from steel 14Kh17N2.

According to the constitutional diagram of Potak and Sagalevich [1], steel 14Kh17N2 belongs to high-alloy steels of the martensitic-ferritic grade, with martensite content of about 70 %, ferrite content of less than 20 %, and traces of retained austenite. Structurally, free ferrite precipitates have the form of strips [2].

Steel 14Kh17N2 is classed with hardenable stainless steels, where the increased chromium content provides sufficient corrosion resistance in a number of low-corrosive environments [3, 4]. However, because of the probability of precipitation of redundant carbide phases, steels of this alloying system [1, 3] exhibit a decreased corrosion resistance in heating to above 500 °C.

Fracture of the airfoil took place during operation on variable-incidence stationary blades in the compressor of unit GTK-25I.

Dye penetrant inspection of the airfoil surface and metallographic examinations allowed revealing local microcracks in the zone of fillets in locations of transition of cylindrical parts of the upper and lower journals to the airfoil (Figure 1) (the presence of fillets, in the opinion of designers, should have decreased the concentration of stresses in these locations); microcracks in locations of nicks on the leading edge of the airfoil; and local (pitting) corrosion damages on the airfoil surface, including in the fillet zones (Figure 2).

Analysis of the state of the upper journal of a variable-incidence blade showed one-sided wear of its cylindrical part on the back side of the airfoil, which seems to be related to the impact by substantial alternating loads on the airfoil (most probably, one-sided impact).

In addition, visual examinations showed the presence of multiple local buckles on the airfoil surface,

Figure 1. Fatigue-corrosion fracture (*1*) of the surface of 14Kh17N2 steel blade formed during operation, and brittle fracture within the nick regions (*2*) formed in emergency fracture

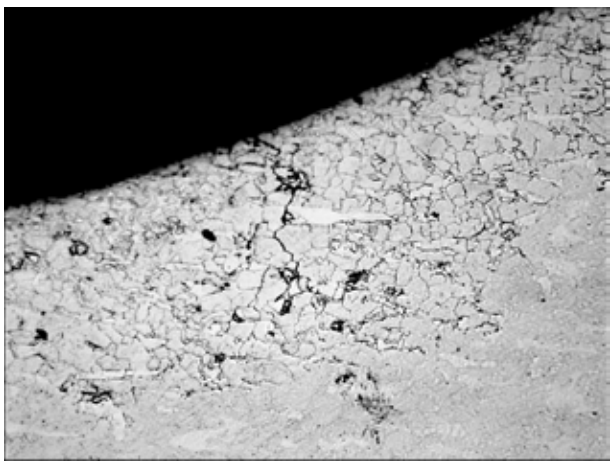

Figure 2. Microstructure with characteristic fatigue-corrosion fracture of 14Kh17N2 steel airfoil within the fillet region (fragment *1* in Figure 1) (×200)

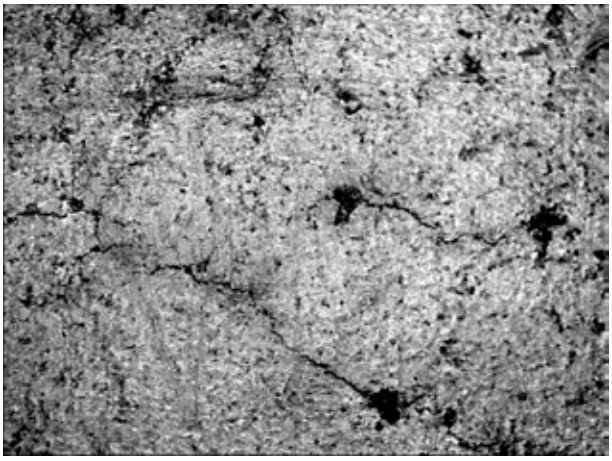

Figure 3. Fragment of the surface of airfoil of variable-incidence blade made from steel 14Kh17N2 with characteristic corrosion cracking (×50)

0.5–1.2 mm in diameter and 0.5 mm deep, with characteristic corrosion cracking (Figure 3).

As determined by metallography, the metal structure consisted of block-type martensite (M) and streak precipitates of δ-ferrite (δ-F) formed, probably, as a result of high-temperature heat treatment. Precipitates of carbides of the $Me_{23}C_6$ type (Figure 4) were seen at the boundaries of the martensite blocks in the bulk of prior austenite grains, and at the interfaces between δ-ferrite and martensitic structural components.

Chemical composition of metal of the variable-incidence blade of steel 14Kh17N2 after service was as follows, wt.%: 0.14 C, 0.46–0.58 Si, 17.85–20.30 Cr, 78.12–79.66 Fe, 1.01–2.03 Ni. Because of different high-temperature solubility of chromium and nickel in γ-austenite and δ-ferrite, some re-distribution of these elements took place between the martensitic and ferritic structural components.

Examinations of the surface of blades after service by using optical microscope «Neophot-32» allowed detailed evaluation of the character of fracture of the

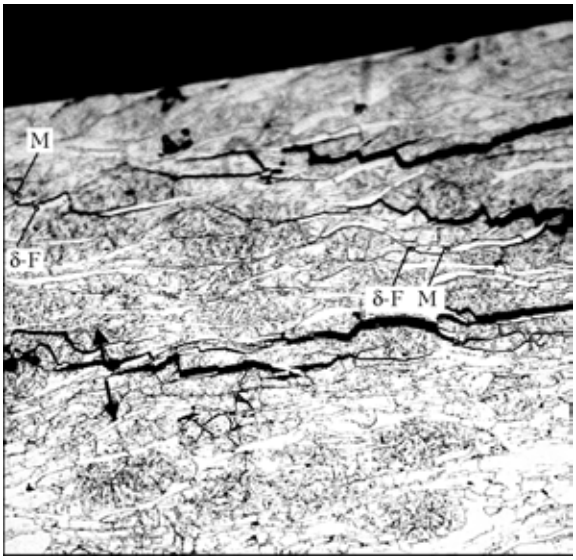

Figure 4. Displacement of local metal regions (shown by arrows) confirming the causes of surface bulges in swelling locations (×100)

Mechanical properties of steel 14Kh17N2 [5]

Product	$\sigma_{0.2}$, MPa	σ_t, MPa	δ, %	ψ, %	*KCU*, J / cm^2	*ÍÂ*
Rolled sections	835	1080	10	30	49	≤ 285
Forgings	539	686	13	35	54	248–293

airfoil formed during operation. First of all, the examinations confirmed the presence of the fatigue-corrosion fracture formed due to fillets in the locations of transition from the upper and lower journals to the airfoil.

Metallography of the polished, but non-etched sections made it possible to evaluate the depth of penetration of corrosion into metal, as well as the character of corrosion. It can be concluded that the intergranular fracture of metal along the boundaries of prior austenite grains, which formed at high temperatures in metal hardening, took place during operation. The examinations confirmed the arbitrary distribution of pitting fractures on the airfoil surfaces, resulting from the corrosion effect.

Mechanical characteristics of metal of the damage-free specimens corresponded to the data given in [5] (Table). Hardness of the 14Kh17N2 steel variable-incidence blade metal was as follows: airfoil ---- *HB* 255, upper journal ---- *HB* 262, and lower journal ---- *HB* 251.

The results obtained allow a conclusion that the first to occur was the fracture along the prior austenite grain boundaries. After that the selective corrosion also took place from the grain boundaries deep into the bulk of grain, primarily along the martensite needles. Some local pitting fractures merged with cracks, thus forming a macro fracture.

As noted above, the substantial amount of corrosion damages can also be related to the local bulges formed on the airfoil surface of the 14Kh17N2 steel blade.

Assumingly, these bulges precede formation of «pitting» fractures. The special procedure for preparation of sections, ensuring the target opening of the centre of such a bulge by the section plane, was developed to reveal the mechanism of formation of such local damages on the surface. The examinations were carried out by using light- and dark-field optical microscopy, as well as scanning electron microscopy. To facilitate identification and evaluation of characteristics of the types of corrosion, analysis of structure of the section surfaces in corrosion fracture locations was conducted without their preliminary etching.

It was found that fatigue fractures within the fillet region were of an intergranular character. Fatigue cracks propagated along the prior austenite grain boundaries, and were located within the field of stresses induced by fillets. The presence of corrosion pits within the fillet region facilitated propagation of the fatigue cracks.

Local bulges were formed as a result of sub-surface exfoliation of metal due to the corrosion processes. At

the initial stage, the corrosion fracture occurred at the grain boundaries and at the martensite–ferrite interface, and then it transformed into an intragnaular fracture along the martensite needles.

The above assumptions on development of local fatigue-corrosion damages are based on the known facts [6], according to which the rate of corrosion under atmospheric conditions strongly depends upon the humidity of air and its content of corrosive admixtures, such as SO_2, H_2S, etc.

It should be noted in conclusion that the main cause of corrosion is a change in the structural state of metal, where the metal becomes depleted of chromium below the passivation threshold, which results from precipitation of chromium carbides on structural components and heat treatment. In addition, selective (local) corrosion fracture takes place on the rear side under the effect of stresses and humid air enriched with corrosive admixtures, such as SO_2, H_2S, etc.

1. (2003) *Reference book on steel and alloy grades*. Ed. by A.S. Zubchenko. Moscow: Mashinostroenie.
2. Potak, Ya.M. (1972) *High-strength steels*. Moscow: Metallurgiya.
3. Chigal, V. (1969) *Intercrystalline corrosion of stainless steels*. Moscow: Khimiya.
4. Lanskaya, K.A. (1976) *High-chromium heat-resistant steels*. Moscow: Metallurgiya.
5. Ulianin, E.A., Svistunova, T.V., Levin, F.L. (1987) *Corrosion-resistant high alloys*. Moscow: Metallurgiya.
6. Melekhov, R.K., Pokhmursky, V.I. (2003) *Structural materials for power generation equipment*. Kiev: Naukova Dumka.

NEW EMISSION SYSTEM WITH TABLET LaB_6 CATHODE

Tablet LaB_6 cathodes have been used for many years in welding guns of the E.O. Paton Electric Welding Institute, which are also manufactured by Sumy PA «Elektron».

PWI is currently supplying to the customers a new emission system, in which the design of the molybdenum cathode holder and control electrodes has been changed, and fused single-crystal tablets of a special shape are used.

Previously used transition bushing

As-assembled unchanged heater component

New transition bushing

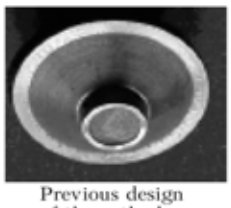

Previous design of the cathode–holder assembly

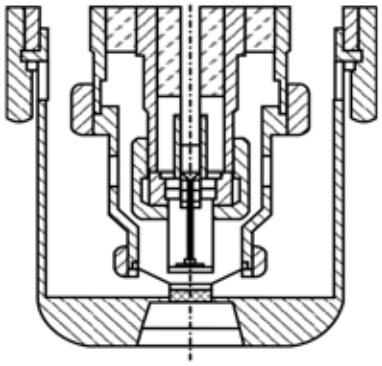

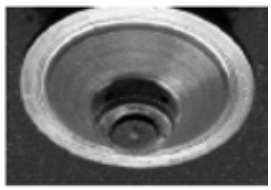

New design of cathode–holder assembly

Previously used control electrode

New control electrode

Development of a new emission system was necessitated primarily by a comparatively short cathode life (10 h). This is attributable to the fact that the emitting surface of a hot-pressed tablet is significantly disrupted because of the recrystallisation processes and ion bombardment. A large contact surface between the tablet and molybdenum holder intensifies the diffusion and evaporation processes leading to reduced dimensions of the tablet, change of its position and increase of the beam peripheral part. Such tablets are also prone to fracture because of cracking.

In order to replace the previously used emission system by a new system it is necessary to use only a new transition bushing, cathode assembled with the holder and control electrode. No other changes in the gun or power source are required. Cathodes and heating spirals are no longer delivered separately, in view of the impossibility of precision assembly of these elements with the holders under the conditions of a non-specialized plant, as well as because of the need for vacuum training of the assembled components.

Cathodes and heating elements are supplied only as-assembled with the holders:

Diameter of the cathode emitting surface, mm	Beam current, mA
1.50	0–-50
3	0–250
3	0–500
4.25	1000

Application. New emission systems are designed for welding guns with accelerating voltage of 30, 60 and 120 kV (U-250A, ELA-15, ELA-30, ELA-60 / 60, ELA-60B, ELA-120-6, etc.).

Advantages of the new emission system:

• cathode life has been extended to 40 to 70 h due to application of single-crystal cathodes and a new design, preventing LaB_6 interaction with the molybdenum holder;

• specific beam power has been increased not less than 2 times due to elimination of its peripheral part, thus providing more narrow and deep welds;

• high reproducibility of welds has been ensured and possibility of beam deflection from the welding gun geometrical axis, and, hence also from the plane of the butt of the edges being welded has been eliminated, due to precision assembly and vacuum training of emission system components.

RANGE OF KL-109, KL-110 AND KL-111 UNIVERSAL MACHINES FOR EBW OF LARGE AND HEAVY WORKPIECES

• PC and programmable controllers are used.

• Electron beam parameters analysis and «black box» type selfdiagnostics of machine by PC.

• Real-time seam tracking and monitoring of EBW process by RASTR system on the basis of the secondary electron emission.

• Gun power source with electron tube flashless system.

Mobile type 15, 30 or 60 kW electron beam gun at accelerating voltage of 60 kV.

Design

The work chamber has two sliding doors. The workpiece table is moved out of the work chamber onto the runout platform of EBW process. The table acommodates rotators with horizontal and vertical axis, and also back centre. The electron gun 3-axis-manipulator has the travelling distance in *Õ*-direction up to 3000 mm, in *Y*-direction up to 730 mm and in *Z*-direction up to 1500 mm. Precision of the guidance and drive system equals that of precision machine tools operation with tolerances in the hundredth-of-a-millimeter range.

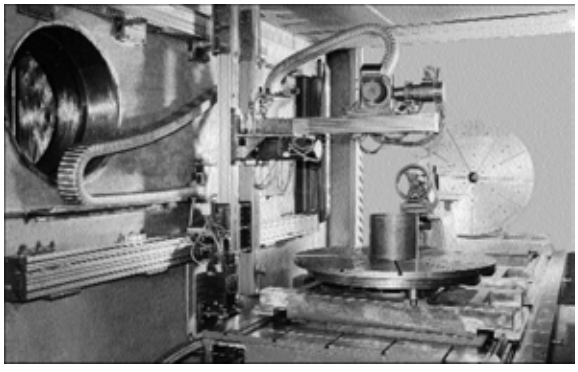

Technical data

Vacuum chamber inner dimensions, m:	
KL-109 and KL-110	$2.5 \times 2.5 \times 5.0$
KL-111	$2.0 \times 2.0 \times 5.5$
Time of evacuation up to the vacuum of $5 \cdot 10^{-4}$ Torr, min	≤ 45
Workpiece weight, kg	max 2500

KL-113 UNIVERSAL MACHINE FOR EBW OF LARGE WORKPIECES

- PC and programmable controllers are used.
- Electron beam parameters analysis and «black box» type selfdiagnostics of the machine by PC.
- Real-time seam tracking and EBW process monitoring by RASTR-5 system on the basis of the secondary electron emission.
- Gun power source with electron tube flashless system.

Machine design

The work chamber has two sliding doors. The workpiece table is moved out of the work chamber onto the charging car. The table acommodates the rotators with horizontal and vertical axis, also the tailstock. The mechanism of electron gun movement has three moving axes *Õ–Õ*, *Y–Y*, *Z–Z*. The gun moves by means of standard linear modules, equipped ball-and-screw gears. The gun is placed on a plate in the rotating support. Rotation may be performed in specified range of 0–90°. Rotation is visually controlled by limb / dial accurate up to 1°, as well as display of rotation angle on the monitor screen.

Vacuum system is assembled on the basis of two roughing-down pumps with capacity of 320 m^3 / h, a single two-rotor ROOTS pump with capacity of 4860 m^3 / h, two high-vacuum pumps D630 with capacity of 16000 l / s each, and turbo-molecular pump with capacity of 110 l / s.

Automated control system (ACS) is a program and hardware complex intended to control the EBW machine equipment (vacuum system, high-voltage source, positioner drive and rotators, RASTR-5M system) both during preparatory operations and EBW performance.

The ACS structure is hierarchic two-level (upper and lower control levels) distributed system. The upper control level (realized in operation medium Windows NT) performs the following functions:

- giving tasks to the lower level subsystems;
- representation of the ACS operation results;
- image of the weldment surface, weld and pool and tracking a joint (RASTR-5M system).

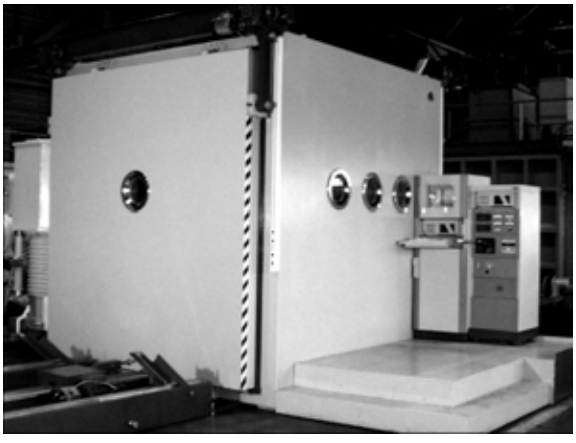

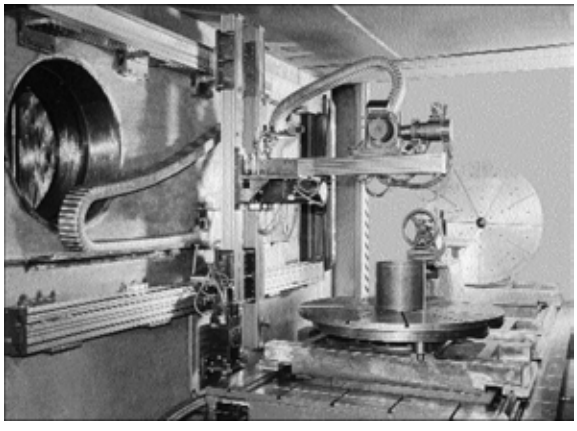

The lower level subsystems software is realized in MS DOS operation medium. The lower level function is direct control of the EB machine equipment. The realized software structure allows using MS DOS realiability at direct control of the machine in real time mode and Windows graphic possibilities (graphic interface) to create a friendly interface for a welding operator with visualization of the EBW processes. The ACS noise immunity is greatly increased due to the lower level subsystems location directly at control objects. Network interchange between the levels is realized by Fast Ethernet network line.

Main technical parameters for KL-113 machine

Overall machine sizes (l × w × h), mm	8450 × 280 × 3470
Weight without high voltage power source, t	32.5
Vacuum chamber internal sizes (l × w × h), mm	3000 × 2500 × 2700
Working pressure in chamber, Torr	not worse than $2 \cdot 10^{-4}$
Time before working pressure in chamber and gun is obtained, min	max 30
EB gun movements with positioning accuracy ±0.1 mm along the coordinates *X*–*X*, *Y*–*Y*, *Z*–*Z*, mm	1800, 800, 1000
Gun tilt angle with 1° accuracy in *X*–*Y* plane, deg	90
EB gun traveling speed along linear coordinates, mm / s	1.66–25
EB gun and source power, kW	15
Accelerating voltage, kV	$60 \pm 0.5 \cdot 10^{-2}$
Beam current, mA	1–250
Beam deflection angle, deg	±3.5
Technical parameters, provided by the Buyer:	
mains	380 V, 50 / 60 Hz
consumed power, kV·À	max 60
cooling water flow rate at temperature of 25 °Ñ and pressure of 2 kg / cm^2, l / h	min 1550
compressed air pressure, kg / cm^2	min 4

KL-114 MACHINE FOR HEATING, DEGASSING, POURING AND VIBRATION COMPACTION OF GRANULES IN CAPSULES WITH SUBSEQUENT HERMETIC SEALING BY MEANS OF EBW

Is intended for fabrication of blanks for aicraft turbine engine parts from high-temperature Ni-based alloys.

Heating and degassing of a capsule to complete removal of adsorbed moisture and gases.

Degassing of the granules during filling in a capsule.

Vibration compaction of the granules in a capsule.

EBW hermetic sealing of a capsule.

PC and programmable controllers are used.

Monitoring of the filling and control of welding processes by RASTR system on the basis of secondary electron emission.

Machine design

The chamber is a rectangular double-wall structure of stainless steel. The partitions forming the cooling system are placed between internal and external walls of the chamber. The door hanger is mounted on the front flange. The rear wall on which the heater is mounted, and the door are cooled by water.

The upper wall of the chamber is equipped with the flange on which the following components are mounted: EB gun with turbo-molecular pump, manipulator of filling, manipulator of placing a plug, manipulator of shield and target, as well as porthole for visual observation of the production process.

The cathode àãåà is isolated bó a vacuum valve to keep the gun under vacuum when the work chamber is vented.

The heater is intended to heat the workpiece before and during the process of its filling with granules. Before starting and during the process of filling-in the capsule with granules, the heater holds uniform (±10 °Ñ) temperature distribution along the workpiece external cylindrical surface.

The three-section heater is designed as a lengthwise split cylinder, supplied with insulating units along the upper and the lower flanges to tighten the filaments on them.

The vibrodrive of eccentric type consists of two parts, first –– located in the vacuum space, and second –– located outside the chamber. The flange, to which the diaphragm of special strengthened rubber is fixed, is mounted on the lower wall of the chamber. It serves to hermetically seal the vibrodrive part placed inside the vacuum chamber.

The charging device is intended to place / unload the tool set together with fixed capsule on / from the vibrodrive landing plate located inside the vacuum chamber.

The automatic control system is a programmable-hardware controlled complex which consists of upper level processor; lower level subsystem, realized on the basis of programmable logical controller; control object interface; operational units (pumps, valves and heating system); visualization system of welding area and alignment device.

The software realizes algorithms of the following functional subsystems control:

- vacuum system;
- high-voltage power supply;
- control and visualization system RASTR;
- workpiece heating system;
- temperature control system.

Main technical data for KL-114 machine

Overall dimensions (l × w × h), mm	5000 × 4400 × 3020
Weight, t	3.5
Internal dimensions of vacuum chamber (l × w × h), mm	940 × 940 × 1065
Dimensions of a capsule (diameter, height), mm	100–400, 100–500
Weight of capsule, kg	max 350
Diameter of weld, mm	max 20
Operating vacuum in vacuum chamber, Pa (mm Hg)	not worse than $2.66 \cdot 10^{-3}$ ($2 \cdot 10^{-5}$)
Temperature of capsule heating, °Ñ	500–600
Amplitude of capsule vibration, mm	0–2
Range of capsule vibration frequency, Hz	10–50
EB gun power source, kW / kV	1.2 / 60
Cycle of preparation, heating, filling and welding of one capsule, working shifts	1

Technical parameters provided by the Buyer

Mains	380 V, 50 / 60 Hz
Power consumption, kV·À	not more than 80
Cooling water flow, l / h	3250
Cooling water inlet temperature, °Ñ	not more than 25
Pressure of cooling water, kg / cm^2	not less than 2
Pressure of compressed air, kg / cm^2	not less than 6
Ambient temperature, °Ñ	not more than 25

UNIVERSAL KL-115 MACHINE FOR EBW WITH 7-AXIS MOTION SYSTEM

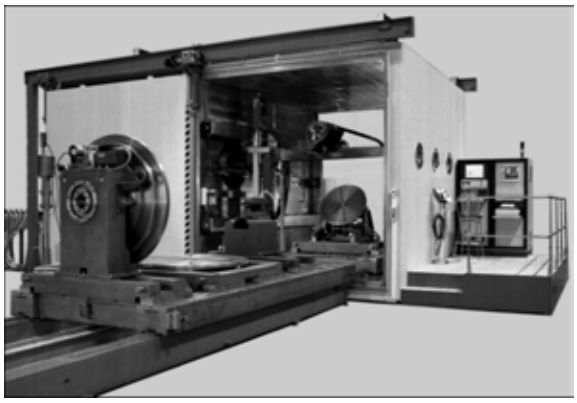

Vacuum chamber and slide doors have two shells, namely a stainless inner shell and outer shell of structural steel connected to each other by frames. The produced box section allows a significant lowering of the structure metal content with preservation of a high rigidity, that guarantees a high accuracy of the displacement mechanisms.

The cantilever mechanism of EB gun displacement allows moving the gun along *X*, *Y*, *Z* axes, as well as rotating it in *X*–*Y* (±90°) and *X*–*Z* (by 90°) planes.

Programmable CNC 7-axes motion control, simultaneous control of 4 coordinates.

Unique high voltage control regulator with vacuum tube detects and suppresses arcing, allowing continuous welding without discontinuties and defects.

Welding control with real time automatic seam tracking by RASTR secondary electron emission system.

Beam analysis system allows the operator to determine actual beam operating conditions prior to welding start and reduce weld parameter development time.

Lanthanum hexaboride cathodes are used for long life of more than 40 h at the power 60 kW, and prevent «beam walking» when the focus position is changed.

PC and programmable controllers are used.

Machine design

The vacuum chamber is a rectangular double-wall welded structure. Two sliding doors are moved letting workpiece to be loaded into the vacuum chamber for the welding. Movement mechanism of the EB gun has three moving axes: *Õ*–*Õ*, *Y*–*Y* and *Z*–*Z*. Accuracy of gun linear positioning along *X*–*X*, *Y*–*Y*, *Z*–*Z* axes is not less than ±0.1 mm. EB gun is mounted on the table along *Y*–*Y* axis and has two rotating axes: rotation — *QG* axis and tilt — *VG* axis. Accuracy of EB gun angular movement on *QG* and *VG* axes is better than 0.1°. Screws in ball-and-screw pairs, linear guides of all linear modules are covered by protective shields or encased to protect them from depositions.

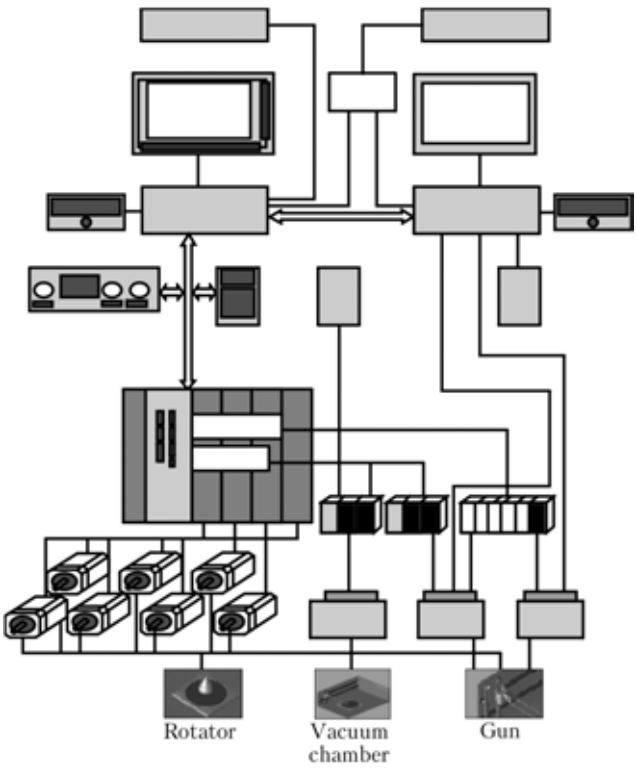

Machine is equipped with three rotators: with horizontal rotation axis, with vertical rotation axis and with tilt rotation axis. Two platforms are functionally designed for the placement of machine mechanisms, mounting of workpieces, their assembling, control of joints to be welded as well as for their transportation into the chamber. This allows assembling and fitting up of workpieces to be done on the one platform while welding of other workpieces is being done on the other platform.

Control system is based on open architecture principles of automation systems for machine tools.

Control system provides implementation of the following features:

- programmable CNC of 7-axes motion (3 linear gun axes, 2 rotary gun axes and 2 rotary rotator axes);
- any 4 axes of the 7 CNC axes selectable for coordinated contouring CNC of motions with linear and circular interpolations;
- full integration of all beam parameters with CNC control;
- operating in a fully automated mode, a semi-automated mode with user defined start and stop locations, and a manual mode including jog function;
- Windows oriented GUI (User Graphic Interface) for programming, system diagnostics, data logging, seam tracking, seam / weld viewing, and real-time process control;
- sequencing blocks of programmed data together into master programs;
- automatic real time teaching and seam tracking via seam tracking system RASTR;
- off-line programming and remote communication;
- PLC control of vacuum system and power supply in all modes;
- diagnostic tools for trouble-shooting faults or errors;
- data logging of process control parameters.

Main technical parameters for KL-115 machine

Overall machine sizes (l × w × h), mm	15960 × 10390 × 3740
Weight, t	48
Vacuum chamber internal sizes (l × w × h), mm	4040 × 2950 × 2950
Working pressure in chamber, Torr	not lower than $1 \cdot 10^{-4}$
Time before working pressure in chamber and gun is obtained, min	max 25
EB gun movements with positioning accuracy of ±0.1 mm along coordinates *X*–*X*, *Y*–*Y*, *Z*–*Z*, mm	3000, 1800, 2000
Gun tilt angle in *X*–*Z* plane, deg	90
Gun rotation angle with 0.1° accuracy in *X*–*Y* plane, deg	not less than ±90
EB gun traveling speed along linear coordinates, mm / s	1.66–33.3

Electron beam gun and power supply

Power, kW	60
Accelerating voltage, kV	$60 \pm 0.5 \cdot 10^{-2}$
Beam current, mA	1–1000
Cathode life, h	40
Beam deflection angle, deg	±3.5

Technical parameters provided by the Buyer

Mains	380 V, 50 / 60 Hz
Consumed power, kV·A	max 250
Cooling water flow rate at temperature of 20 °Ñ and pressure of 4 kg / cm^2, l / h	2630
Compressed air pressure, kg / cm^2	6

Prof. Nazarenko O.K.
Head of Department 57
E-mail: nazarenko@technobeam.com.ua
http: / / www.nas.gov.ua / pwj / beam
http: / / paton.kiev.ua / eng / inst / ntkstructure / deplist / 571.html